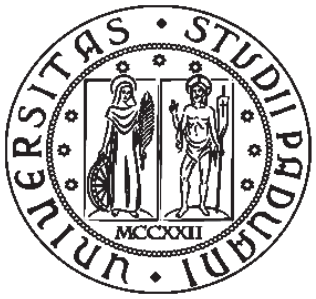

University of Padova

Department of Management and Engineering

PhD school in : Mechatronics and Product Innovation Engineering

27° cycle

MODELLING AND OPTIMIZATION OF THE MECHANICAL PROPERTIES OF POLYMER NANOCOMPOSITES

PhD school director : Alessandro Persona, PhD, Professor

Supervisor : Michele Zappalorto, PhD

PhD candidate : Alessandro Pontefisso

To who is.
And to who is no more.

SUMMARY

The research activity here reported spans different areas of the nanocomposite material science, giving a contribution toward the advancement in its state of the art.

The study of the effects of the filler distribution on the mechanical properties of nanomodified polymers is a major research topic which is carried out. Different computational and theoretical approaches have been developed, considering statistics, finite element analyses and micromechanics.

Several nanomodified epoxy resins have been manufactured along with glass fibre reinforced laminates with nanomodified matrix. The effects of the nanomodification on the mechanical properties of these composites have been studied, in order to validate predictive models and supply technical data to material designers.

The results obtained so far highlight the importance, in this class of materials, of the study of interactions at the nanoscale between the nanoreinforcement and the matrix.

The thesis is articulated in an introduction, followed by two sections, dedicated to the experimental activity and the modelling one, and by an appendix.

The introduction presents a brief overview on nanocomposites giving a primer to a reader devoid of prior experience with this class of materials.

The experimental activity section is constituted by four chapters. The first one contains the results of mechanical tests performed on a nanoparticle reinforced epoxy, alongside an analysis on the processing parameters employed in the composite preparation. The enhancement in the nanocomposite fracture toughness is compared with a theoretical model, showing a satisfactory agreement. The second chapter reports the study of the effect of the testing temperature on the fracture toughness of the same material. The analysis highlights the fundamental importance of the processing parameters and of the testing temperature on the nanomodification effects. The third chapter considers a different aspect of the nanomodification: a nanoplatelet reinforced epoxy is used to prepare notched specimens and the strength analysis of the notched component is carried out. The fourth chapter reports the research activity performed on the study of the matrix nanomodification of glass fibre reinforced laminates. The effects on the matrix dominated

mechanical properties and the feasibility in the production of a laminate with antibacterial bulk properties are analysed.

The modelling section is constituted by three chapters. The first one contains a comparison between two approaches for the estimation of the elastic properties of a nanocomposite material, considering explicitly the presence of an interphase surrounding the nanoreinforcements. The first approach implements a two-step micromechanical model, while the second one is based on a finite element analysis. The second chapter reports the research activity carried out on the generation of representative volume elements of nanoparticle reinforced materials. A statistically based algorithm is implemented to minimize the volume element size while retaining its representativeness. The study of the interphase extent and of the overall elastic modulus, through finite element analyses, is reported. The third chapter extends these considerations to the generation of volume elements for nanoplatelet reinforced materials. The random sequential absorption approach is implemented and its hidden effects on the filler distribution highlighted. A new version of the algorithm is proposed to remove these unwanted behaviours.

The appendix section is dedicated to the implementation activity of approaches which have not been completed yet. The results obtained on the use of molecular dynamics in the simulation of polymers and nanomodified polymers are reported. While a detailed procedure for the simulation of epoxy resins is listed, the approach for the study of nanoplatelet-epoxy interactions is still in progress.

SOMMARIO

L'attività di ricerca riportata nella presente tesi riguarda diverse aree della scienza dei materiali nanocompositi e mira a dare un contributo nell'avanzamento del suo stato dell'arte.

Uno degli ambiti principali di indagine è stato inerente allo studio degli effetti della distribuzione dei rinforzi sulle proprietà meccaniche esibite dai polimeri nanomodificati. Diversi approcci, computazionali e teorici, sono stati sviluppati, sfruttando considerazioni statistiche, l'analisi agli elementi finiti e la modellazione micromeccanica.

E' stata eseguita la nanomodificazione di diverse resine epossidiche e la produzione di laminati in fibra di vetro con matrici nanomodificate. Sono quindi stati studiati gli effetti della nanomodificazione sulle proprietà meccaniche di questi compositi, al fine di validare modelli previsionali e fornire dati ai progettisti di materiali.

I risultati finora conseguiti evidenziano l'importanza che, in questa classe di materiali, ricopre lo studio delle interazioni alla nanoscala che si sviluppano tra i nanorinforzi e la matrice.

La tesi è articolata in una introduzione, seguita da due sezioni dedicate all'attività sperimentale e alla modellazione, e da una appendice a concludere.

La sezione inerente l'attività sperimentale è costituita da quattro capitoli. Il primo contiene i risultati dei test sperimentali eseguiti su resine epossidiche nanomodificate, volti ad indagarne le proprietà meccaniche includendo l'effetto dei parametri di processo. E' inoltre riportato il confronto tra l'incremento della tenacità a frattura misurato sperimentalmente e le previsioni di un modello teorico, evidenziando una soddisfacente congruenza dei risultati. Il secondo capitolo riporta lo studio degli effetti della temperatura sulla tenacità a frattura dello stesso materiale. Tale analisi rimarca la fondamentale importanza dei parametri di processo e della temperatura di prova sugli effetti della nanomodificazione. Il terzo capitolo considera un diverso aspetto della nanomodificazione, ovvero la resistenza di campioni intagliati, prodotti con resine epossidiche rinforzate con nanoplatelets. Il quarto capitolo riporta l'attività di ricerca portata avanti sull'impiego di matrici nanomodificate in laminati rinforzati in fibra di

vetro. Oggetto di analisi sono le proprietà meccaniche dipendenti dalla matrice e la possibilità di produrre laminati con proprietà antibatteriche.

La sezione inerente l'attività di modellazione è invece costituita da tre capitoli. Il primo contiene un confronto tra due approcci volti alla stima delle proprietà elastiche di un materiale nanocomposito, considerando in modo esplicito la presenza di una interfase che circonda i nanorinforzi. Il primo degli approcci implementati è un modello micromeccanico in due passi, mentre il secondo è basato su una analisi agli elementi finiti. Il secondo capitolo riporta l'attività di ricerca inerente la creazione di volumi rappresentativi di materiali rinforzati da nanoparticelle. Tale studio si basa sull'impiego di un algoritmo in grado di considerare aspetti statistici volti alla riduzione della dimensione del volume di controllo, pur mantenendone la rappresentatività. Sono quindi riportate le analisi sull'estensione dell'interfase e sulle proprietà elastiche globali del composito, valutate tramite analisi agli elementi finiti. Il terzo capitolo estende i concetti esposti nel precedente per la generazione di volumi rappresentativi di materiali rinforzati con nanoplatelets. Un approccio basato sull'algoritmo di *random sequential absorption* è stato implementato, evidenziando gli effetti che questo comporta sulla distribuzione dei rinforzi. E' stata quindi proposta una nuova versione di questo algoritmo, capace di rimuovere queste conseguenze indesiderate.

L'appendice è dedicata all'esposizione dell'attività svolta nell'implementazione di approcci che però non sono ancora stati completati. In essa sono riportati i risultati finora conseguiti sull'uso della dinamica molecolare nella simulazione di polimeri e nanocompositi. In particolare è elencata una procedura dettagliata per la simulazione di resine epossidiche, e la prima parte di un approccio per lo studio di resine epossidiche rinforzate con nanoclay.

LIST OF PUBLICATIONS

On International Journals

1. "AN EFFICIENT RVE FORMULATION FOR THE ANALYSIS OF THE ELASTIC PROPERTIES OF SPHERICAL NANOPARTICLE REINFORCED POLYMERS", A. Pontefisso, M. Zappalorto, M. Quaresimin, Computational Materials Science, Volume 96, Part A, January 2015, Pages 319–326.

2. "NOTCH EFFECT IN CLAY-MODIFIED EPOXY: A NEW PERSPECTIVE ON NANOCOMPOSITE PROPERTIES", M. Zappalorto, M. Salviato, A. Pontefisso, M. Quaresimin, Composite Interfaces, Volume 20, Issue 6, 2013, Pages 405-419.

3. "INFLUENCE OF INTERPHASE AND FILLER DISTRIBUTION ON THE ELASTIC PROPERTIES OF NANOPARTICLE FILLED POLYMERS", A. Pontefisso, M. Zappalorto, M. Quaresimin, Mechanics Research Communications, Volume 52, September 2013, Pages 92-94.

4. "MECHANICAL BEHAVIOUR OF EPOXY/SILICA NANOCOMPOSITES: EXPERIMENTS AND MODELLING", M. Zappalorto, A. Pontefisso, A. Fabrizi, M. Quaresimin, **accepted for publication** on Composites Part A: Applied Science and Manufacturing.

5. "ADVANCED MULTIFUNCTIONAL POLYMER NANOCOMPOSITES WITH ENHANCED MECHANICAL AND ANTI-MICROBIAL PROPERTIES", M. Quaresimin, R. Bertani, M. Zappalorto, A. Pontefisso, F. Simionato, A. Bartolozzi, **under review** on Composites Part B: Engineering.

6. "STUDY OF THE RANDOM SEQUENTIAL ABSORPTION ALGORITHM IN THE GENERATION OF NANOPLATELET VOLUME ELEMENTS", A. Pontefisso, M. Zappalorto, M. Quaresimin, **Under preparation**.

At International Conferences

7. "MULTIFUNCTIONAL NANOCOMPOSITES WITH ENHANCED MECHANICAL AND ANTI-MICROBIAL PROPERTIES", R. Bertani, M. Quaresimin, M. Zappalorto, A. Pontefisso, F. Simionato, 16th European Conference on Composite Materials, 22-26 June 2014, Seville, Spain.

8. "FRACTURE BEHAVIOR OF EPOXY/NANOPARTICLE NANOCOMPOSITES AT LOW AND HIGH TEMPERATURE", M. Zappalorto,

A. Pontefisso, M. Quaresimin, A. Fabrizi, 16th European Conference on Composite Materials, 22-26 June 2014, Seville, Spain.

9. "EXPERIMENTAL STUDY ON THE NOTCH EFFECT IN CLAY-MODIFIED EPOXY RESINS", M. Zappalorto, M. Salviato, A. Pontefisso, M. Quaresimin, 3rd International Conference on Nanomechanics and Nanocomposites, 22-25 May 2014, Hong Kong, China.

10. "FRACTURE TOUGHNESS AND NOTCH SENSITIVITY OF CLAY-EPOXY NANOCOMPOSITES UNDER MIXED MODE LOADINGS", M. Quaresimin, M. Zappalorto, M. Salviato, A. Pontefisso, Proceedings of The 4th International Conference from Nanoparticles and Nanomaterials to Nanodevices and Nanosystems, 16-20 June 2013, Corfù Island, Greece.

11. "MODELLING OF THE ELASTIC PROPERTIES OF NANOPARTICLE FILLED RESINS", A. Pontefisso, M. Zappalorto, M. Quaresimin, 15th European Conference on Composite Materials, 24-28 June 2012, Venice, Italy.

12. "FRACTURE TOUGHNESS OF NANOMODIFIED EPOXY RESINS AND GLASS REINFORCED LAMINATES", M. Salviato, A. Pontefisso, M. Zappalorto, M. Santi, N. De Rossi, M. Quaresimin, 15th European Conference on Composite Materials, 24-28 June 2012, Venice, Italy.

At National Conferences

13. "NANOCOMPOSITI AVANZATI CON PROPRIETA' MULTIFUNZIONALI", R. Bertani, A. Pontefisso, M. Quaresimin, F. Simionato, M. Zappalorto, 43rd conference of Associazione Italiana Analisi Sollecitazioni, 9-12 September 2014, Rimini, Italy.

14. "RESISTENZA E TENACITÀ DI NANOCOMPOSITI IN EPOSSIDICA/SILICE", A. Pontefisso, M. Zappalorto, A. Fabrizi, N. De Rossi, M. Quaresimin, 43rd conference of Associazione Italiana Analisi Sollecitazioni, 9-12 September 2014, Rimini, Italy.

15. "EFFETTO DELLA MORFOLOGIA SULLE PROPRIETA' MECCANICHE DEI NANOCOMPOSITI", A. Pontefisso, 42nd conference of Associazione Italiana Analisi Sollecitazioni, 11-14 September 2013, Salerno, Italy.

16. "MODELLAZIONE DELLE PROPRIETA' ELASTICHE DI POLIMERI RINFORZATI CON NANOPARTICELLE", A. Pontefisso, 41st conference of Associazione Italiana Analisi Sollecitazioni, 5-9 September 2012, Vicenza, Italy.

INDEX

SUMMARY v

SOMMARIO vii

LIST OF PUBLICATIONS ix

INTRODUCTION 1

EXPERIMENTAL ACTIVITY 9

Mechanical behaviour of epoxy/silica nanocomposites: experiments and modelling 11

The effect of the testing temperature on the fracture toughness in a nanosilica modified epoxy resin 33

Notch effect in clay-modified epoxy: a new perspective on nanocomposite properties 45

Advanced multifunctional polymer nanocomposites with enhanced mechanical and anti-microbial properties 67

MODELLING 85

Influence of interphase and filler distribution on the elastic properties of nanoparticle filled polymers 87

An efficient RVE formulation for the analysis of the elastic properties of spherical nanoparticle reinforced polymers 97

Study of the Random Sequential Absorption algorithm in the generation of nanoplatelet Volume Elements 121

APPENDIX 139

Molecular dynamics simulation of nanoscale interactions in epoxy nanocomposites 141

ACKNOWLEDGEMENTS 163

INTRODUCTION

This introduction contains a brief overview on the main characteristics of polymer nanocomposites, and it is intended as a primer for the reader. More information can be found in the several reviews [1-4] and books[5-7] available in the literature, as well as in the introduction of each of the following chapters.

1. WHAT IS A POLYMER NANOCOMPOSITE?

Literally, polymer nanocomposites indicate those composites having polymer matrixes reinforced by fillers with at least one sub-micrometer dimension [2]. These nano-fillers display a surface-over-volume ratio which is orders of magnitude higher than in the case of micro-fillers, giving rise to the so called "nano-effect" [3]. Due to molecular interactions between the nanoreinforcement and the polymer matrix, an interphase zone of thickness comparable to the filler size is developed [8]. This interphase is constituted by polymer chains affected by thermo-chemic-mechanical interactions with the nanoreinforcement and it displays properties different from those of the filler and the matrix [8], thus giving rise to a distinctive phase within the material (see Figure 1). The reduction of the filler size to the nanoscale also modifies the mechanical properties displayed by the same filler (e.g. increase the material strength), thus affecting the properties of the whole composite [5].

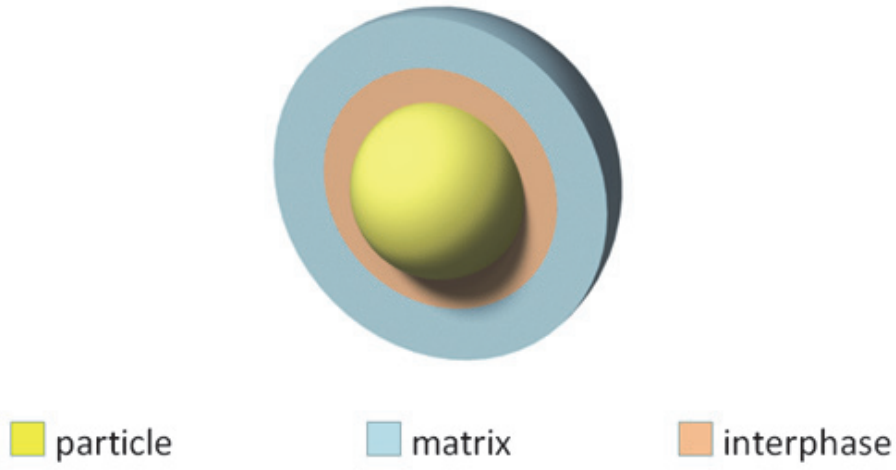

Figure 1. Representation of the material phases developed within nanocomposites.

2. WHY ARE POLYMER NANOCOMPOSITES IMPORTANT?

Polymers are a fundamental class of materials in the 21st century manufacturing technology [9]. They show peculiar processability properties as well as functional ones, offering effective and efficient design solutions otherwise impossible with other materials [10]. However, their use is hampered by their relative modest mechanical properties: for instance high-performance epoxy resins have mechanical properties which are 1-2 order of magnitude lower than steels. To solve this issue several types of reinforcements have been used, such as Carbon fibres, obtaining composite materials which display outstanding mechanical properties [11] and give the possibility of tailoring materials for specific applications [11].

In this scenario nanoreinforcements offer the possibility to further engineer these composites, giving new functional properties or enhanced mechanical ones to their matrices, and thus to the whole composites [12].

Nanocomposites can also be used on their own, such is the case of the nanoclay reinforced polymers used to produce films with enhanced mechanical [13] and gas-barrier properties [14]. Or they can be used to obtain materials with flame-retardant ones, increasing the safety of vehicles and buildings [15]. Another possibility they offer is the production of polymers which display bulk antibacterial properties, thus avoiding the need of coatings [16], or electrically conductive polymers which can be used, for example, in damage sensing solutions [17].

In general, polymer nanocomposites offer an endless amount of possibilities in the engineering of polymer matrixes, resulting in a fundamental tool for the material designer.

3. NANOREINFORCEMENT PROPERTIES AND CHARACTERISTICS

In terms of the nanoreinforcement geometries, three categories can be defined, as a function of the number of sub-micrometer dimensions they possess [4]:

1. With one dimension there are "nanoplatelets", such as Montmorillonite nanoclays, which have thickness of the order of 10^0nm, while the width and the length range up to more than 10^0μm (see Figure 2a).
2. With two dimensions there are "nanofibres" and "nanotubes", such as the Carbon Nano-Tubes (CNTs), which are cylindrical tubes with a diameter in the order of 10^1nm and a length which can be more than 10^2μm.

3. With all three dimensions in the nanoscale there are "nanoparticles", such as silica nanoparticles which can have a diameter in the order of 10^1nm (see Figure 2b).

Regardless of the nanoreinforcement geometry, one fundamental characteristic which they must possess is a sufficient compatibility with the polymer: usually the matrix is hydrophobic while the nanofiller hydrophilic, thus resulting in a segregated material morphology, with micrometer-size clusters of nanoreinforcements [18]. Clearly this behaviour is unwanted because all the benefits due to the nanomodification are lost. Two approaches are then implemented to avoid this behaviour:

1. The nanoreinforcement surface is modified with a surfactant, capable of binding the filler and the matrix [18]. This procedure is common, but it may affect some of the nanoreinforcement properties.
2. The processing of the material includes high-energy dispersing solutions (e.g. shear-mixing [19] or sonication [20]) capable of breaking nanofiller clusters and disperse them within the matrix.

In terms of nanoreinforcement prices, they range from few euro per kilogram (such is the case of Montmorillonite nanoclays) up to hundreds of euro per gram (such is the case of high quality single-wall CNTs), as a function of the nanoreinforcement availability and quality. In fact, the material cost is one of the major issues concerning the employment of nanocomposites in mass-productions [21].

One final remark is about health hazards. It is still unclear what the consequences of prolonged expositions to nanocomposites or nanoreinforcements could be. In the case of CNTs, their capability to penetrate deeply in the lungs and produce a toxic response, time and dose-dependent, has been proved [22]. The same is true for nanoclays [23], which penetrate the lung cell membrane and accumulate within. However the lacking of standardized testing procedures does not help in having a clear picture [22].

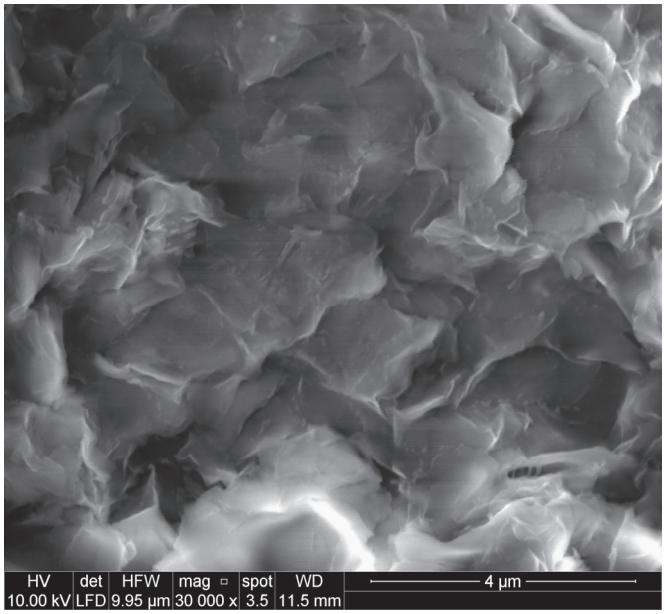

(a)

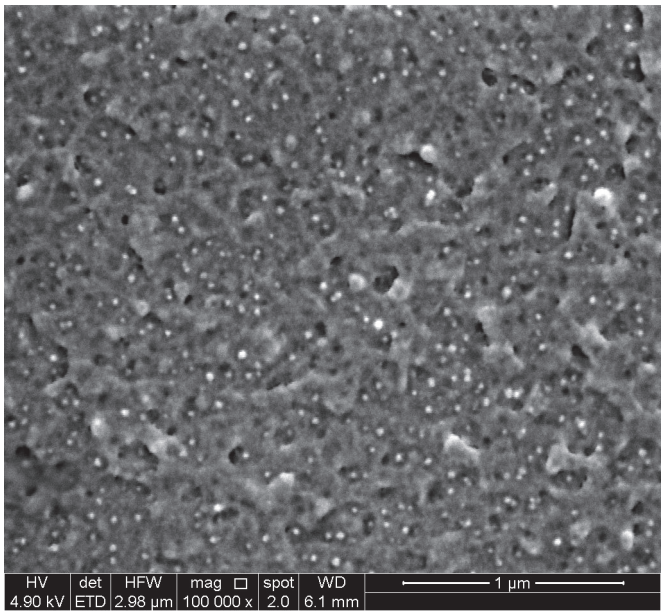

(b)

Figure 2. (a) SEM image of a Montmorillonite nanoclay cluster: clay edges appear as clear lines. (b) SEM image of a silica nanoparticle reinforced epoxy: the white points are the filler.

4. MODELLING AND OPTIMIZATION OF THE MECHANICAL PROPERTIES OF POLYMER NANOCOMPOSITES

Considering the concepts reported above, it should be clear that the employment of nanocomposite materials involves a remarkable complexity. The number of parameters which must be taken into account, and the boundless number of polymer-nanoreinforcement combinations can only be handled through a methodical approach. Whichever aspect of the nanocomposite science and technology a researcher is working on, an overall comprehension of the cross-relationships with the other aspects and in their advancements is fundamental. No modelling effort will truly be successful without considering the processing limitations, which result in the actual nanocomposite filler morphology, or the properties of the interphase due to polymer-filler interactions. No processing procedure can be optimized without considering the chemical compatibility between the composite constituents or the optimal morphology which the models demand. It is from the understanding of this complexity that the author of this PhD thesis resolved to perform his research activities on different aspects of the nanocomposite science and technology, from the production of nanomodified epoxy resins and the testing of their mechanical properties, to their employment as matrixes in glass fibre reinforced laminates, from the proposal of models able to take into account the nanocomposite filler morphology, to the use of molecular dynamic simulations to study the polymer-filler interactions at the nanoscale. All these efforts are reported in the following chapters, in a journal-like structure, each chapter organized as a stand-alone article, with its introduction and bibliography.

REFERENCES

[1] Tjong, S. C. (2006). Structural and mechanical properties of polymer nanocomposites. Materials Science and Engineering: R: Reports, 53(3), 73-197.

[2] Hussain, F., Hojjati, M., Okamoto, M., & Gorga, R. E. (2006). Review article: polymer-matrix nanocomposites, processing, manufacturing, and application: an overview. Journal of composite materials, 40(17), 1511-1575.

[3] Paul, D. R., & Robeson, L. M. (2008). Polymer nanotechnology: nanocomposites. Polymer, 49(15), 3187-3204.

[4] Hu, H., Onyebueke, L., & Abatan, A. (2010). Characterizing and modeling mechanical properties of nanocomposites-review and evaluation. Journal of Minerals and Materials Characterization and Engineering, 9(04), 275.

[5] Bandyopadhyay, A. K., & Bandyopadhyay, A. K. (2008). Nano materials. New Age International.

[6] Ajayan, P. M., Schadler, L. S., & Braun, P. V. (2006). Nanocomposite science and technology. John Wiley & Sons.

[7] Liu, W. K., & Karpov, E. (2005). Nano mechanics and materials: theory, multiple scale analysis, and applications.

[8] Odegard, G. M., Clancy, T. C., & Gates, T. S. (2005). Modeling of the mechanical properties of nanoparticle/polymer composites. Polymer, 46(2), 553-562.

[9] Ashby, M. F. (1987). Technology of the 1990s: Advanced Materials and Predictive Design. Royal Society of London Philosophical Transactions Series A, 322, 393-403.

[10] Kalpakjian, S., & Schmid, S. R. (2010). Manufacturing processes for engineering materials (Vol. 5). Pearson education.

[11] Gay, D., Hoa, S. V., & Tsai, S. W. (2002). Composite materials: design and applications. CRC press.

[12] Quaresimin, M., & Varley, R. J. (2008). Understanding the effect of nano-modifier addition upon the properties of fibre reinforced laminates. Composites Science and Technology, 68(3), 718-726.

[13] Tang, Z., Kotov, N. A., Magonov, S., & Ozturk, B. (2003). Nanostructured artificial nacre. Nature materials, 2(6), 413-418.

[14] Duncan, T. V. (2011). Applications of nanotechnology in food packaging and food safety: barrier materials, antimicrobials and sensors. Journal of colloid and interface science, 363(1), 1-24.

[15] Kiliaris, P., & Papaspyrides, C. D. (2010). Polymer/layered silicate (clay) nanocomposites: an overview of flame retardancy. Progress in Polymer Science, 35(7), 902-958.

[16] Roy, B., Bharali, P., Konwar, B. K., & Karak, N. (2014). Modified hyperbranched epoxy/clay nanocomposites: A study on thermal, antimicrobial and biodegradation properties. International Journal of Materials Research,105(3), 296-307.

[17] Abot, J. L., Song, Y., Vatsavaya, M. S., Medikonda, S., Kier, Z., Jayasinghe, C., ... & Schulz, M. J. (2010). Delamination detection with carbon nanotube thread in self-sensing composite materials. Composites Science and Technology, 70(7), 1113-1119.

[18] LeBaron, P. C., Wang, Z., & Pinnavaia, T. J. (1999). Polymer-layered silicate nanocomposites: an overview. Applied clay science, 15(1), 11-29.

[19] Yasmin, A., Abot, J. L., & Daniel, I. M. (2003). Processing of clay/epoxy nanocomposites by shear mixing. Scripta Materialia, 49(1), 81-86.

[20] Park, C., Ounaies, Z., Watson, K. A., Crooks, R. E., Smith Jr, J., Lowther, S. E., ... & Clair, T. L. S. (2002). Dispersion of single wall carbon nanotubes by in situ polymerization under sonication. Chemical physics letters, 364(3), 303-308.

[21] Wijewardane, S. (2009). Potential applicability of CNT and CNT/composites to implement ASEC concept: a review article. Solar Energy, 83(8), 1379-1389.

[22] Helland, A., Wick, P., Koehler, A., Schmid, K., & Som, C. (2008). Reviewing the environmental and human health knowledge base of carbon nanotubes.Ciência & Saúde Coletiva, 13(2), 441-452.

[23] Verma, N. K., Moore, E., Blau, W., Volkov, Y., & Babu, P. R. (2012). Cytotoxicity evaluation of nanoclays in human epithelial cell line A549 using high content screening and real-time impedance analysis. Journal of Nanoparticle Research, 14(9), 1-11.

EXPERIMENTAL ACTIVITY

1 Mechanical behaviour of epoxy/silica nanocomposites: experiments and modelling

KEYWORDS: A. Nano-structures; B. Fracture toughness; C. Mechanical properties; D. Analytical modelling;

ABSTRACT
In the present chapter the mechanical behaviour of an epoxy/silica nanocomposite system is analysed, discussing the results from tensile and fracture tests.
Moreover a study on the effect of the curing cycle on the mechanical properties of nanocomposites is carried out, considering two different curing conditions. Results indicate that the curing cycle has a significant effect on the overall mechanical behaviour of the nanocomposite. Indeed, while nanomodification always enhances the fracture toughness of the epoxy resin, the strength and the notch strength are shown either to increase or to decrease, depending on the specimen curing process.
Fracture properties are compared to theoretical predictions based on a multiscale and multimechanism model recently developed by the research group, showing a satisfactory agreement.

1. INTRODUCTION

The possibility to obtain outstanding improvements of mechanical properties at low nanofiller contents has arisen significant interest in the use of nano-modified epoxy resins from the scientific community. Among the different types of nanofillers many authors focused their attention on the use of nanoparticles to strengthen and toughen polymer resins.

Chen et al. [1] investigated the mechanical properties of epoxy resins filled with 12-nm spherical silica nanoparticles dispersed with minimal aggregation and obtained, for filler contents lower than 10%, substantial improvements of the tensile modulus and the fracture toughness. Similar results were obtained by Ma et al. [2] on two epoxy systems loaded with silica nanoparticles.

The nanoparticle size effect was studied experimentally by Liang and Pearson [3] and Dittanet et al. [4] who agree that the Young's modulus and the fracture toughness of epoxy resins can be significantly improved by nanomodification, the effect of particle size being almost negligible. In agreement with previous findings by Hsieh et al. [5],

Dittanet et al. [4] noted the presence of nanoparticle debonding, matrix void growth, and shear banding on the surfaces of fractured specimens.

Different from the above mentioned works where a clear size effect was absent, Zamanian et al. [6] showed that the mechanical properties of an epoxy resin were largely improved by the addition of silica nanoparticles with different size, the better improvements being obtained with the smaller nanoparticles.

Liu et al. [7] carried out a study on the effects of silica and rubber nano-particles on the fracture toughness behaviour of an epoxy polymer by analyzing the results from mode I fracture toughness tests of binary silica/epoxy, binary rubber/epoxy and ternary silica/rubber/epoxy nanocomposites with different particle weight fractions. The major conclusion drawn by the authors is that the G_{Ic} of the epoxy resin is significantly increased by incorporating either rubber or silica nano-particles, but hybrid nanocomposites do not display any synergistic effect.

In the present chapter the mechanical behaviour of an epoxy/silica nanocomposite system is analysed, discussing the results from tension and fracture tests. Moreover a study on the effect of the curing process on the mechanical properties of nanocomposites is carried out considering two different curing cycles:

A. Curing at room temperature for 72 hours.
B. Curing at room temperature for 72 hours and post-curing in an oven at 60°C for 15 hours.

In both cases, it is found that nanomodification significantly enhances the fracture toughness of the epoxy resin.

As far as the strength and the notch strength are concerned, a significant effect of the curing process is noted. In more details, nanomodification results in an increase of the strength and the notch strength for specimens post-cured in oven; instead a decrease of those properties is noted when specimens are cured at room temperature only.

Eventually, the experimental results from fracture tests are compared to the theoretical predictions based on a multiscale and multimechanism model recently developed by the present authors.

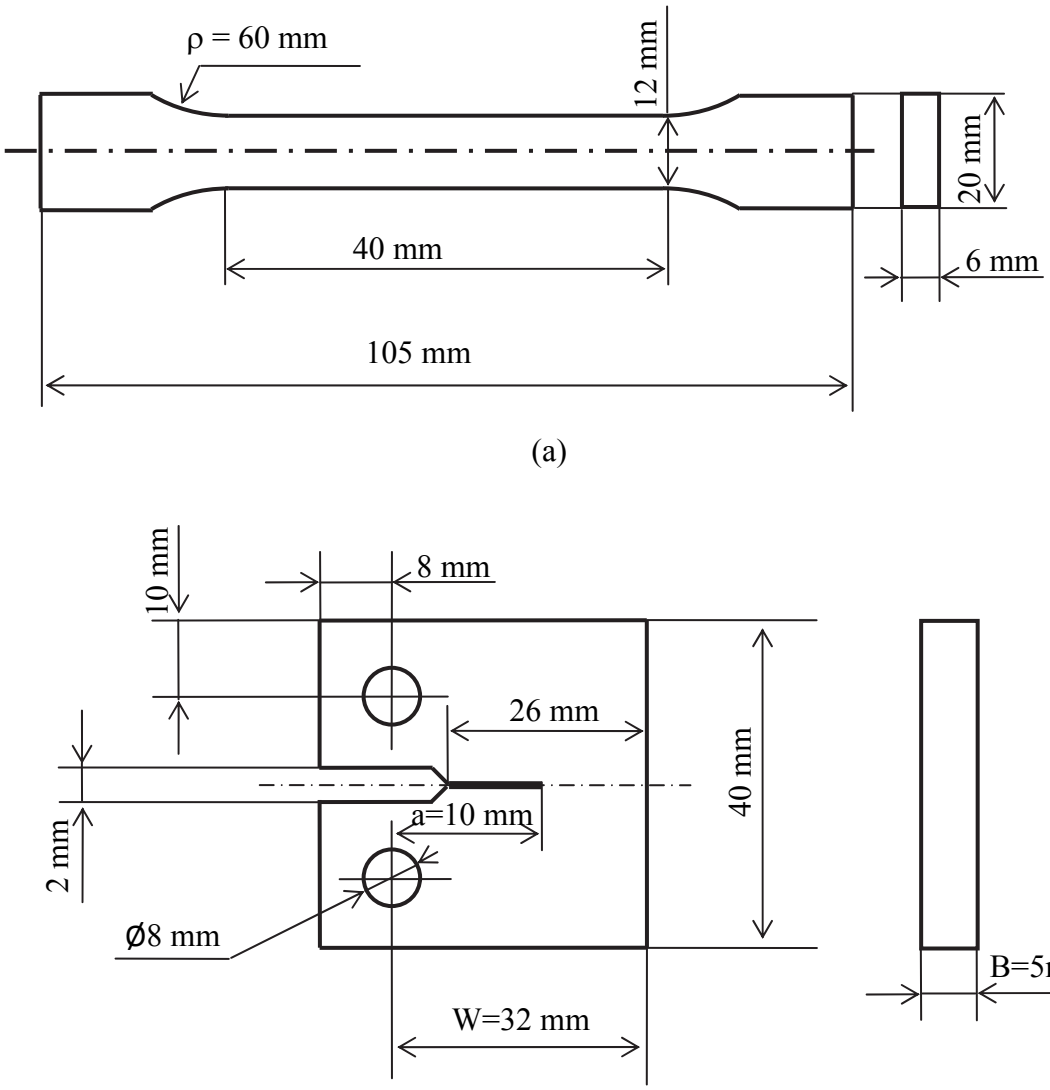

Figure 1. Dog-Bone (DB) specimens (a), Compact Tension (CT) specimens (b) and Double Edge Notch Tension (DENT) specimens (c) used in the tests.

2. MATERIALS AND SPECIMENS EMPLOYED IN THE EXPERIMENTAL ANALYSIS

A DGEBA-based epoxy resin from ELANTAS ITALIA was used (EC157 with W152LR hardener) as the matrix for the nanocomposites investigated.

Nanopox F400 from Evonik was used for nanomodification. It is a masterbatch of 40%wt of silica nanoparticles, with an average diameter of about 20nm and a maximum diameter of 50nm, dispersed in a DGEBA epoxy resin. The following nanofiller weight fractions have been used: 1, 3, 5 and 8%wt.

Dog-Bone (DB) specimens, Double Edge Notch Tension (DENT) specimens as well as Compact Tension (CT) specimens have been manufactured according to the following steps:

1. *Preparation of the masterbatch*. As suggested by the supplier the masterbatch was heated for 15 minutes at 50°C to reduce its viscosity.
2. *Mixing of the composite components*. The masterbatch was then added to the resin and shear mixing was carried out with a DISPERMAT TU shear blender from VMA-Getzmann with a 70mm diameter blade (1200rpm for 5 minutes). Afterwards the blend was sonicated through a HIELSCHER UP 200S sonicator using a 40mm diameter sonotrode for 15 minutes (amplitude 160W and duty cycle 1). Eventually the hardener was added and shear mixing at 350rpm for 5 minutes was carried out.
3. *Degassing and moulding of the blend*. During the shear mixing process, a large amount of air was trapped into the matrix thus requiring a careful degassing process. To this end, a low-vacuum pump was used to induce a very low pressure in the resin pot, promoting bubbles explosion. After half an hour of degassing the nanomodified resin was slowly poured into silicone rubber moulds.
4. *Post-curing of the specimens*. All specimens were cured at room temperature for 3 days. Subsequently, once de-moulded, half of the specimens were post-cured in an oven at 60°C for 15 hours.
5. *Finishing*. Finally specimens were lapped. Moreover CT specimens were pre-cracked by manual tapping with a razor blade, obtaining artificial short cracks. 10 mm long cracks (half the specimen width, according to [9]) were finally obtained by applying some zero-to-tension fatigue cycles.

3. EXPERIMENTAL TESTING AND RESULTS

3.1 Tensile tests

Tensile tests on Dog-Bone (DB) specimens were carried out with the aim to determine the failure stress, σ_R, the elastic modulus, E and the strain to failure, ε_R of the neat epoxy and nanomodified resins. The specimen geometry, shown in Figure 1a, complies with the ISO 527-2 suggestions [10]. A MTS809 servo-hydraulic machine equipped by a 25kN load cell has been used, with crosshead speed equal to 2mm/min and a MTS 632.29F-30 extensometer was used for accurate strain measurements. For each material configuration, at least three specimens were tested. In all the tests performed failure took place in the gauge length of the specimens.

The effect of the weight content of silica particles upon the nanocomposite tensile properties is shown in Figures 2-4. In particular the values of the Young's modulus, E, are shown in Figure 2. A modulus of 3.5GPa was measured for the Non-Post-Cured (NPC) specimens made of unmodified epoxy resin and a maximum modulus of 3.85GPa was measured for the NPC epoxy polymer with 8%wt of particles, with an increase of about 10% compared to that of the unmodified epoxy resin. Generally speaking nanomodification results in a moderate monotonic increase of the longitudinal elastic modulus with an almost negligible effect of the post curing process.

The results for the tensile strength and strain to failure are shown in Figures 3 and 4. Different from before, in this case it is evident that Post-Cured (PC) and Non-Post-Cured (NPC) specimens exhibit a different mechanical behaviour. As far as NPC specimens are concerned, nanomodification has a detrimental effect: nanocomposite strength is indeed continuously decreased from about 70MPa (neat resin) to about 50MPa (8%wt nanoparticle) with a 30% reduction of σ_R. The trend for the strain to failure is similar, which is reasonable considering that the elastic modulus is about constant and the behaviour linear elastic. This negative effect is not present on the results from PC specimens. It seems that the nanomodification hinder the reticulation process of the resin, affecting the resistance of the material, but the post-curing compensates this behaviour and allows a complete curing. Unfortunately the authors do not have the facilities to perform a quantitative analysis on the nanocomposite curing and to verify this hypothesis. Instead, a qualitative analysis has been performed, immerging the specimens for 24 hour in Acetone solvent: NPC specimens displayed an extensive damaging, which increased proportionally to the amount of nanoreinforcements they contained, while PC specimens

resulted unaffected, regardless the filler volume fraction. A similar approach has been used in [8], where the authors used MEK instead of Acetone to test the curing of an epoxy-γAl_2O_3 nanocomposite. Pictures of the specimens removed from the Acetone are reported in Figure 5, confirming that nanomodification without post-curing affects negatively the material curing.

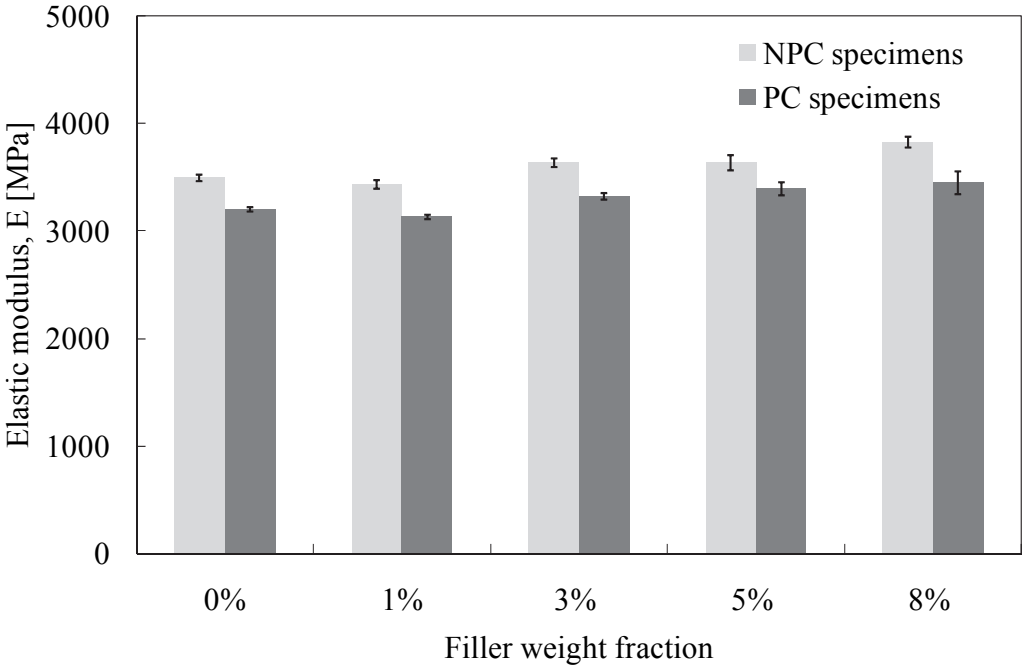

Figure 2. Results of tensile tests on neat and nanomodified DB specimens. Elastic modulus E.

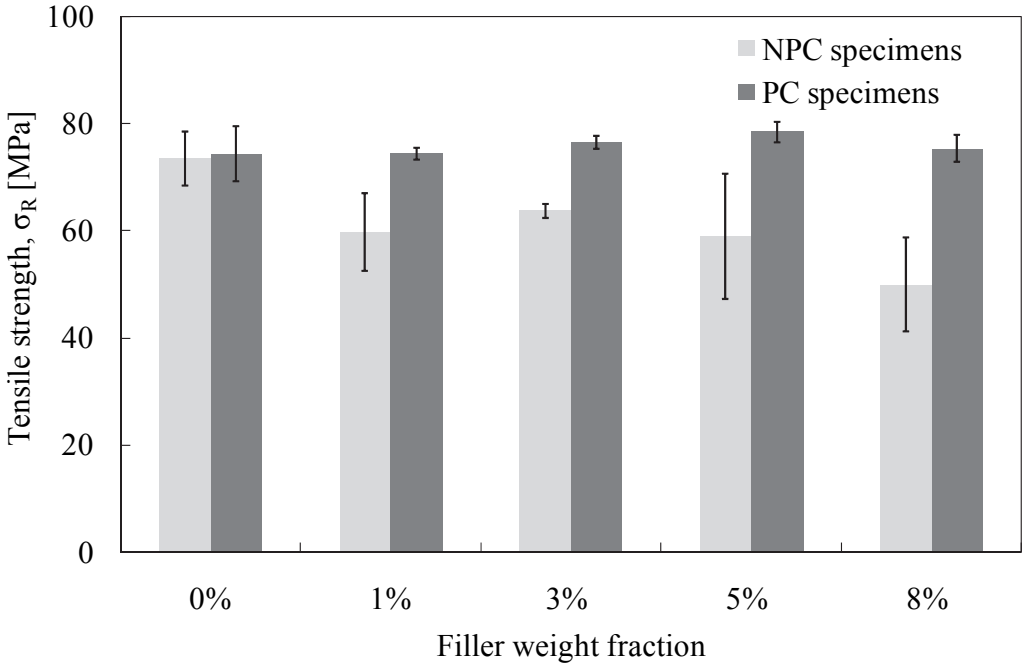

Figure 3. Results of tensile tests on neat and nanomodified DB specimens. Tensile strength, σ_R.

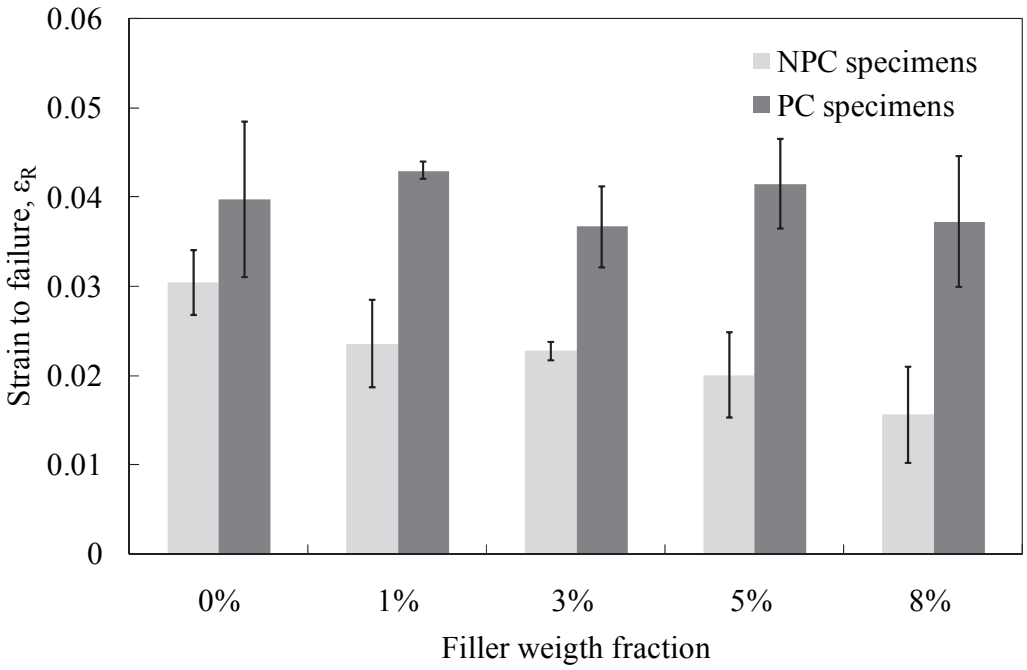

Figure 4. Results of tensile tests on neat and nanomodified DB specimens. Strain to failure, ε_R.

(a) *(b)*

Figure 5. Tested Dog-Bone specimens after immersion for 24h in Acetone. (a) NPC specimens with 8%wt nanosilica particles. (b) PC specimens with the same filler loading.

3.2 Mode I fracture tests

Fracture tests have been carried out on Compact Tension specimens (Figure 1b) according to the ASTM D5045-99 suggestions [9]. A MTS858 servo-hydraulic machine equipped with a 2.5kN load cell has been used. At least three values for each material have been used.

Mode I fracture toughness has been computed by the following expression [9]:

$$K_{Ic} = \frac{P_{cr}}{B W^{0.5}} f\left(\frac{a}{W}\right) \tag{1}$$

where P_{cr} is the critical load, B, a and W are defined in Figure 1b, and f(a/W) can be assessed as [9]:

$$f\left(\frac{a}{W}\right) = \frac{\left(2+\frac{a}{W}\right)\left[0.886+4.64\frac{a}{W}-13.32\left(\frac{a}{W}\right)^2+14.72\left(\frac{a}{W}\right)^3-5.6\left(\frac{a}{W}\right)^4\right]}{\left(1-\frac{a}{W}\right)^{1.5}} \tag{2}$$

with $0.2 < \frac{a}{W} < 0.8$.

A summary of all experimental data from CT tests, expressed in terms of K_{Ic} according to Eq. (1), is shown in Figure 6. It is evident that nanomodified specimens, independently whether PC or NPC, exhibit a fracture toughness higher than that of the pure resin.

In more details, it can be noted that, as far as NPC specimens are concerned, the addition of nanosilica particles initially increases the nanocomposite fracture toughness, up to a maximum value (for 5 %wt) of 1.19MPa·$m^{0.5}$, 35% higher than the neat resin. Increasing again the nanosilica content, the trend reverses and K_{Ic} decreases.

Differently, PC specimens exhibit a monotonic amelioration of the K_{Ic}, up to a maximum value (for 8%wt of silica nanoparticles) of 1.26MPa·$m^{0.5}$, about 60% higher than that of the PC specimens made of neat resin.

The different trend of fracture toughness data, passing from 5%wt to 8%wt, exhibited by NPC and PC specimens might be attributed to competing effects between the fracture toughness enhancement, due to the increasing amount of filler, and the reduction in the polymer reticulation, due to a reduced mobility of the polymer chains. PC specimens take advantage from the post-curing process and compensate the chain mobility reduction with an higher curing temperature.

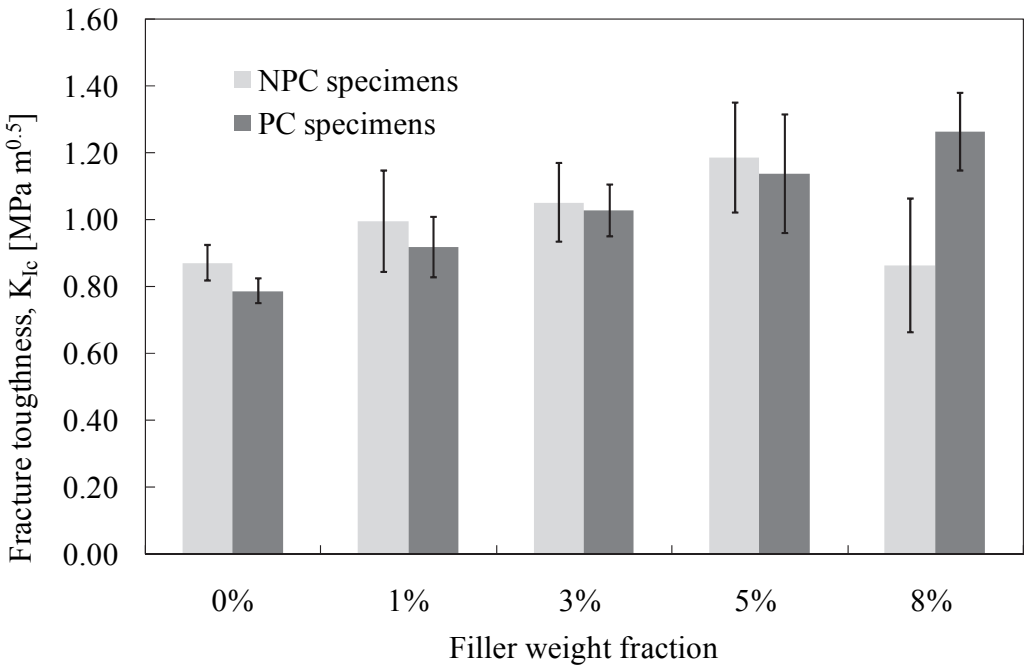

Figure 6. Results of mode I fracture tests on neat and nanomodified CT specimens.

3.3 Tests on notched specimens

Tensile tests on DENT specimens (Figure 1c) were carried out with the aim to determine the failure stress, σ_t, of notched components. A MTS809 servo-hydraulic machine equipped by a 25kN load cell has been used, with crosshead speed equal to 2mm/min. For each material configuration, at least three specimens were tested. In all the performed tests failure took place in the net area of the specimen.

The effect of the weight content of silica nanoparticles upon the strength of notched specimens is shown in Figure 7; results are reported in terms of the maximum notch stress to failure, σ_t, the stress concentration factor on the net area being K_{tn}=1.86 [11]. It is evident that the results are consistent with those obtained from Dog-Bone specimens (see section 3.1)*:* as far as NPC specimens are concerned, nanomodification has a detrimental effect, whereas this negative effect is not present on the results from PC specimens.

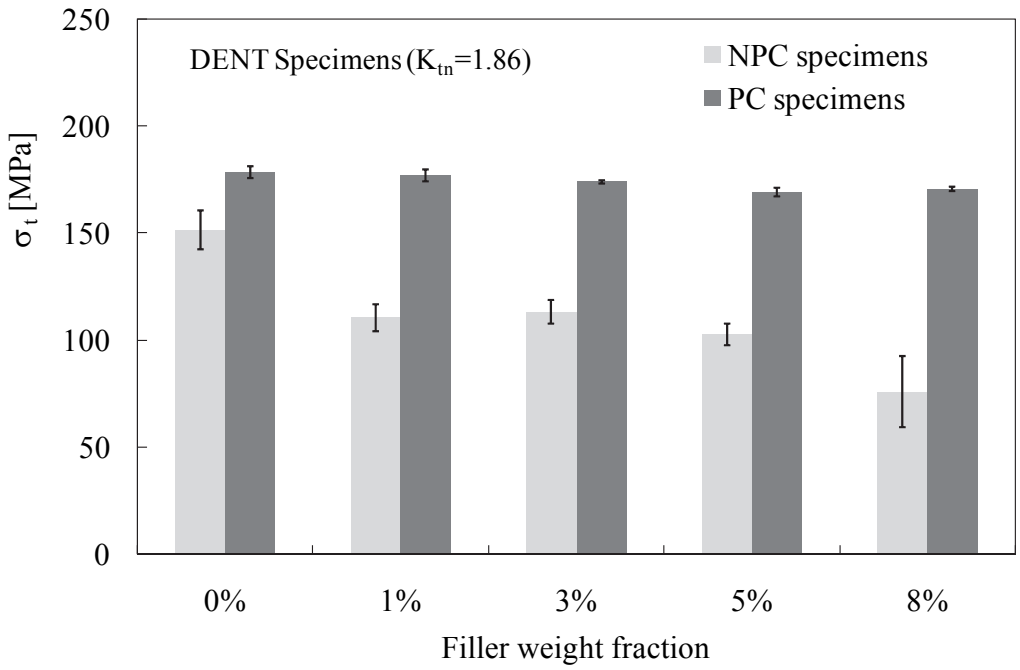

Figure 7. Results of tensile tests on neat and nanomodified DENT specimens in terms of the maximum notch stress to failure, σ_t.

3.4 Some remarks on the experimental results

In the previous subsections, it has been shown that the curing process can alter the mechanical behaviour of silica/epoxy nanocomposites, PC and NPC specimens being characterised by different mechanical properties.

Indeed, even if all nanomodified specimens exhibit a fracture toughness higher than that of the pure resins, the highest value of K_{Ic} has been obtained with 8%wt loaded post-cured samples. Moreover, PC specimens exhibit a monotonic amelioration of K_{Ic}, whereas NPC specimens are characterized by an initial improvement of the fracture toughness for low contents, followed by a reversed trend for weight fractions higher than 5%. Accordingly it can be concluded that silica nanoparticles act as toughen agent in the epoxy matrix for both the curing cycles considered, only for weight fractions lower than 5%. Increasing the filler content the interaction between nanoparticles and epoxy molecules makes it necessary a more effective curing, improving the degree of polymer crosslinking. A similar results was obtained by Tcherbi-Narteh et al.[12] for DGEBA epoxy resin composites modified with montmorillonite nanoclay.

Moving to the nanocomposite strength the scenario is much more complicated: while indeed for NPC specimens nanomodification is found to have a detrimental effect on σ_R,

post-cured DB samples, as well as DENT specimens, were found to be characterised by a strength comparable or slightly higher than that of the neat resin (see Figures 4,7).

This result is extremely important; indeed, for notch root radii large enough, the brittle failure of notched nanomodified specimens is a strength-controlled phenomenon [13]. Accordingly, it might happen that nanomodification, while enhancing the polymer fracture toughness, might have a detrimental effect on the strength of notched components, so that particular care should be used when using nanomodified resins for structural applications in the presence of notches or holes [13] − this concept is dealt with in third chapter. This is not the case of PC specimens analysed in this work, for which nanomodification allowed to improve the polymer fracture toughness without penalizing its strength and notch sensitivity.

As a major conclusion it can be stated that in the epoxy/silica nanocomposite system studied in this work, silica nanoparticles effectively act as strengthening agent only in the case of PC specimens, for which an increased curing time probably allows to increase the degree of cross-linking of the polymer.

This result disagrees with those reported in the literature for MWNT/epoxy nanocomposites [14-16] where the effect of the reinforcement was more evident for a less cured resin. In the case of CNTs, however, the same papers report how the nanomodification does not affect the strain to failure, which can reasonably motivate the different behaviour.

4. MORPHOLOGICAL ANALYSES

The fracture surfaces of PC nanomodified resins were analysed by using Field Emission Gun Scanning Electron Microscope (FEG-SEM, Quanta FEG 250 FEI) at an accelerating voltage of about 5kV. Prior to SEM observation, the fracture surfaces were gold-sputtered for about 10s.

FEG-SEM micrographs of the fracture surfaces of a 5%wt nanomodified CT specimen are shown in Figures 8, where a very satisfactory degree of dispersion and distribution of the nanofillers can be noted. The mean diameter of the particles was found to be approximately 25nm, very close to the data provided by the supplier (20nm).

It is also evident that the fracture surface is very rough, documenting the presence of damage evolution and energy dissipation, probably due to nanoparticle debonding and nanovoid deformation taking place during crack propagation. This corroborates the idea

that fracture toughness improvements can be attributed to the energy absorption mechanisms taking place at the nanoscale.

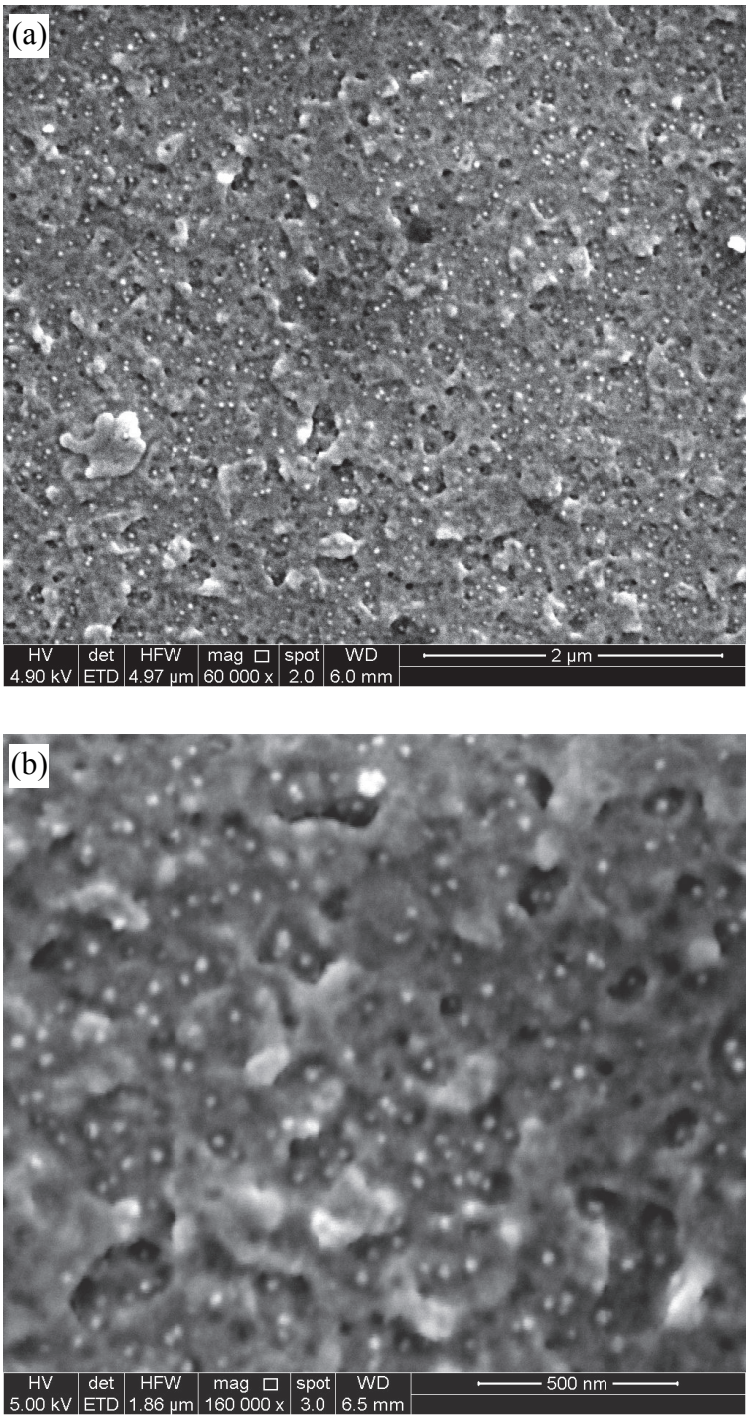

Figure 8. Analysis of the fracture surfaces of 5%wt nanomodified resins by using Field Emission Gun Scanning Electron Microscope.

5. MODELLING STUDIES

The fracture toughness assessment of nanoparticle reinforced polymers was recently tackled in Refs. [17-19] considering the following material system at the nanoscale (see Figure 9):

1. a spherical nanoparticle of radius r_0;
2. a surrounding interphase of external radius a, thickness t and uniform properties;
3. a volume of matrix, much larger than the interphase and the nanoparticle.

This system accounts for molecular interactions at the nanoscale through the size and elastic properties of the interphase layer [17-19] which is supposed to be homogeneous and isotropic.

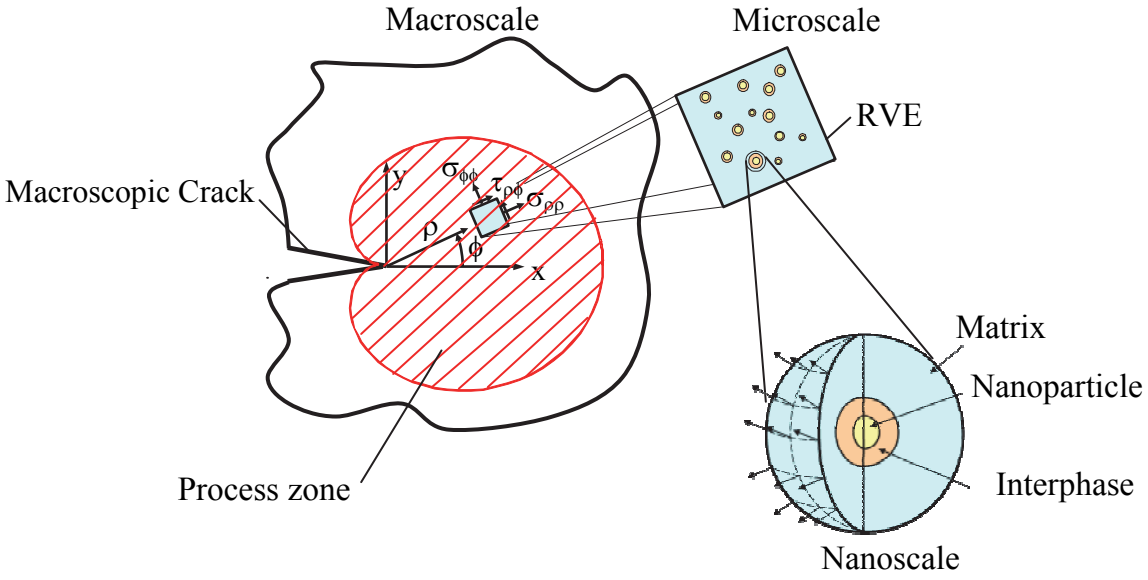

Figure 9. Description of the multiscale system for the assessment of the fracture toughness of nanoparticle filled polymers [18].

A cracked nanocomposite is considered at the macro-scale (see again Figure 9). At this larger scale, it is assumed that the crack stress fields give rise to a process zone containing all the sites of nanoscale damage and energy dissipation, resulting, in turn, in the enhanced fracture toughness of the nanocomposite material.

Through the analysis of the energy dissipation at the nanoscale the normalised fracture toughness of nanoparticle filled polymers can be written as follows [17]:

$$\frac{G_{Ic}}{G_{Im}} = \frac{1}{1 - f_{p0}\left(\psi_{db} + \psi_{p} + \psi_{SB}\right)} \tag{3}$$

where G_{Im} is the unloaded polymer toughness, f_{p0} is the filler volume fraction while parameters ψ_i quantify the energy dissipation caused by each damaging mechanisms, namely, nanoparticle debonding (i = db), plastic yielding of nanovoids (i = p) and shear banding (i=SB) [17-19]:

$$\psi_{db} = \frac{2}{3\pi} \times \frac{\gamma_{db}}{r_0} \times \frac{1+\nu_o}{1-\nu_o} \times \frac{E_o}{\sigma_{cr}^2 (C_h)^2} \tag{4}$$

$$\psi_{p} = \frac{4}{9\pi C_h} \cdot \frac{E_o}{E_m} \frac{(1+\nu_o)(1+\nu_m)}{1-\nu_o} \frac{\sigma_{Ym}}{\sigma_{cr}} \left(\frac{a}{r_0}\right)^{3\times\left(1-\frac{\sigma_{Ya}}{\sigma_{Ym}}\right)} e^{\left(3C_h \frac{\sigma_{cr}}{\sigma_{Ym}} - 1\right)} \tag{5}$$

$$\psi_{SB} = \frac{I_{SB}}{4\pi\sigma_{yca}^2 (1 - \mu/\sqrt{3})^2} \frac{E_o}{1-\nu_o^2} \times \Gamma \tag{6}$$

In Eq. (4) E_o and ν_o are the elastic properties of the nanocomposite, σ_{cr} is the critical debonding stress [20]:

$$\sigma_{cr} \cong \sqrt{\frac{4\gamma_{db}}{r_0} \frac{E_m}{1+\nu_m}} \sqrt{\frac{\chi(4+\xi) - \xi(\chi-1)(r_0/a)^3}{4+\xi+4(\chi-1)(r_0/a)^3}} \tag{7}$$

C_h is the reciprocal of the hydrostatic part of the global stress concentration tensor, estimable as [20]:

$$C_h = \frac{K_m}{K_p} \frac{(\xi+4)(3K_p/G_m + 4\chi)}{(\xi+4\chi)(3K_m/G_m + 4)} + \frac{(4\xi - 12K_p/G_m)(1-\chi)}{(\xi+4\chi)(3K_m/G_m+4)} \left(\frac{r_0}{a}\right)^3 \tag{8}$$

where E_m and ν_m are the elastic modulus and Poisson's ratio of the matrix, K_m, K_a and K_p the bulk moduli of the matrix, the interphase and the nanoparticle, G_m and G_a are the shear elastic moduli of the matrix and the interphase, $\chi = G_a / G_m$ and $\xi = 3K_a / G_m$.

Instead, in Eq. (5) and Eq. (6) σ_{Ym} and σ_{Ya} are the yield stress of the matrix and the interphase, μ is a dimensionless pressure coefficient, σ_{yca} is the interphase yielding stress under compression, whereas function Γ quantifies the energy produced at the nanoscale and I_{SB} accounts for the stress concentration around nanoparticles [19]:

$$\Gamma = \tau_{ym}\gamma_{fm} \left\{ \left(\frac{\pi}{6f_{p0}}\right)^{\frac{1}{3}} - \frac{52}{63} \frac{\tau_{ya}\gamma_{fa}}{\tau_{ym}\gamma_{fm}} - \left(1 - \frac{\tau_{ya}\gamma_{fa}}{\tau_{ym}\gamma_{fm}}\right) A \right\} \tag{9}$$

$$, A = \left[\frac{32}{21} Q \left(\frac{1}{3} + \frac{\bar{a}^4}{5} \right) + \frac{\bar{a}^2}{315} \left(4S - 32\bar{a}^4 Z + 128\bar{a}^6 M \right) \right]$$

$$I_{SB} = \frac{1}{2\pi} \left(p H_{vM}^2 + k \mu H_h H_{vM} + j \mu^2 H_h^2 \right) \tag{10}$$

$$\bar{a} = \frac{a}{r_0} \qquad Q = \sqrt{\bar{a}^2 - 1} \qquad M = \bar{a} - Q \qquad S = 105\,\bar{a} - 88Q \qquad Z = 9\,\bar{a} - 7Q \tag{11}$$

where τ_{ym} and τ_{ya} are the shear yielding stress of the matrix and of the interphase, γ_{fm} and γ_{fa} the shear fracture strains, parameters p,k,j are functions of the Poisson's ratio [19], $H_h=1/C_h$ and H_{vM} is the deviatoric component of the global stress concentration tensor which can be evaluated either numerically or analytically [19, 21].

It is evident that in order to apply Eq. (3) the properties and size of the interphase need to be determined. As discussed in [17], the elastic properties and the thickness of the interphase can be computed by means of Molecular Dynamics (MD) analyses [22,23], or, alternatively determined a posteriori by fitting the experimental values for the elastic properties of the nanocomposite by a multi-phase micromechanical model.

In this paper the last mentioned approach has been adopted, and the two-step analytical model based on the Hashin-Shtrikman solution developed by the authors [24] has been used – more information about this model are reported in chapter 6. In Ref. [24] the three-phase nanocomposite material showed in Figure 8 has been considered, and each particle and the surrounding interphase have been changed for an "Equivalent Homogeneous Particle (EHP)" of total radius $a=r_0+t$ with bulk and shear elastic moduli, K' and G', given by:

$$K' = K_a \left\{ 1 + \frac{\left(\frac{r_0}{a} \right)^3 \left(\frac{K_p}{K_a} - 1 \right)}{1 + \left[1 - \left(\frac{r_0}{a} \right)^3 \right] \frac{1+\nu_a}{3(1-\nu_a)} \left(\frac{K_p}{K_a} - 1 \right)} \right\} \tag{12}$$

$$G' = G_a \left\{ 1 + \frac{\left(\frac{r_0}{a} \right)^3 \left(\frac{G_p}{G_a} - 1 \right)}{1 + \left[1 - \left(\frac{r_0}{a} \right)^3 \right] \frac{8-10\nu_a}{15(1-\nu_a)} \left(\frac{G_p}{G_a} - 1 \right)} \right\} \tag{13}$$

where $(r_0/a)^3$ is the volume fraction of the nanoparticle within the EHP. As a second step, the elastic properties of the nanocomposite, K_o and G_o, can be assessed as:

$$K_o = K_m \left\{ 1 + \frac{f_{p0}\left(\frac{a}{r_0}\right)^3 \left(\frac{K'}{K_m} - 1\right)}{1 + \left[1 - f_{p0}\left(\frac{a}{r_0}\right)^3\right] \frac{1+\nu_m}{3(1-\nu_m)} \left(\frac{K'}{K_m} - 1\right)} \right\} \tag{14}$$

$$G_o = G_m \left\{ 1 + \frac{f_{p0}\left(\frac{a}{r_0}\right)^3 \left(\frac{G'}{G_m} - 1\right)}{1 + \left[1 - f_{p0}\left(\frac{a}{r_0}\right)^3\right] \frac{8-10\nu_m}{15(1-\nu_m)} \left(\frac{G'}{G_m} - 1\right)} \right\} \tag{15}$$

where $f_{p0}(a/r_0)^3$ is the volume fraction of the *EHPs* [23]. Finally the modulus of elasticity in tension of the nanocomposite is $E_o = 9K_oG_o/(3K_o + G_o)$. Using Eqs. (12-15) in combination with the experimental data for the elastic modulus given in Section 3, the resulting best fitting values have been found to be χ=1.3 and t=4 nm, respectively (see Figure 10). For the sake of simplicity, instead, the plastic properties of the interphase zone have been supposed to equate those of the matrix according to [17].

Moreover, the following properties have been used into Eqs. (5,6,9): σ_{ym} = 88MPa, σ_{ycm} = 120MPa, $\gamma_{fm} = \gamma_{fa}$ = 0.75, μ = 0.2, as taken from Ref. [5] where a similar epoxy resin was analysed.

Figures 11 and 12 show a comparison between the fracture toughness predicted by Eq. (3) and experimental results. It is evident that the agreement is extremely satisfactory for PC specimens which exhibit a monotonic amelioration of the fracture toughness (Figure 11). For NPC specimens the agreement is satisfactory up to the maximum value of the normalised fracture toughness (Figure 12).

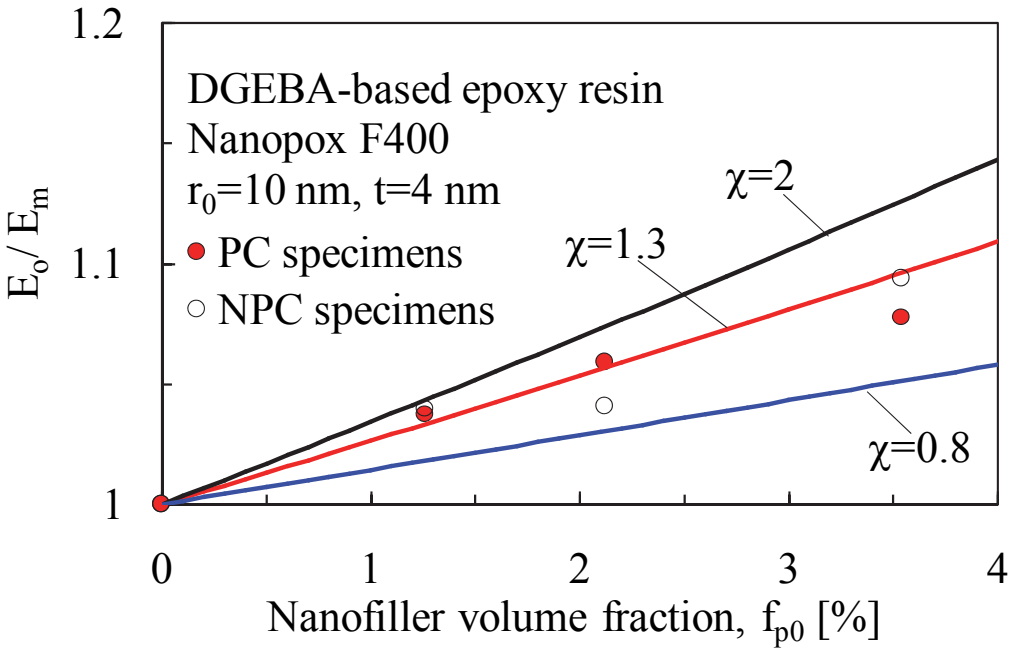

Figure 10. Estimation of the interphase thickness and elastic properties by best fitting of experimental data through Eqs. (12-15).

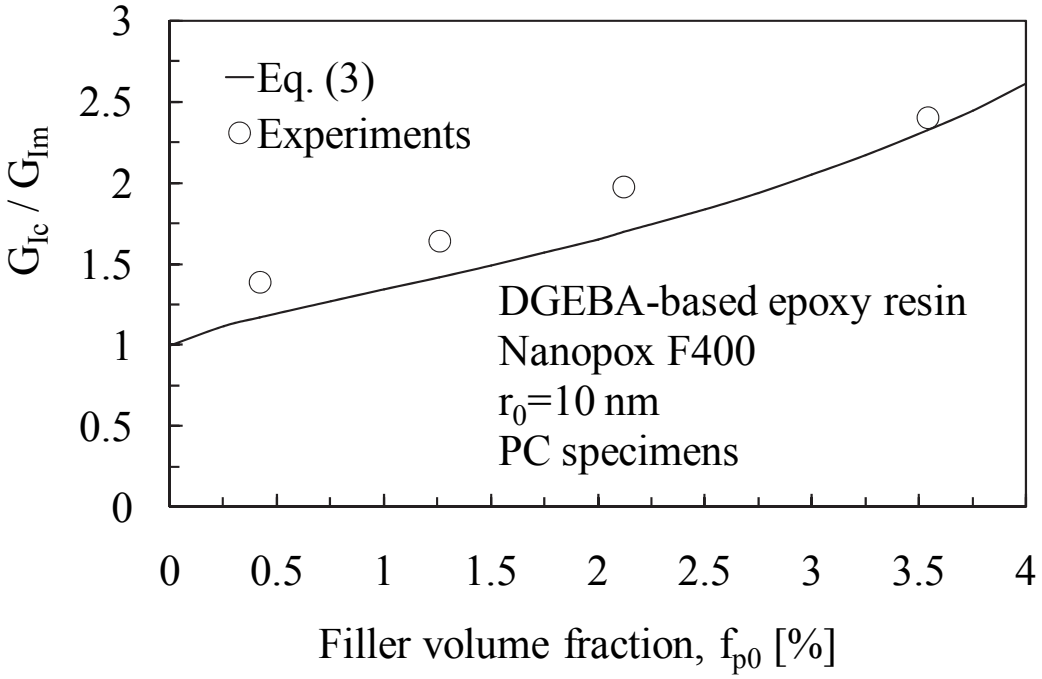

Figure 11. Comparison between Eq. (3) (solid line) and the experimental data from PC CT specimens.

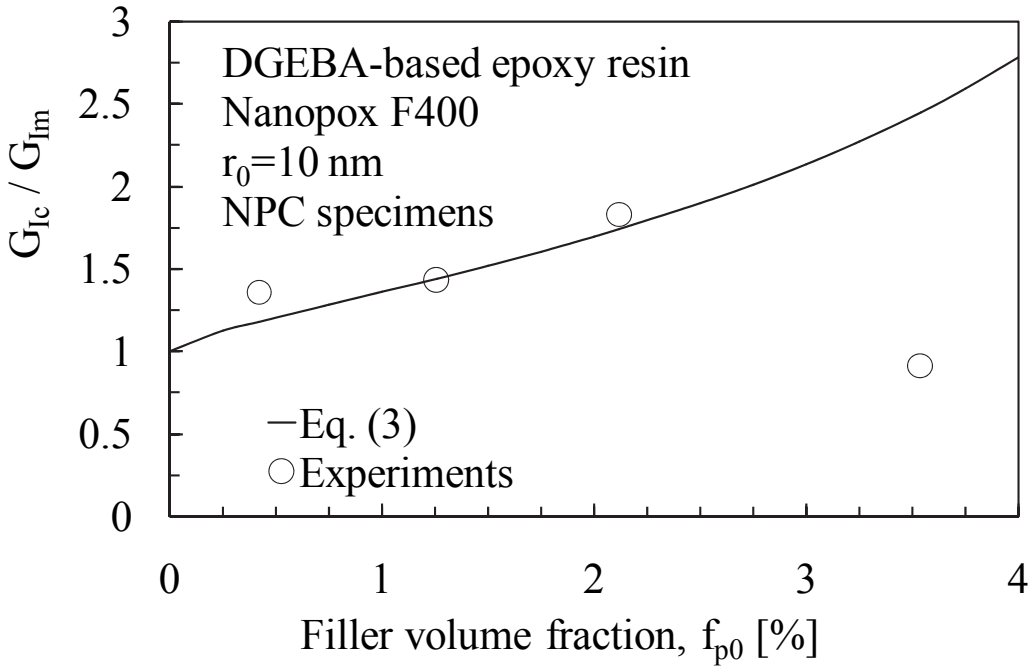

Figure 12. Comparison between Eq. (3) (solid line) and the experimental data from NPC CT specimens.

6. CONCLUSION

In the present paper the mechanical behaviour of an epoxy/silica nanocomposite system has been analysed, taking advantage of the results from tension and fracture tests carried out on DB, DENT and CT specimens made of DGEBA epoxy resin and Nanopox F400. Moreover a study on the effect of curing on the mechanical properties of nanocomposites has been carried out, considering two different processes:

A. Curing at room temperature for 72 hours (NPC specimens).
B. Curing at room temperature for 72 hours and post-curing in an oven at 60°C for 15 hours (PC specimens).

The results indicate that the curing process can alter the mechanical behaviour of silica/epoxy nanocomposites, PC and NPC specimens being characterised by different properties. In particular, even if all nanomodified specimens exhibit a fracture toughness higher than that of the pure resins, the highest value of K_{Ic} was obtained with 8%wt loaded post-cured samples. Moreover, PC specimens exhibited a monotonic amelioration of K_{Ic}, whereas NPC specimens are characterized by an initial improvement of the fracture toughness for low contents, followed by a reversed trend for weight fractions higher than 5%.

The curing cycle highly affects the nanocomposite tensile strength as well. While indeed for NPC specimens nanomodification is found to have a detrimental effect on σ_R, post-cured DB samples, as well as DENT specimens, were found to be characterised by a strength comparable or slightly higher than that of the neat resin.

Eventually, the mode I fracture toughness evaluated from CT tests has been compared to the theoretical predictions based on a multiscale and multimechanism model recently developed by the present authors, showing a satisfactory agreement.

ACKNOWLEDGEMENTS

The authors acknowledge the financial support to the activity by Veneto Nanotech, the Italian cluster of Nanotechnology, by CARIVERONA Foundation, (within the frame "Contributo di Fondazione Cariverona a valere sui finanziamenti alla ricerca scientifica e tecnologica per l'anno 2012") and by the CARIPARO foundation.

The authors would like also to thank Dr. Stephan Sprenger (Evonik) for kindly providing the Nanopox F400 used in the experimental analyses.

REFERENCES

[1] Chen, C., Justice, R. S., Schaefer, D. W., & Baur, J. W. (2008). Highly dispersed nanosilica–epoxy resins with enhanced mechanical properties.Polymer, 49(17), 3805-3815.

[2] Ma, J., Mo, M. S., Du, X. S., Rosso, P., Friedrich, K., & Kuan, H. C. (2008). Effect of inorganic nanoparticles on mechanical property, fracture toughness and toughening mechanism of two epoxy systems. Polymer, 49(16), 3510-3523.

[3] Liang, Y. L., & Pearson, R. A. (2009). Toughening mechanisms in epoxy–silica nanocomposites (ESNs). Polymer, 50(20), 4895-4905.

[4] Dittanet, P., & Pearson, R. A. (2012). Effect of silica nanoparticle size on toughening mechanisms of filled epoxy. Polymer, 53(9), 1890-1905.

[5] Hsieh, T. H., Kinloch, A. J., Masania, K., Lee, J. S., Taylor, A. C., & Sprenger, S. (2010). The toughness of epoxy polymers and fibre composites modified with rubber microparticles and silica nanoparticles. Journal of materials science, 45(5), 1193-1210.

[6] Zamanian, M., Mortezaei, M., Salehnia, B., & Jam, J. E. (2013). Fracture toughness of epoxy polymer modified with nanosilica particles: Particle size effect. Engineering Fracture Mechanics, 97, 193-206.

[7] Liu, H. Y., Wang, G. T., Mai, Y. W., & Zeng, Y. (2011). On fracture toughness of nano-particle modified epoxy. Composites Part B: Engineering, 42(8), 2170-2175.

[8] Chen, C. H., Jian, J. Y., & Yen, F. S. (2009). Preparation and characterization of epoxy/γ-aluminum oxide nanocomposites. Composites Part A: Applied Science and Manufacturing, 40(4), 463-468.

[9] ASTM D 5045. Standard Test Methods for Plane-Strain Fracture Toughness and Strain Energy Release Rate of Plastic Materials (1999).

[10] ISO 527-2. Plastics-Determination of tensile properties (2012).

[11] Peterson, R. E., & Plunkett, R. (1975). Stress concentration factors. Journal of Applied Mechanics, 42, 248.

[12] Tcherbi-Narteh, A., Hosur, M., Triggs, E., Owuor, P., & Jelaani, S. (2014). Viscoelastic and thermal properties of full and partially cured DGEBA epoxy resin composites modified with montmorillonite nanoclay exposed to UV radiation. Polymer Degradation and Stability, 101, 81-91.

[13] Zappalorto, M., Salviato, M., Pontefisso, A., & Quaresimin, M. (2013). Notch effect in clay-modified epoxy: a new perspective on nanocomposite properties.Composite Interfaces, 20(6), 405-419.

[14] Ci, L., & Bai, J. (2006). The reinforcement role of carbon nanotubes in epoxy composites with different matrix stiffness. Composites Science and Technology, 66(3), 599-603.

[15] de Villoria, R. G., Miravete, A., Cuartero, J., Chiminelli, A., & Tolosana, N. (2006). Mechanical properties of SWNT/epoxy composites using two different curing cycles. Composites Part B: Engineering, 37(4), 273-277.

[16] Montazeri, A., Khavandi, A., Javadpour, J., & Tcharkhtchi, A. (2010). The effect of curing cycle on the mechanical properties of MWNT/Epoxy nanocomposite. International Journal of Polymer Analysis and Characterization, 15(3), 182-190.

[17] Quaresimin, M., Salviato, M., & Zappalorto, M. (2014). A multi-scale and multi-mechanism approach for the fracture toughness assessment of polymer nanocomposites. Composites Science and Technology, 91, 16-21.

[18] Zappalorto, M., Salviato, M., & Quaresimin, M. (2012). A multiscale model to describe nanocomposite fracture toughness enhancement by the plastic yielding of nanovoids. Composites Science and Technology, 72(14), 1683-1691.

[19] Salviato, M., Zappalorto, M., & Quaresimin, M. (2013). Plastic shear bands and fracture toughness improvements of nanoparticle filled polymers: a multiscale analytical model. Composites Part A: Applied Science and Manufacturing, 48, 144-152.

[20] Zappalorto, M., Salviato, M., & Quaresimin, M. (2011). Influence of the interphase zone on the nanoparticle debonding stress. Composites Science and Technology, 72(1), 49-55.

[21] Zappalorto, M., Salviato, M., & Quaresimin, M. (2012). Stress distributions around rigid nanoparticles. International Journal of Fracture, 176(1), 105-112.

[22] Odegard, G. M., Clancy, T. C., & Gates, T. S. (2005). Modeling of the mechanical properties of nanoparticle/polymer composites. Polymer, 46(2), 553-562.

[23] Yu, S., Yang, S., & Cho, M. (2009). Multi-scale modeling of cross-linked epoxy nanocomposites. Polymer, 50(3), 945-952.

[24] Pontefisso, A., Zappalorto, M., & Quaresimin, M. (2013). Influence of interphase and filler distribution on the elastic properties of nanoparticle filled polymers. Mechanics Research Communications, 52, 92-94.

[25] Hashin, Z., & Shtrikman, S. (1963). A variational approach to the theory of the elastic behaviour of multiphase materials. Journal of the Mechanics and Physics of Solids, 11(2), 127-140.

2 The effect of the testing temperature on the fracture toughness in a nanosilica modified epoxy resin

KEYWORDS: A. Temperature; B. Fracture toughness; C. Processing parameters; D. Epoxy resin; E. Nanocomposites;

ABSTRACT

In this chapter the fracture toughness of an epoxy system is evaluated at different testing temperatures. In particular neat and nanosilica reinforced epoxy resins have been manufactured, with and without post-curing, and compact tension specimens have been prepared and tested. The results show the importance of the post-curing treatment of the epoxy resin on its fracture toughness, and suggest the capability of nanoparticles to smooth the variation of this mechanical property due to the different testing temperature.

1. INTRODUCTION

The employment of nanoreinforcements to enhance the mechanical properties of polymers is a growing research field, fuelled by new discoveries and outstanding results. Focussing on epoxies, many authors reported significant increases of the elastic modulus, strength and fracture toughness [1-4] through the addition of few point percent in weight of nanoreinforcements in the polymer matrix.

However one parameter is often disregarded in these analyses: the testing temperature. From one side this, is due to the need of expensive equipment to enable testing temperature control, from the other, this parameter does not seem so important when dealing with the effects of nanomodification relative to the neat matrix. In truth, many authors highlighted a significant influence of this parameter on the fracture toughness of neat and nanomodified epoxy resins [5-8].

In 1971 Lange and Radford [5] analysed the fracture energy of a DGEBA reinforced with alumina microparticles at room temperature and at about -200°C. They measured an increase of about 2 times of the elastic modulus and G_{Ic} at low temperature with respect to room temperature, for the neat epoxy.

Kim et al. [6] studied the properties of epoxy resins at low temperature, as well. In particular they used a modified bisphenol-A epoxy adhesive nanoreinforced with carbon

black and montmorillonite clay, performing tests from -150°C up to room temperature. Their results for the neat resin agree with those of Lange and Radford, showing a substantial increase of K_{Ic} at lower temperatures as well as an increase of the elastic modulus and strength. Considering the effects of nanomodification, they showed that nanoreinforcements reduce the fracture toughness at low temperature, while they enhance the same property at room temperature. Studying SEM images they concluded that at low temperatures the intermolecular forces within the epoxy polymer networks are more dominant than the nanoreinforcement toughening effect. As a consequence they highlighted the need of considering the working temperature when deciding if nanoparticles are to be used for a particular application.

Zhang et al. [7] considered the effect of nanomodification of an epoxy resin at room temperature and at 80°C. In particular they employed a DGEBF resin reinforced with nanosilica and performed DMTA, DSC and CT fracture tests. They reported a reduction of the elastic and strength properties at 80°C with respect to room temperature, regardless of the filler fraction. Considering the fracture toughness, the neat epoxy showed a reduction at higher temperature, but nanomodification managed to transform this reduction in an increase proportionately to the amount of nanofiller. They reported an unstable stick-slick crack propagation at both test temperatures and, considering the connection between this phenomenon and the crack tip blunting, they concluded that high temperatures and low strain rates should favourite this ductile failure mechanism. Taking into account the nanomodification, they reported an increase of this phenomenon, which implies an increase of crack tip deformations due to nanoparticles.

Han and Cho [8] studied the fracture toughness of reinforced epoxy composites from room temperature up to 175°C, considering a byphenil epoxy resin reinforced with silica micro and nano particles. They derived the strain energy release rates from the elastic properties evaluated by means of DMA tests and the data from testing SENB specimens. Considering only the neat and nanomodified epoxies, they reported an increase in the fracture toughness, G_{Ic}, for both cases up to a certain temperature, followed by a drastic reduction. They attributed this increase to an improved molecular mobility of the polymer chains, followed by the yielding of the epoxy resin. Moreover they highlighted how, at room temperature, the addition of nanosilica resulted in an increase of the G_{Ic}, while at higher temperatures it reduced the peak of G_{Ic} improvement shown by the neat epoxy.

In the present chapter the results of fracture tests performed on a nanosilica modified epoxy resin are reported. Three testing temperatures are considered (-20°C, 20°C and

40°C) for testing CT specimens of unreinforced and reinforced epoxy resin. Weight fraction of 1%, 3% and 5% have been used. Post-curing in oven is performed on half of the specimens to test the effect of this treatment. The results suggest the capability of nanoparticles to smooth the variation of fracture toughness due to the different testing temperature, but more analyses will be required to support this thesis.

2. MATERIALS AND SPECIMENS EMPLOYED IN THE EXPERIMENTAL ANALYSIS

In this analysis, a DGEBA-based epoxy resin from ELANTAS ITALIA is employed (EC157 with W152LR hardener). The main mechanical properties of the epoxy system, as reported in the datasheet from the supplier, are summarized in Table 1.

E [GPa]	σ_R [MPa]	ε_R [%]	μ [mPas]
3.2 – 3.6	67 – 75	6.0 – 8.0	150 – 250

Table 1. Properties of the neat epoxy resin (EC157+W152LR): E, elastic modulus, σ_r, ultimate tensile strength, ε_r, fracture strain, and μ, viscosity at 25°C.

In addition, a masterbatch of 40%wt of silica nanoparticles in a DGEBA-based epoxy resin from EVONIK is used (Nanopox F400). This masterbatch is diluted in EC157 at different weight fractions and a part of W152LR is used to balance the equivalent epoxy weight of the masterbatch. The silica nanoparticles have an average diameter of about 20nm and a maximum diameter of 50nm, as from the datasheet.

Compact Tension (CT) specimens have been manufactured according to the following steps:

1. *Preparation of the resin*. The masterbatch is heated for 15 minutes in an oven, at 60°C. This is performed in order to reduce its viscosity (which is about 60,000mPas at 25°C) as suggested by the supplier.
2. *Mixing of the composite components*. The masterbatch is added to the resin and they are mixed by means of shear mixing. The shear mixing is carried out with a DISPERMAT TU shear blender from VMA-Getzmann (Figure 1a), at about 3500rpm for 5 minutes. Then, the blend is sonicated using a HIELSCHER UP 200S sonicator (Figure 1b), set at amplitude 1 and duty cycle 1, for 10 minutes, in order to improve particle dispersion. After the sonication, an intermediate degassing has been performed at 60°C, to remove as much air trapped within the

resin as possible, before the addition of the hardener. Finally, the hardener is added and a further shear mixing at 300rpm for 5 minutes is performed.

3. *Degassing and moulding of the blend*. In order to the remove the air trapped within the blend as a consequence of the shear mixing, degassing is carried out. To this end a low vacuum pump is employed to reach a relative pressure of -1bar and, at the same time, mechanical shaking of the blend is performed. After 30 minutes the composite is poured in silicone moulds.
4. *Post-curing of the specimens*. After a curing at room temperature for 3 days, a set of specimens is post-cured in an oven at 60°C for 2h, and then at 90°C for 15h.
5. *Finishing of the specimens*. Finally, the specimens are lapped and cracks are generated tapping on a razor blade placed in the notch.

CT specimens are moulded at nanoparticle weight fractions of: 0%, 1%, 3% and 5%. To analyse the effects of post-curing, along with the specimens Post-Cured according to point 4 above (from hereafter "PC"), specimens cured at Room Temperature for about one and a half month have been tested (from hereafter "RT").

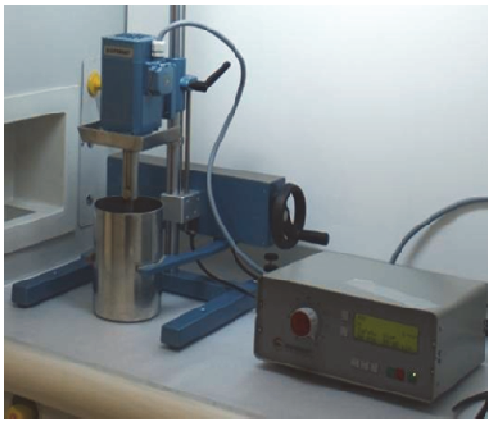

(a)

(b)

Figure 1. (a) Mixer used to carry out the shear mixing. (b) Sonicator.

3. EXPERIMENTAL TESTING AND RESULTS

Fracture tests have been carried out on CT specimens on a servo-hydraulic machine equipped with a 2.5kN load cell, according to the ASTM D5045-99 suggestions. Tests have been performed at 10mm/min at -20°C, 20°C and 40°C by means of a dedicated temperature control equipment. Specimen temperature has been controlled by means of a

thermocouple inserted in a hole drilled on the specimens (see Figure 2) and each specimen has been kept at testing temperature for 2 minutes before performing the test. Pre-cracking of the specimens has been performed tapping a razor blade in the notches and 4 values for each material have been obtained.

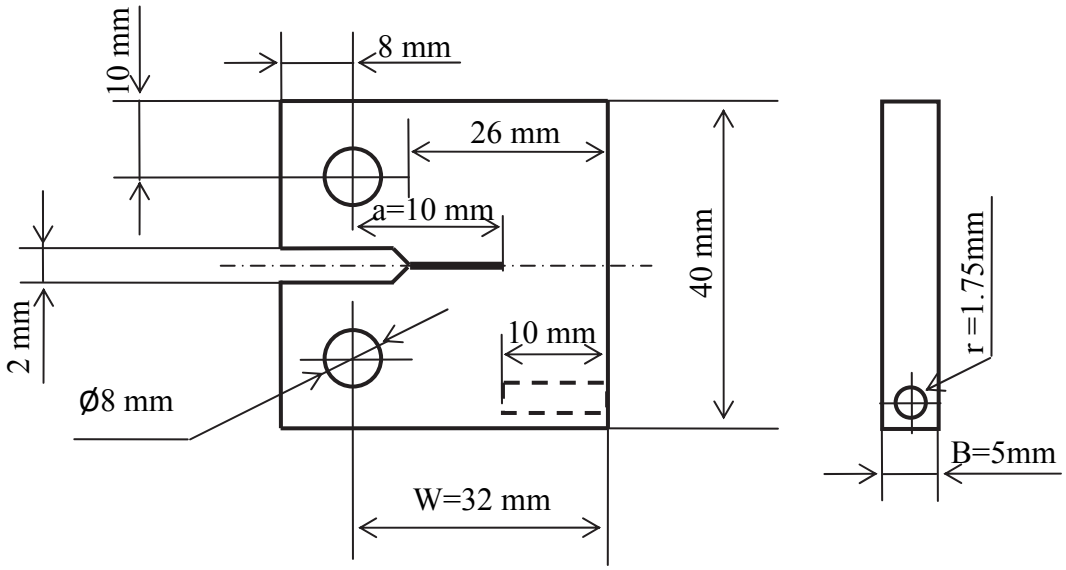

Figure 2. Geometries of the specimens used in testing neat and nanomodified resin.

Mode I fracture toughness can be computed from the following expression [9]:

$$K_{Ic} = \frac{P_{cr}}{B\,W^{0.5}}\, f\left(\frac{a}{W}\right) \tag{1}$$

where P_{cr} is the critical load while B, a and W are defined in Figure 2. The suggested expression for f(a/W) is:

$$f\left(\frac{a}{W}\right) = \frac{\left(2+\frac{a}{W}\right)\left[0.886 + 4.64\frac{a}{W} - 13.32\left(\frac{a}{W}\right)^2 + 14.72\left(\frac{a}{W}\right)^3 - 5.6\left(\frac{a}{W}\right)^4\right]}{\left(1-\frac{a}{W}\right)^{1.5}} \tag{2}$$

with $0.2 < \frac{a}{W} < 0.8$.

The experimental results in term of K_{Ic} have been computed applying Eq.(2) and have been reported in Figure 3 and 4. In Figure 5 a comparison among representative force-displacement curves obtained testing CT specimens is reported. While the curve peak value depends on the crack length and specimen width, the shape is a function of the failure mechanisms which take place.

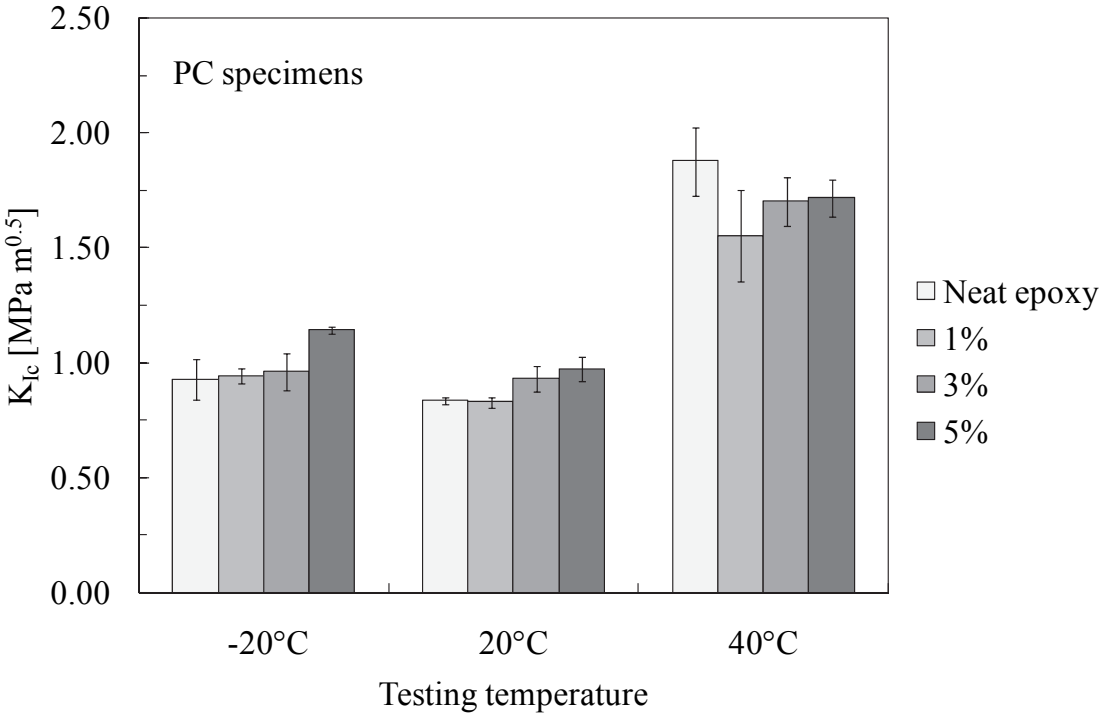

Figure 3. Composite fracture toughness as a function of the testing temperature and filler weight fraction in case of PC specimens.

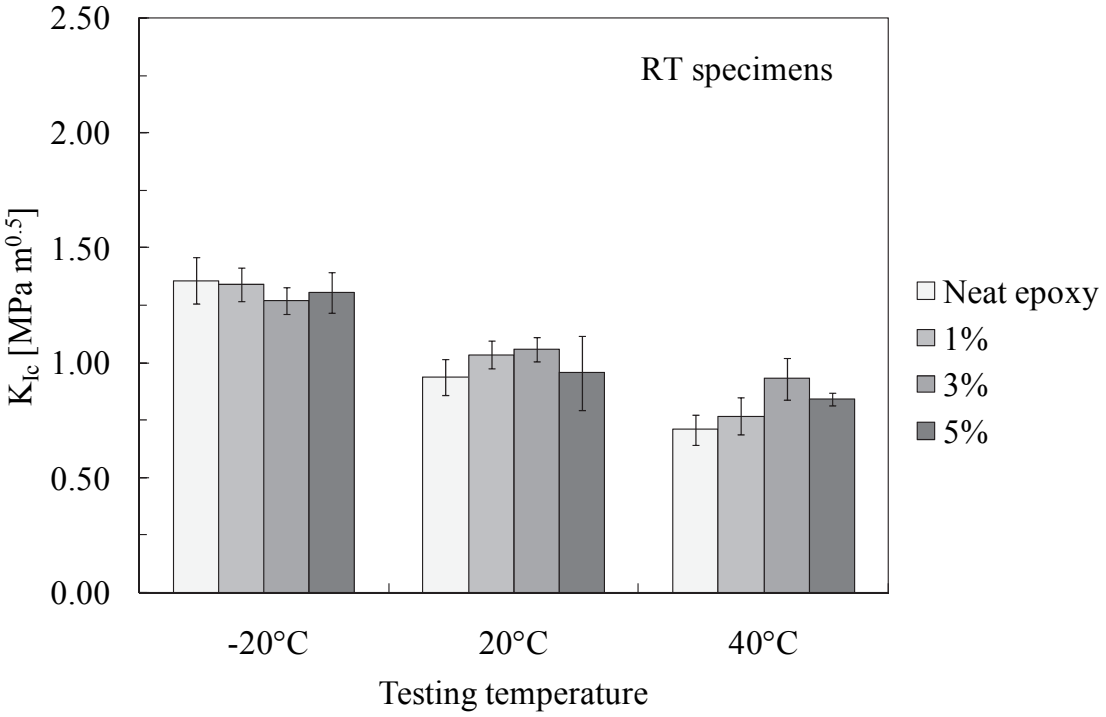

Figure 4. Composite fracture toughness as a function of the testing temperature and filler weight fraction in case of RT specimens.

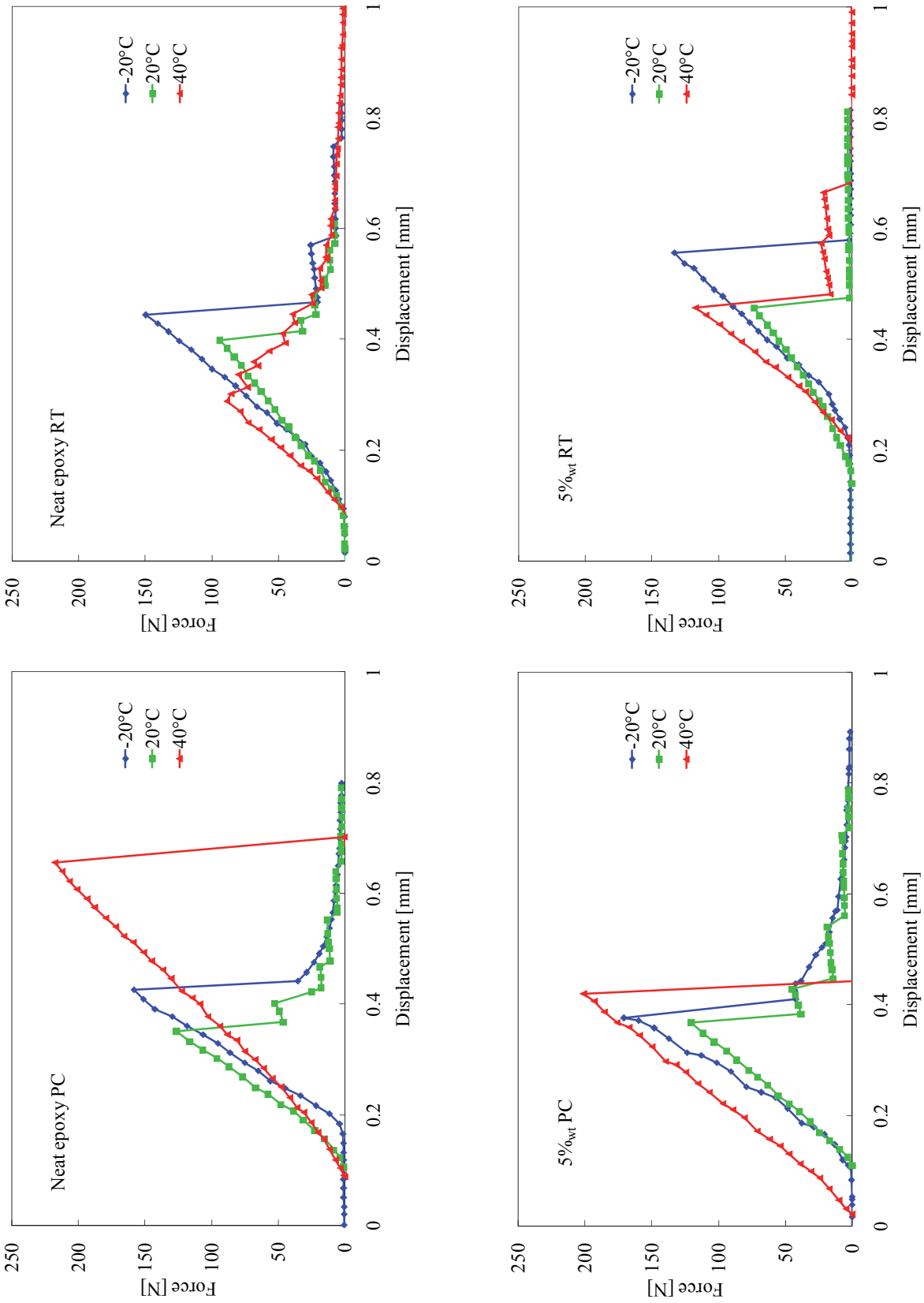

Figure 5. Typical force-displacement curves from CT tests in case of neat epoxy and 5%wt reinforced epoxy, both PC and RT.Only the shape of the curve is to be considered, the peak value depends on the specimen geometry.

4. RESULTS AND DISCUSSION

4.1 General trend of the fracture toughness of epoxy resins

The results highlight that the nanomodification induces only a marginal effect on the overall fracture toughness, being the property of the neat epoxy the dominant term. Therefore in order to interpret the results of the experimental tests, it is necessary to understand the general trend of the fracture toughness of the neat epoxy resin as a function of the temperature. To this end the papers reported in the introduction [5-8] allow to plot a qualitative graph of this property from cryogenic to high temperatures, as reported in Figure 6. It is possible to identify 3 zones: a low temperature zone, a room temperature zone and a high temperature zone:

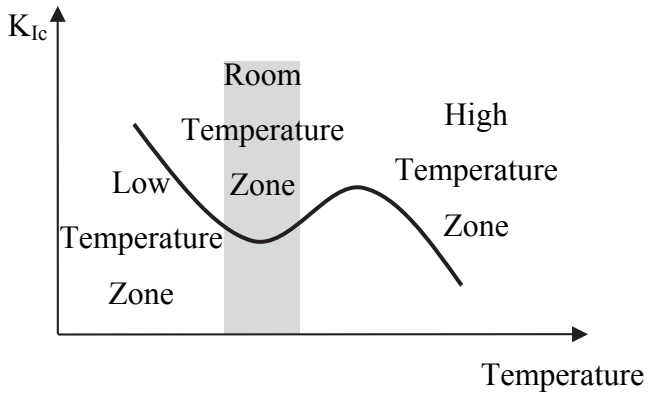

Figure 6. General trend of the fracture toughness in epoxy resins as a function of the temperature.

1. In the Low Temperature Zone (LTZ) the fracture toughness of the epoxy resin is inversely proportional to the temperature. According to the literature, in this zone the intermolecular forces among polymer networks are the dominant term which influences the fracture toughness.
2. In the Room Temperature Zone (RTZ) the fracture toughness of the epoxy resin is quite constant. The failure mechanisms which take place in this zone have been widely studied by several authors [10-12]. This zone is the easiest to analyse, because it does not require temperature control equipment, and at the same time it is the most important, because the majority of the applications works in this condition.
3. In the High Temperature Zone (HTZ) epoxy resins exhibit a toughening followed by a steep decrease of the fracture toughness. The toughening seems related to an

enhanced plasticity, which is a consequence of the higher mobility of the polymer chains. However, too high temperatures affect negatively the fracture toughness.

4.2 Effect of the curing treatment on the neat epoxy

Considering the experimental results, the different curing of the neat epoxy generates significant differences in the resin behaviour:

1. PC specimens exhibit the same K_{Ic} at -20°C and at 20°C, followed by an increase of about 100% at 40°C, regardless of nanomodification. Considering Figure 5, general trends for -20°C and 20°C are similar, with stepped crack propagation (in particular at 20°C stick-slip crack propagation is developed). Differently, at 40°C, the material loses its crack-arrest capability but earns an increase in K_{Ic} thanks to an enhanced elongation at failure.
2. RT specimens exhibit a well different behaviour: at -20°C K_{Ic} is at maximum, with a progressive decrease while the temperature rises. Again in the neat epoxy at -20°C and at 20°C stick-slip crack propagations are developed, but at 40°C the curve is significantly different: the material shows a reduction in the linear elastic elongation followed by yielding.

These differences between RT and PC specimens could be explained considering the effect of the curing on the epoxy resin. Post-curing results in a double effect: it reduces the amount of un-reticulated resin and, at the same time, it allows the polymer chains to move and reach a lower entropic state.

It seems reasonable that at -20°C the behaviour of PC and RT specimens is different: RT specimens are "more glassy", because the polymer chains have not had the possibility to set and, therefore, they have a reduced mobility compared to that of PC specimens. It seems likely that PC specimens need a far lower temperature to reach the same state of RT specimens and, as a consequence, PC specimens at -20°C belong to the RTZ, while RT specimens at -20°C belong to the LTZ.

At the same time, at 40°C the differences in behaviour between PC and RT specimens could be explained in this way: RT specimens have a greater amount of un-reticulated epoxy groups, therefore higher temperatures allows a greater plastic flow with respect to PC specimens. However this plastic flow is paid with a reduced amount of cross-links in the polymer and this affects significantly the resin: while PC specimens are able to gain advantages by this plastic flow, RT specimens are not. Therefore PC specimens at 40°C

belong to the first part of the HTZ of Figure 6, while RT specimens do not develop the enhancement in fracture toughness and belong to the HTZ at higher temperatures.

4.3 Effect of the nanomodification

In the following section, the effect of the nanomodification is considered separately for LTZ, RTZ, HTZ and considers the results reported in Figures 3, 4 and 5:

1. *LTZ*. According to [6] nanomodification at very low testing temperature should reduce the fracture toughness of the epoxy, but it should also be considered that in the analysis carried out the testing temperature is relative high (-20°C) compared to the cryogenic one. Following the assumption that only RT specimens at -20°C belong to this zone (as explained in section 4.2) the effects of nanomodification seem lost: the fracture toughness is not affected by the addition of nanoreinforcements.
2. *RTZ*. In this zone the nanomodification of the epoxy resin improves the fracture toughness in accordance with behaviours widely reported in the literature [10-12] and in the previous chapter. The general trend consists in an improvement proportional to the amount of nanoreinforcement, with a stick-slip crack propagation. RT 5%wt reinforced specimens show a decrease in the fracture toughness, with respect to the other filler weight fractions; this trend agrees with the observations reported in the literature [13] and in the previous chapter and may be due to clustering of reinforcements and lower reticulation.
3. *HTZ*. In this zone the effect of nanomodification differs for PC and RT specimens. In the former ones it shows a reduction in fracture toughness with respect to neat epoxy resin, but the specimens exhibit the same fracture behaviour in Figure 5. In the latter ones nanomodification improves the resin fracture toughness, modifying the fracture behaviour: differently from the evident plasticity in the case of neat-epoxy, $5\%_{wt}$ RT specimens show stick-slip crack propagation, which is more similar to the behaviour in the RTZ and shows a similar value for K_{Ic}. The effects of nanomodification in the HTZ agree with those reported in [8], but for PC specimens differ from those in [7], where nanomodification enhances the nanocomposite fracture toughness.

Trying to infer a general trend, considering also the results reported in [6] and [8], it seems that nanomodification smoothes the variations of K_{Ic} in case of different testing temperatures. Moreover the RTZ is the zone with the lower value of K_{Ic} (not considering

higher temperatures in the HTZ, where the resin loses its structural properties) and in that zone nanomodification improves the polymer fracture toughness. From these considerations it is possible to plot the graph reported in Figure 7.

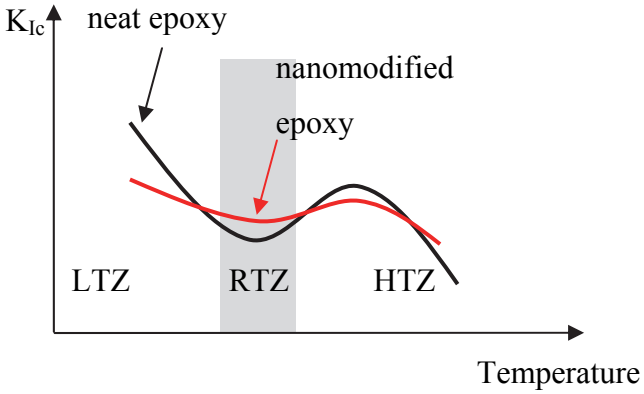

Figure 7. General trend of the fracture toughness in nanomodified epoxy resins as a function of the temperature.

A final remark on the differences between the presented results and [7]: these differences could reasonably be ascribed to the differences in the chemical nature between the two nanocomposite systems. More data needs to be collected in this regard.

CONCLUSIONS

In this chapter the fracture toughness of an epoxy system has been evaluated at different testing temperatures, above and below room temperature. In particular neat and nanosilica reinforced epoxy resins have been manufactured, with and without post-curing, and compact tension specimens have been prepared and tested. The results highlight a competitive effect of the nanomodification on K_{Ic} when compared to the effect of the testing temperature. Moreover the results show the importance of the epoxy resin post-curing treatment on its fracture toughness, and suggest the capability of silica nanoparticles to smooth the variation of this mechanical property due to the different testing temperature. However the latter observation needs more evidences supporting it.

ACKNOWLEDGEMENTS
The authors would like to thank Dr. Stephan Sprenger (Evonik) for kindly providing the Nanopox F400 used in the experimental analyses.

REFERENCES

[1] Chen, C., Justice, R. S., Schaefer, D. W., & Baur, J. W. (2008). Highly dispersed nanosilica–epoxy resins with enhanced mechanical properties.Polymer, 49(17), 3805-3815.

[2] Ma, J., Mo, M. S., Du, X. S., Rosso, P., Friedrich, K., & Kuan, H. C. (2008). Effect of inorganic nanoparticles on mechanical property, fracture toughness and toughening mechanism of two epoxy systems. Polymer, 49(16), 3510-3523.

[3] Carballeira, P., & Haupert, F. (2010). Toughening effects of titanium dioxide nanoparticles on TiO2/epoxy resin nanocomposites. Polymer Composites,31(7), 1241-1246.

[4] Liu, W., Hoa, S. V., & Pugh, M. (2005). Organoclay-modified high performance epoxy nanocomposites. Composites Science and Technology, 65(2), 307-316.

[5] Lange, F. F., & Radford, K. C. (1971). Fracture energy of an epoxy composite system. Journal of Materials Science, 6(9), 1197-1203.

[6] Kim, B. C., Park, S. W., & Lee, D. G. (2008). Fracture toughness of the nano-particle reinforced epoxy composite. Composite Structures, 86(1), 69-77.

[7] Zhang, H., Tang, L. C., Zhang, Z., Friedrich, K., & Sprenger, S. (2008). Fracture behaviours of in situ silica nanoparticle-filled epoxy at different temperatures. Polymer, 49(17), 3816-3825.

[8] Han, J. T., & Cho, K. (2006). Nanoparticle-induced enhancement in fracture toughness of highly loaded epoxy composites over a wide temperature range.Journal of materials science, 41(13), 4239-4245.

[9] ASTM D 5045. Standard Test Methods for Plane-Strain Fracture Toughness and Strain Energy Release Rate of Plastic Materials (1999).

[10] Zappalorto, M., Salviato, M., & Quaresimin, M. (2012). A multiscale model to describe nanocomposite fracture toughness enhancement by the plastic yielding of nanovoids. Composites Science and Technology, 72(14), 1683-1691.

[11] Dittanet, P., & Pearson, R. A. (2012). Effect of silica nanoparticle size on toughening mechanisms of filled epoxy. Polymer, 53(9), 1890-1905.

[12] Hsieh, T. H., Kinloch, A. J., Masania, K., Lee, J. S., Taylor, A. C., & Sprenger, S. (2010). The toughness of epoxy polymers and fibre composites modified with rubber microparticles and silica nanoparticles. Journal of materials science, 45(5), 1193-1210.

[13] Wang, K., Chen, L., Wu, J., Toh, M. L., He, C., & Yee, A. F. (2005). Epoxy nanocomposites with highly exfoliated clay: mechanical properties and fracture mechanisms. Macromolecules, 38(3), 788-800.

3 Notch effect in clay-modified epoxy: a new perspective on nanocomposite properties

KEYWORDS: A. Nanocomposites; B. Nanoclay; C. Notch effect; D. Mixed Mode;

ABSTRACT

In this chapter an experimental investigation of the notch effect on clay-modified epoxy resins is carried out, discussing the results from Single Edge Notch Bending (SENB) tests and Double Edge Notch Tension (DENT) tests on notched components.
It is found that when the notch root radius is greater than a limit value, which depends on the clay content, the brittle failure of notched nanomodified specimens is controlled by the material strength. Under this circumstances nanomodification, while enhancing the polymer fracture toughness, might have a detrimental effect on the strength of notched components. This study brings to light a new feature of nanomodification according to which particular care should be used when using nanomodified resins for structural applications in the presence of notches or holes.

1. INTRODUCTION

Nanocomposites are new multifunctional materials endowed with exceptionally improved mechanical and physical properties at very low filler concentrations [1-3]. This behaviour, often regarded as the "nano-effect", is acknowledged to be due to the molecular structure of the material. Indeed, in the presence of nanofiller reinforced polymers the specific surface is extremely large, and this makes surface properties the dominant factor, providing unique properties with widespread applications in many industrial sectors.

Moreover, as the reinforcement size is comparable with that of polymeric chains, molecular interactions with the matrix produce an interphase "layer" with properties potentially different from those of the constituents. In the recent literature it has been demonstrated that the properties of the interphase might significantly affect the overall mechanical properties of the nanocomposite, depending also on the filler size and geometry [4-7].

Nanoclays are layered silicates of which the platelets are micro-sized in area, about 1 nm thick and disposed in stacks called tactoids. Once dispersed in the polymeric matrix three typical nanoclay morphologies are possible, namely, exfoliated, intercalated and phase separated.

Experimental results from the literature reveal that nanoclays are suitable to improve the tensile elastic modulus, the fracture toughness of polymeric systems [8-10] and the fatigue threshold [11-12], while conflicting results have been reported with reference to the strength of nanoclay reinforced resins, which has been proven either to increase [13–14] or to decrease [12,14–16], depending on the investigated system.

In the perspective to use nanomodified polymers as toughened matrixes in ternary, fiber reinforced, nanocomposites the fracture toughness is acknowledged to be the most important mechanical property to be improved [11, 12, 17-21]. This explains the great efforts dedicated by several researchers to study the fracture toughness of binary nanocomposites (polymer matrix plus nanofillers) [13, 22-25]. All the above mentioned works are referred to the pure mode I fracture toughness of nanofilled polymers. Only very recently, inspired by the argument that in practice the stress state ahead of a crack is often of the mixed type, the attention has been moved also onto the mixed mode fracture behaviour of cracked nanoclay/epoxy specimens [26] and nanotubes/epoxy specimens [27]. In particular Zappalorto et al. [26] found that nanomodified specimens exhibit a higher fracture toughness, independently of the loading mode, but ranging from pure mode I to pure mode II improvements are less pronounced.

Despite the fact that geometrical variations unavoidably exist in engineering components, in the best of the authors' knowledge the effects of notches on the mechanical behaviour of clay-modified epoxy resins have been completely ignored in the previous literature. With the aim to fill this gap, in this study the brittle notch fracture behavior of an epoxy resin filled with montmorillonite nanoclays is analysed. To this end, different kind of specimens have been manufactured and tested:

1. Double Edge Notch Tension (DENT) specimens with 4mm radius semicircular notches;
2. Single Edge Notch Bending (SENB) specimens with U-notches characterised by three different values for the notch root radius (0.5, 1 and 2mm).

The effect of nanoclay content on the strength of notched component is discussed in detail. In particular, for the material systems and geometries investigated in this work,

nanomodification is found to have a detrimental effect on the strength of notched components. This behaviour is due to the fact that for notch root radii greater than a limit value, which depends on the clay content, the brittle failure of notched nanomodified specimens is a strength- controlled phenomenon. In all these cases the disadvantageous role played by nanoclay addition on the strength of polymeric resins [12,14–16] is transferred to the notch effect on nanomodified specimens.

This important result makes it evident a new feature of nanocomposites: even if the fracture toughness of nanofilled polymers is generally higher with respect to that of the neat resin, particular care should be taken when using binary nanomodified resins for structural applications in the presence of notches or holes.

A summary of all the experimental results is eventually presented in terms of both the maximum principal stress at the notch edge and the generalised stress intensity factors.

2. MATERIALS AND SPECIMENS USED IN THE EXPERIMENTAL ANALYSIS

In this study, a DGEBA-based epoxy resin (EC157 with W152LR hardener) from ELANTAS-Camattini (Italy) is chosen as polymer matrix. The mechanical properties of the epoxy system, as specified by the supplier, are summarized in Table 1.

E [GPa]	σ_R [MPa]	ε_R [%]	μ [mPas]
3.2 – 3.6	67 – 75	6.0 – 8.0	150 – 250

Table 1. Properties of the neat epoxy resin (EC157+W152LR): E, elastic modulus, σ_r, ultimate tensile strength, ε_r, fracture strain, and μ, viscosity at 25°C.

In addition, a montmorillonite clay, Cloisite 30B® from Southern Clay Products, is used as nanosized reinforcement, considering different weight fractions. 30B nanoclays are characterised by 1 nm thick lamellae, lateral dimensions from 70 to 150 nm and average d-spacing of about 18,5 Å.

Different kind of specimens have been manufactured and tested:

1. Double Edge Notch Tension (DENT) specimens with 4 mm radius semicircular notches (Figure 1a);
2. Single Edge Notch Bending (SENB) specimens with U-notches. In this case the notch depth is equal to 10 mm and three different values for the notch root radius have been used: 0.5, 1 and 2 mm (Figure 1b).

In the best of authors' knowledge there is no standard available for fracture tests on notched components. Accordingly, as far as tests on SENB specimens are concerned, the same specimen size and geometry suggested for mode I fracture tests [29] have been used.

The specimens were manufactured according to the following steps:

1. *Dispersion of the filler within the resin*. Nanoclays were dispersed within the polymer resin through shear mixing followed by sonication. The shear mixing process was carried out with a DISPERMAT TU shear blender from VMA-Getzmann, at an average rate of 2000 rpm for about 1 hour. The sonication process, instead, was performed using a HIELSCHER UP 200s Sonicator, set on 140W (70% of the maximum power) and a duty cycle of 50%, for 10 minutes. After sonication, the hardener was added and the obtained blend was mixed at low rate (1000 rpm) for further 5 minutes.
2. *Degassing and moulding of the obtained blend*. As a major drawback of the shear mixing process, a large amount of air is trapped into the matrix. Thus, in order to prevent bubbles in the specimens, a careful degassing process was carried out. To this end, a low-vacuum pump was used to induce a very low pressure in the resin pot, promoting bubbles explosion. 1 hour of degassing process was enough to obtain a clear and translucent nanomodified resin which was later slowly poured into silicone rubber moulds. The different stages of the degassing process are shown in Figure 2.
3. *Milling and surface polishing*. Once de-moulded, the specimens were milled to cut out the upper surface, where some inclusions and voids due to the pouring process could have been present, and polished up to the final thickness.

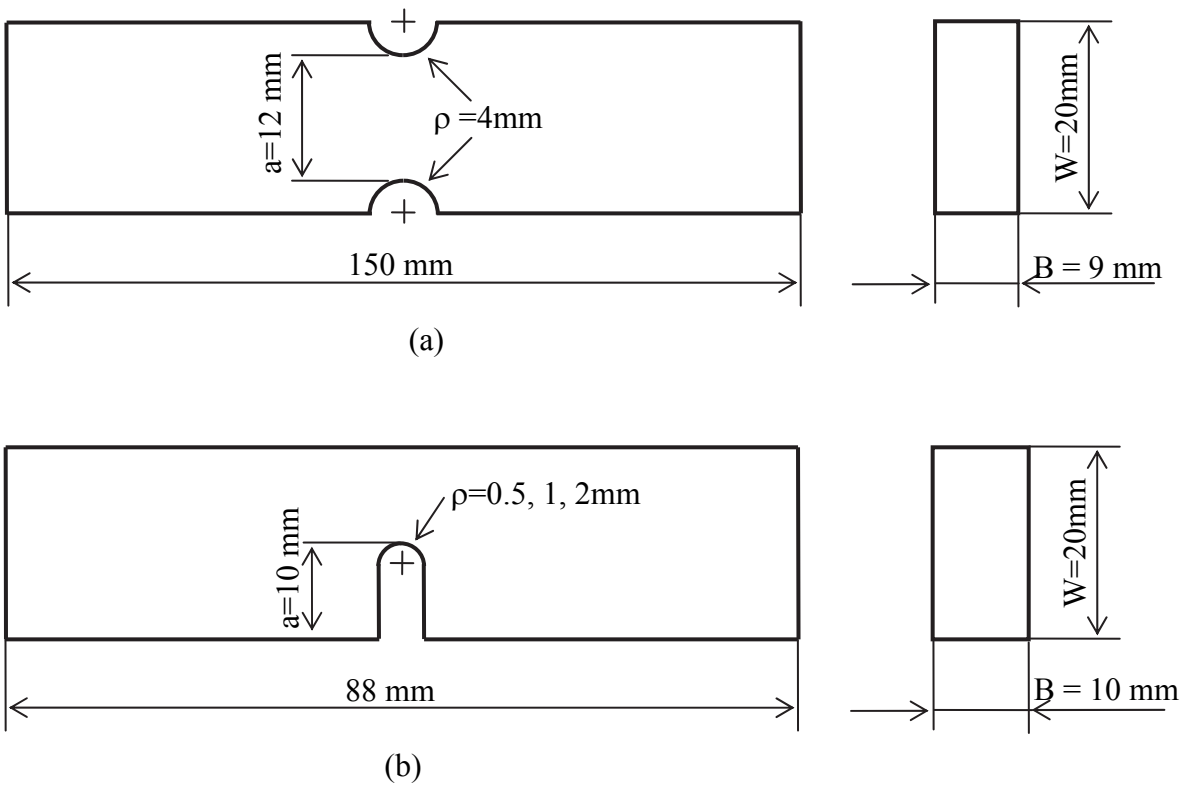

Figure 1. (a) Double Edge Notch Tension (DENT) specimens and (b) Single Edge Notch Bending (SENB) used in the tests

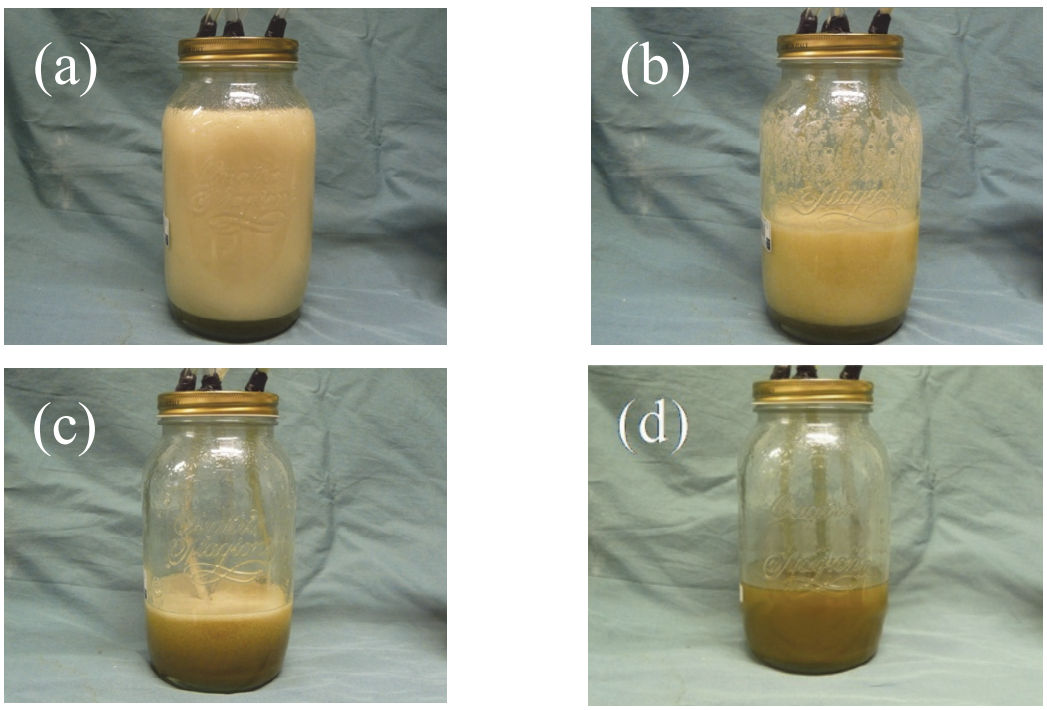

Figure 2. Degassing process of the nanomodified resin (5wt% of nanoclay). (a) Nanomodified resin at low pressure as just poured into the pot; (b) after 10 minutes under vacuum; (c) after 25 minutes and (d) after 35 minutes. At the end of the process, the mixture is devoid of any bubble.

The morphology of the systems analyzed in this work has been investigated using Scanning Electron Microscopy, in order to identify the presence of nanofiller agglomerates. As an example, Figure 3 shows some SEM images for 3 wt% loaded resins. The filler presents a satisfactory distribution within the matrix but some traces of clay agglomeration are evident, the size of the largest agglomerates among those detected being about 15 mm. A similar morphology was found in Ref. [12]; in that case an increase of about 35% of the mode fracture toughness was found.

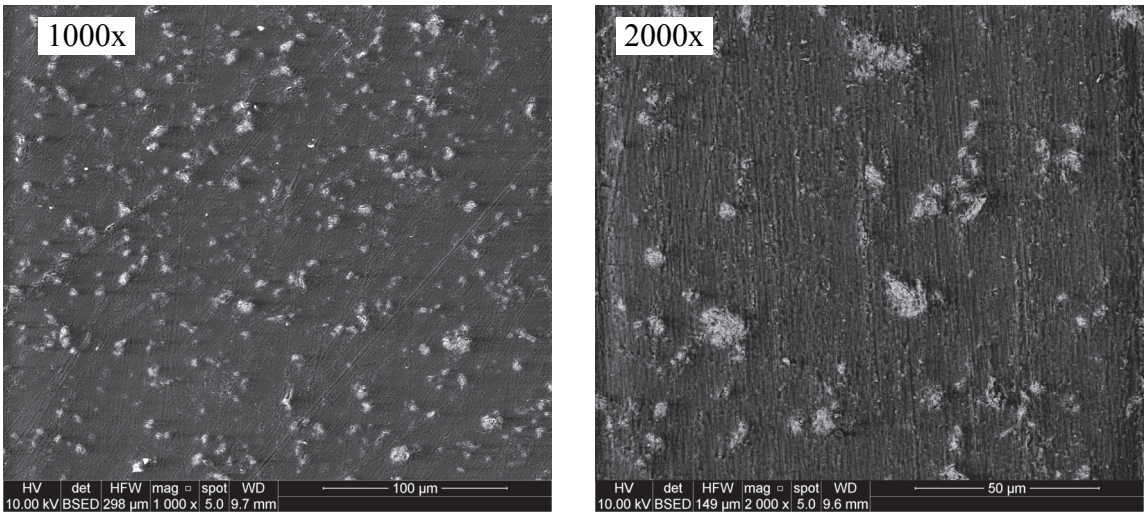

Figure 3. Morphology of 3%wt clay-loaded resins. Scanning electron micrographs at different magnifications.

3. EXPERIMENTAL EQUIPMENT AND TESTS

All tests described in the following have been carried out by using a MTS 858 servo-hydraulic machine, equipped with a 2.5/25 kN load cell.

3.1 Double Edge Notch Tension tests

Tensile tests on DENT specimens made of neat epoxy and nanomodified resins were carried out, by using a crosshead speed equal to 2 mm/min. For each material configuration, five specimens were tested.

It is worth mentioning here that the theoretical stress concentration factor referred to the net area for the DENT specimens used in the present analysis is equal to 1.866 [28].

3.2 Single Edge Notch Bending tests

As far as SENB tests are concerned, different loading conditions have been applied, resulting in different stress states ahead of the notch tip, from pure mode I (completely symmetric stress state) to pure mode II (completely skew-symmetric stress state).

The experimental tests have been carried out using a crosshead speed equal to 10 mm/min, as suggested in [29-30] for cracked components. For every loading condition and every filler weight fraction three specimens were tested.

The testing device consisted of two steel plates, 18 mm thick, one fixed on the load cell, the other attached to a vertical moving ram. One or two pin supports could be mounted on each plate.

Three different kind of loading conditions have been analysed;

1. Symmetric Three-Point Bending tests (S3PB) which result in a purely symmetric stress state close to the notch tip (pure mode I loading conditions);
2. Non-Symmetric Three-Point Bending tests (NS3PB) which result in a mixed (symmetric plus skew-symmetric) stress state close to the notch tip;
3. Non-Symmetric Four-Point Bending tests (NS4PB) which result in a purely skew-symmetric stress state close to the notch tip (pure mode II loading conditions).

Some pictures of the loading system are shown in Figures 4 while schematics of the loading conditions are reported in Figure 5.

The maximum principal stress at the notch edge of SENB specimens can be evaluated as:

$$\sigma_{p,max} = K \cdot \sigma_{n,n} \qquad \text{for S3PB and NS3PB} \tag{1a}$$

$$\sigma_{p,max} = K \cdot \tau_{n,n} \qquad \text{for NS4PB} \tag{1b}$$

where $\sigma_{n,n}$ and $\tau_{n,n}$ are the maximum nominal stresses on the net section, evaluated according to the beam theory:

$$\sigma_{nn} = \frac{6M}{B(W-a)^2} \qquad \tau_{nn} = \frac{3}{2}\frac{Q}{B(W-a)} \tag{2a-b}$$

In Eqs. (2a) and (2b) M and Q are the bending moment and the shear force evaluated on the notch bisector resulting from static equilibrium equations:

$$M = F\frac{L_3 - L_1}{L_3 + L_4}L_4 \qquad Q = F\left(\frac{L_1}{L_1 + L_2} - \frac{L_3}{L_3 + L_4}\right) \tag{3}$$

Stress concentration coefficients K to be used in Eq. (1a,b) have been evaluated by means of finite element analyses and are listed in Table 2.

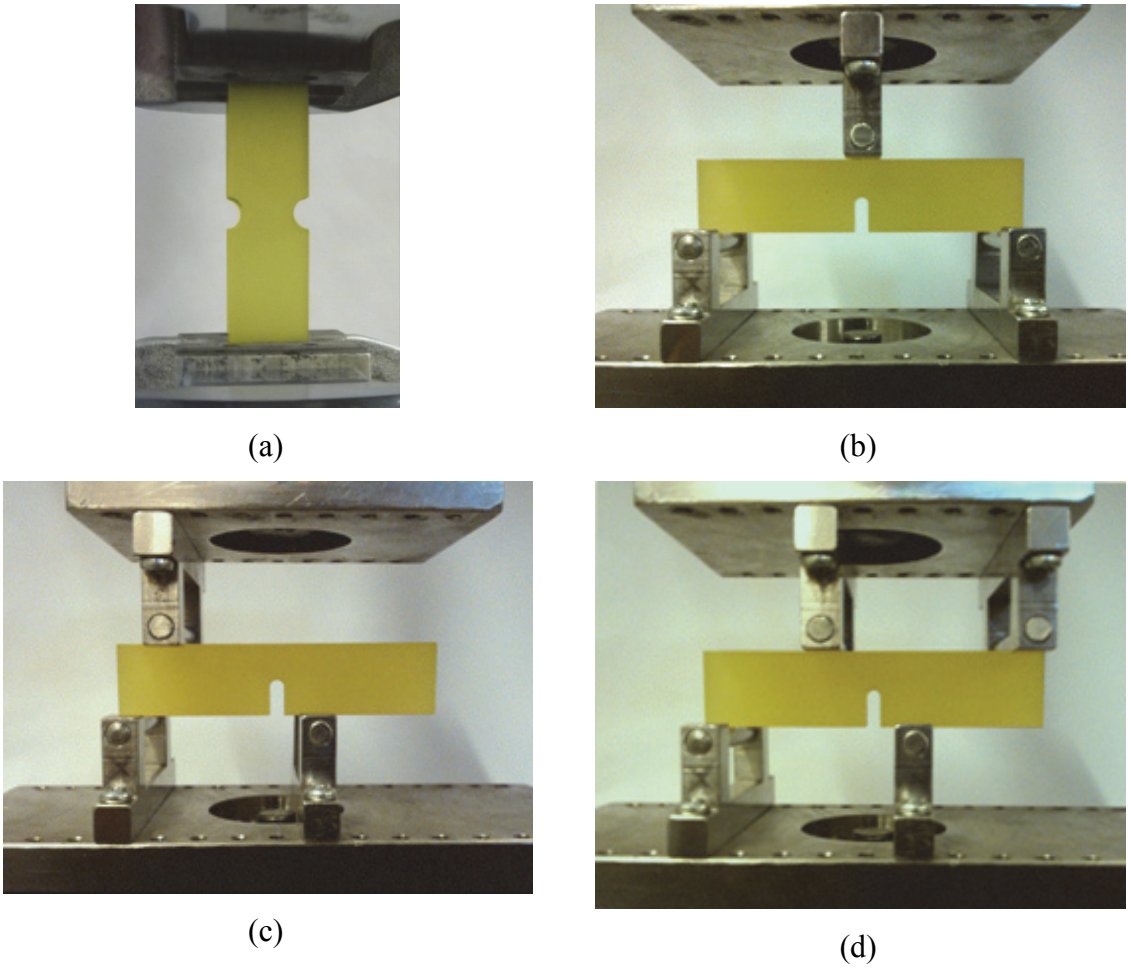

Figure 4. Loading configurations for DENT tests (a), Symmetric three Point Bending (S3PB) tests (b), non-Symmetric three Point Bending (NS3PB) tests (c) and non-Symmetric four Point Bending (NS4PB) tests (d)

ρ [mm]	S3PB	NS3PB	NS4PB
0.5	3.436	4.265	6.062
1	2.518	3.165	4.626
2	1.903	2.433	3.696

Table 2. Values of stress concentration coefficient K for SENB specimens.

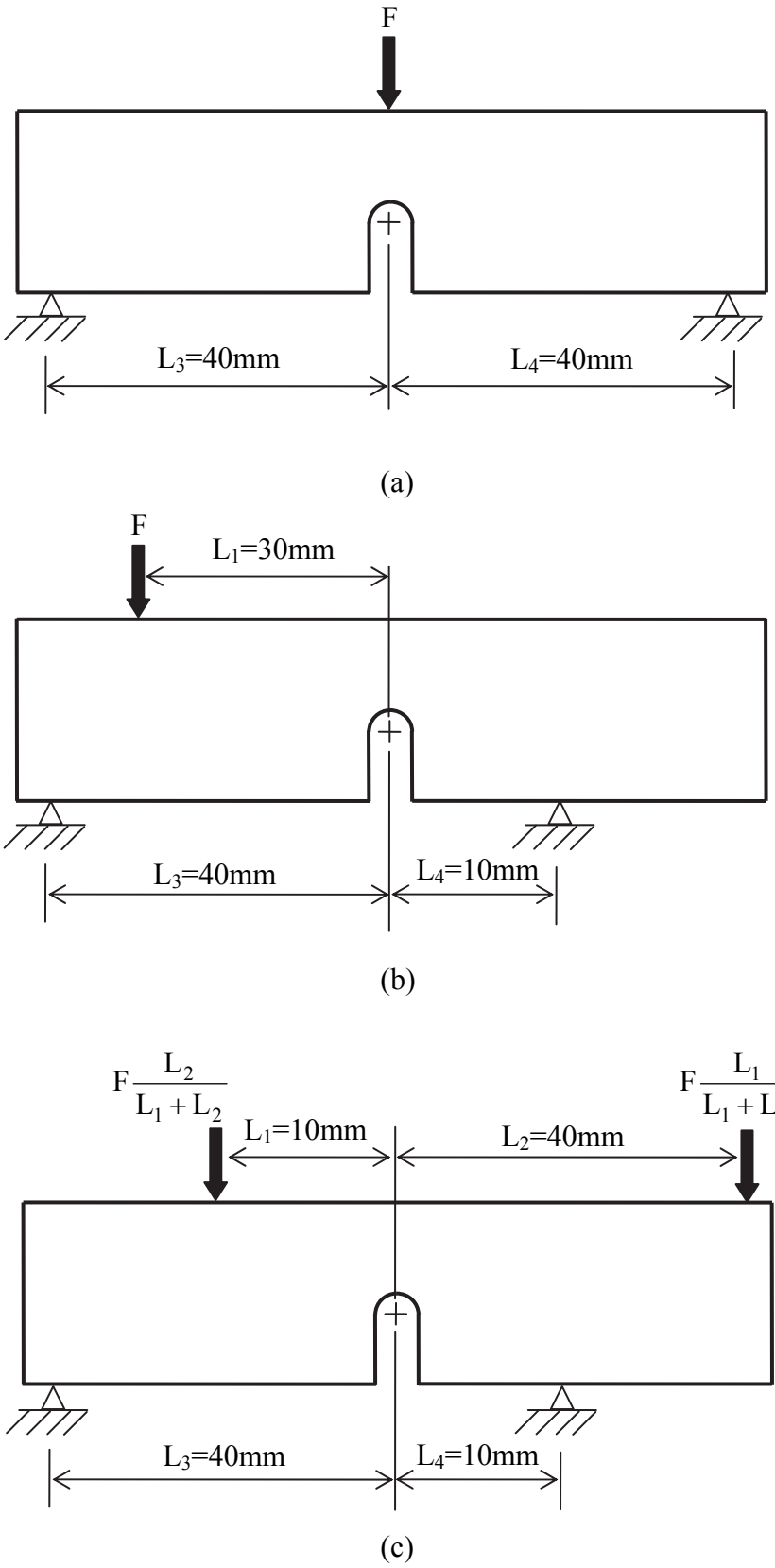

Figure 5. Schematic of (a) the Symmetric three Point Bending (S3PB), (b) Non-symmetric three Point Bending (NS3PB) and (c) of the non-Symmetric four Point

EXPERIMENTAL RESULTS

Brittle failure assessments of cracked and blunt notched components are usually based on fracture toughness or strength criteria, respectively. In the former case, according to the Fracture Mechanics approach, the stress intensity factors at the crack tip are compared to the fracture toughness of the material. In the latter case, according to classical Notch Theory, the stresses computed in the stress concentration regions are compared to the static strength properties of the material.

In the presence of a blunt notch, namely a notch with a finite value of the root radius ρ, the singularity of the linear elastic crack stress fields disappears. Notwithstanding this, the Linear Elastic Fracture Mechanics approach continues to be valid up to a critical value of ρ which varies from material to material according to the following expression [31]:

$$\rho^* = \frac{4}{\pi}\left(\frac{K_{Ic}}{\sigma_t}\right)^2 \tag{4}$$

For notch root radii greater than the limit value ρ^*, the notch sensitivity is full and the strength of the notched components is controlled by the elastic peak stress value at the notch edge.

A gradual transition between a Fracture Mechanics-based approach and the peek stress-based approach can be obtained by using local parameters (see, among the others [32-34]).

While discussing the influence of the root radius of crack-like notches on the static fracture load of brittle components, Kullmer and Richard [35] found a relationship similar to that provided by Atzori and Lazzarin [31] for ρ^*, where 4.5 substitutes 4.0.

K_{Ic} and σ_t to be used in Eq. (4) are the mode I fracture toughness and the critical tensile strength of the material, respectively. While the value of K_{Ic} can be unambiguously determined according to the ASTM-D5045-99 standard [29-30], particular attention should be paid to the choice of critical material tensile strength. In the literature, indeed, it is suggested to estimate σ_t on the basis of the strength of notched components [34, 36, 37]. In particular, Seweryn [36] suggested that σ_t should be determined as "the maximum normal stress existing at the edge at the moment preceding the cracking" and, to this end, recommended to use tensile specimens with semicircular notches [37]. Thus, according [34, 36, 37], in the present work σ_t has been measured evaluating the stress at failure occurring at the tip of DENT specimens. A summary of the obtained σ_t values for the neat and nanomodified epoxy resins is shown in Figure 6. It is evident that, even if 30B clay-

modified epoxy resins exhibit an enhanced fracture toughness [12, 26], nanomodification has a detrimental effect on the critical material tensile strength. In more details, σ_t is decreased from about 151 MPa (neat resin) to about 105.7 MPa (5% wt nanoclay) with a reduction of about 30%. This decrease approximately equates that detected, for the same material systems, on the tensile strength as measured from tensile tests on Dog Bone specimens [12, 26].

The limit values for the notch root radius, ρ^*, for the neat resin and the clay-modified resin evaluated by Eq. (4) are listed in Table 3. In all cases ρ^* is smaller than 0.5 mm, namely the smallest value of the notch root radius used in the present analysis, thus indicating that all the specimens analyzed in the present work are characterized by a full notch sensitivity.

Accordingly, all experimental data from SENB and DENT specimens with the same nanoclay weight content have been summarised in terms of the maximum principal stress evaluated at the notch edge. The summaries are shown in Figures 7-10 where it is evident that data coming from specimens made of the same material but characterized by different values of the notch root radius and different loading conditions fall within the same narrow scatter band. The scatter bands have been drawn by using for each material configuration the mean values of σ_t ±2 standard deviations.

Thus, for all the notched specimens investigated in this work, nanomodification has a detrimental effect on brittle failure, being it a strength-controlled phenomenon ($\rho>\rho*$ for all cases). Under these conditions, the disadvantageous role played by nanoclay addition on the strength of polymeric resins [12,14-16] is directly transferred to the notch effect on nanomodified specimens. Accordingly, in the engineering practice, particular care should be taken when using binary nanomodified resins for structural applications in the presence of notches or holes.

Clay content %wt	K_{Ic} [MPa $m^{0.5}$] [26]	σ_t [MPa]	a_0 [mm]	ρ^* [mm]
0	1.001 ± 0.024	151.0 ± 3.9	0.013991	0.0559
1	1.489 ± 0.036	137.9 ± 2.33	0.037153	0.1486
3	1.306 ± 0.01	110.8 ± 0.85	0.044274	0.1770
5	1.188 ± 0.034	106.7 ± 2.62	0.039511	0.1580

Table 3. Fracture toughness, tensile properties and limit notch root radius of neat epoxy and nanomodified polymers.

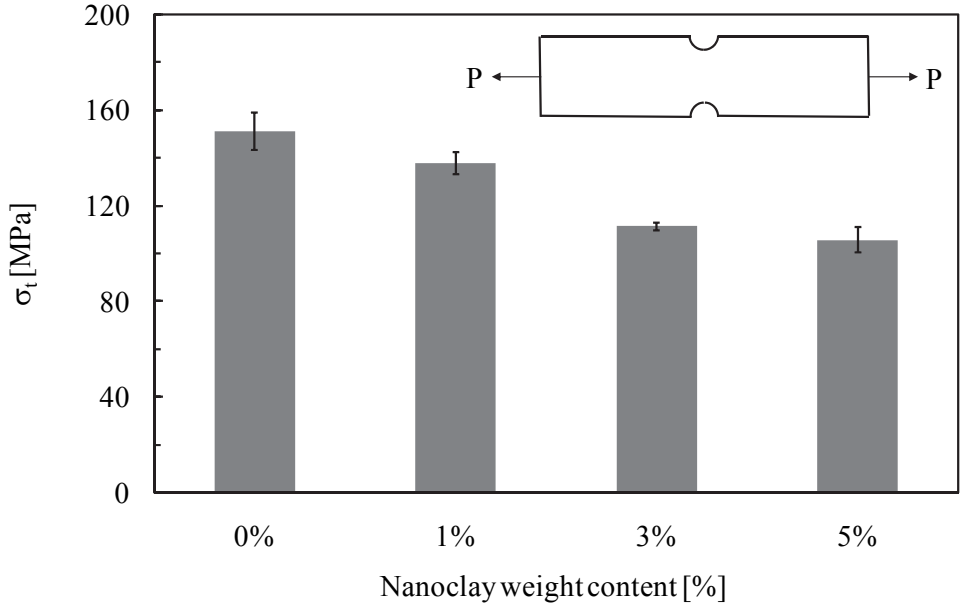

Figure 6. Critical tensile stress, σ_t, of the neat and nanomodified epoxy resins (results from DENT tests). Errors bars: +/- 2 standard deviations.

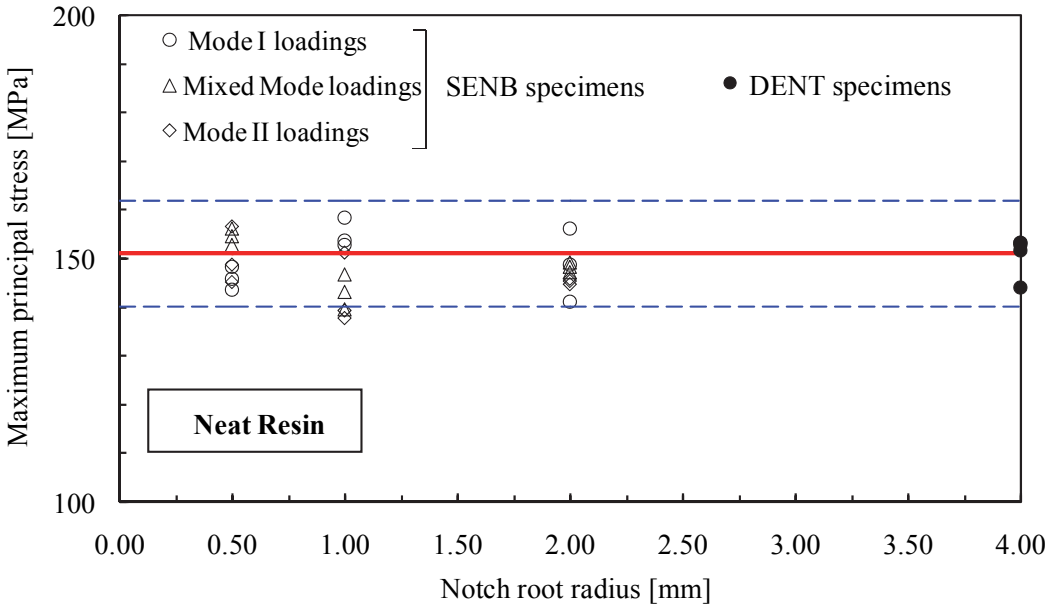

Figure 7. Experimental data from SENB and DENT specimens calculated in terms of the maximum principal stress on the notch edge. Neat resin. Scatter band: mean value +/- 2 standard deviations.

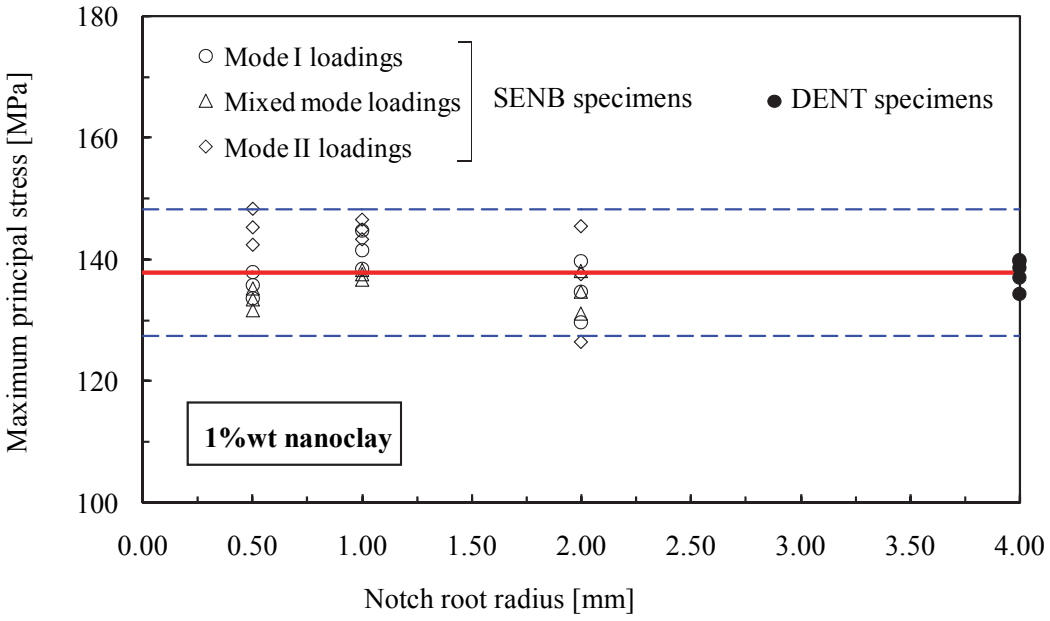

Figure 8. Experimental data from SENB and DENT specimens calculated in terms of the maximum principal stress on the notch edge. 1%wt nanoclay. Scatter band: mean value +/- 2 standard deviations.

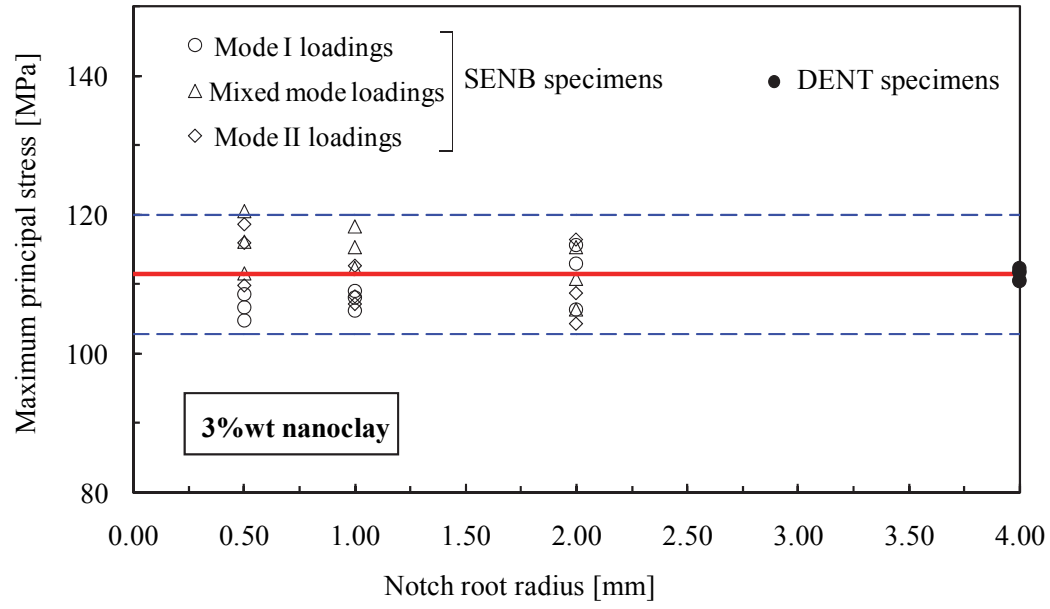

Figure 9. Experimental data from SENB and DENT specimens calculated in terms of the maximum principal stress on the notch edge. 3%wt nanoclay. Scatter band: mean value +/- 2 standard deviations.

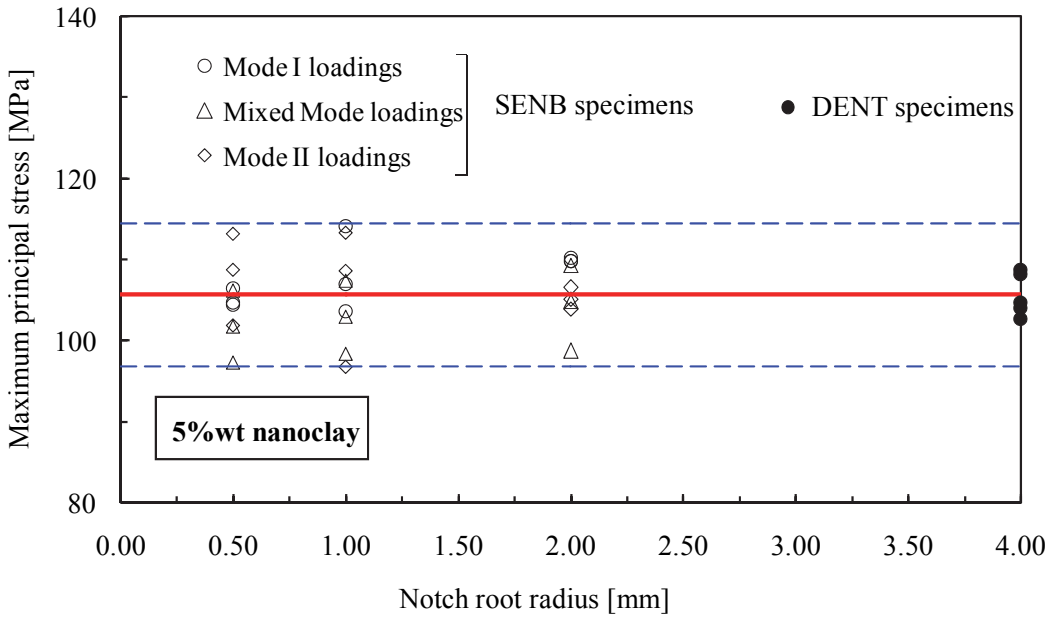

Figure 10. Experimental data from SENB and DENT specimens calculated in terms of the maximum principal stress on the notch edge. 5%wt nanoclay. Scatter band: mean value +/- 2 standard deviations.

EXPERIMENTAL DATA IN TERMS OF APPARENT FRACTURE TOUGHNESS

In this section, the experimental results from SENB specimens already discussed in the previous paragraph will be presented in terms "apparent fracture toughness" by using the concept of "Generalised Stress Intensity Factor" (GSIF).

The Stress Intensity Factors (SIFs) quantify the intensities of the asymptotic linear elastic stress distributions of cracks and are mathematically defined as [38, 39]:

$$K_I = \lim_{r\to 0}\sqrt{2\pi r}\,\sigma_{\theta\theta} \qquad K_{II} = \lim_{r\to 0}\sqrt{2\pi r}\,\tau_{r\theta} \tag{5}$$

When the tip radius is different from zero, the crack becomes a U-notch and the near-the-tip stress field diverges from the singular sharp-crack solution. In this case, Eq. (5) should be modified to account for the stress redistribution caused by the presence of a finite value of the notch root radius [40, 41]:

$$K_{I\rho} = \frac{8\sqrt{2\pi r}\;\sigma_{\theta\theta}}{8+5\left(\frac{\rho}{r}\right)+6\left(\frac{\rho}{r}\right)^2+5\left(\frac{\rho}{r}\right)^3} \tag{6}$$

$$K_{II\rho} = \frac{8\sqrt{2\pi r}\ \tau_{r\theta}}{8+13\left(\frac{\rho}{r}\right)-6\left(\frac{\rho}{r}\right)^2-15\left(\frac{\rho}{r}\right)^3} \quad (7)$$

$K_{I\rho}$ and $K_{II\rho}$ are commonly regarded as Generalised Stress Intensity Factors (GSIFs). In Eqs. (6) and (7), r is the distance from the centre of the curvature radius (see Figure 11), ρ is the notch root radius and $\sigma_{\theta\theta}$ and $\tau_{r\theta}$ are stress components along the notch bisector line, to be determined from finite element analyses. It is worth noting that the units of measure of $K_{I\rho}$ and $K_{II\rho}$ remains MPa $m^{0.5}$, as for the crack case. Accordingly, unlike the theoretical stress concentration factor K_t, the scale effect is fully accounted for by the GSIFs: notched components simply scaled in geometrical proportion have the same K_t value, but different GSIF values.

The concept of generalized stress intensity factors, coupled with the cohesive zone model, has been used by Gómez et al. [42] to build a master curve for estimating fracture loads in deep rounded notched components. A generalised equivalent stress intensity fracture, obtained as a generalisation of Glinka's NSIF [43] for mode I simply replacing σ_{tip} by the maximum elastic stress at the notch edge, was later used by Gomez et al. [44] to summarise fracture tests from U-notched specimens made of PMMA.

A failure criterion based on the mode I and II GSIFs has also been proposed by Ayatollahi and Torabi and applied to summarize a large number of experimental data from Brazilian disc specimens made of PMMA [45] and polycrystalline graphite [46].

The definition or the use of a brittle fracture criterion based on the GSIFs being out of scope of the present research work, in this section GSIFs are used with the only aim to enforce the conclusions drawn in the previous section about the influence of nanomodification on the notch effect on clay-modified epoxy resins. To this end, $K_{I\rho}$ and $K_{II\rho}$ have been evaluated from FE analyses for all SENB specimens and loading conditions considered in the present work, and the experimental results, reconverted in terms of "apparent fracture toughness" have been summarised in $K_{I\rho}$- $K_{II\rho}$ diagrams (Figures 12-14). It is evident that nanomodified specimens exhibit a lower apparent fracture toughness independently of the notch root radius. Moreover, differently to what happened for cracked components where ranging from pure mode I to pure mode II less pronounced improvements of the fracture toughness has been found [26], no evident effect of the loading mode can be noted here.

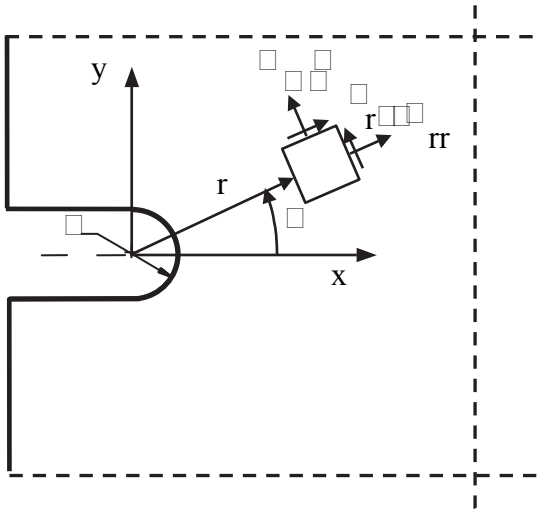

Figure 11. U shaped notch and polar coordinate system to be used in Eq. (6) and Eq. (7).

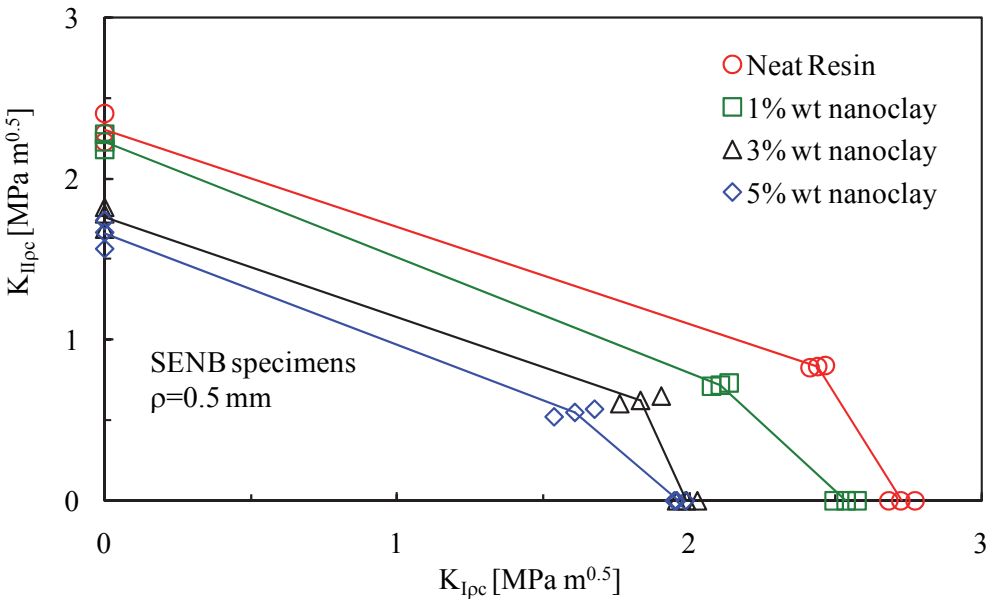

Figure 12. Apparent fracture toughness of neat and nanomodified specimens under various loading conditions. SENB specimens with ρ=0.5mm.

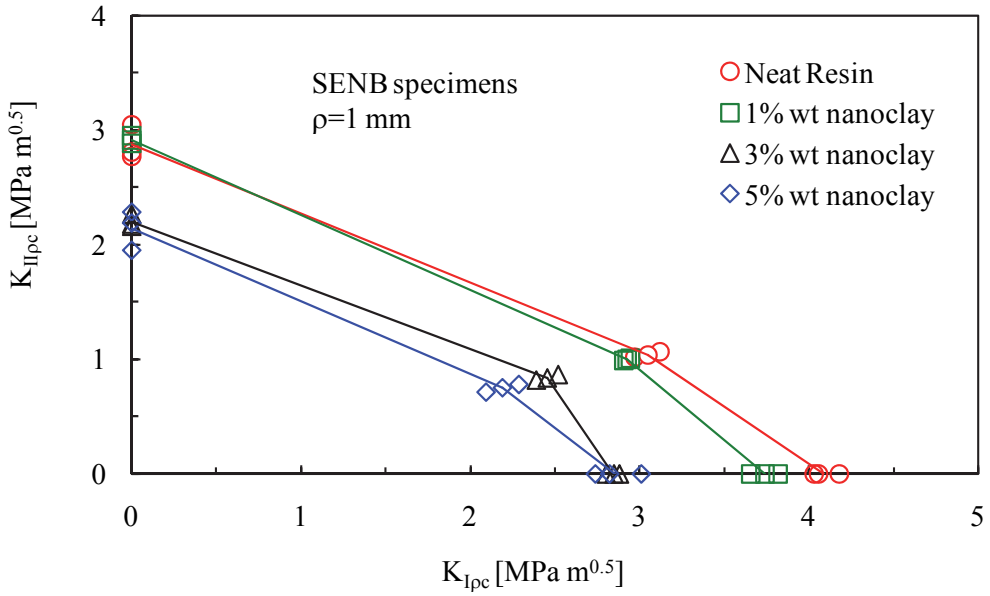

Figure 13. Apparent fracture toughness of neat and nanomodified specimens under various loading conditions. SENB specimens with ρ=1mm.

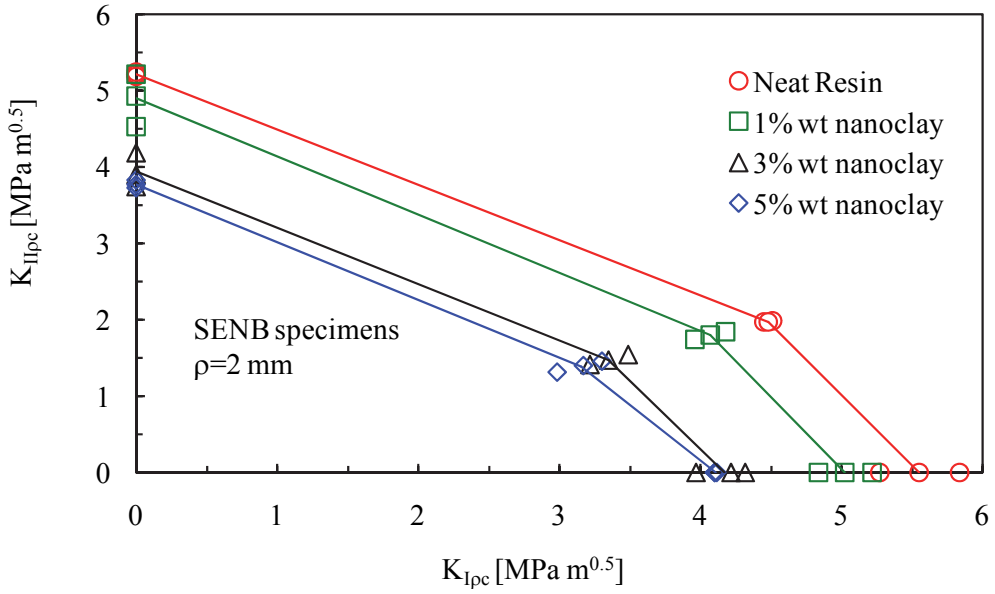

Figure 14. Apparent fracture toughness of neat and nanomodified specimens under various loading conditions. SENB specimens with ρ=2mm.

CONCLUSION

In the present work the effects of nanoclay addition on the brittle notch fracture behavior of an epoxy resin have been studied. Different kind of notched specimens have been manufactured and tested:

1. Double Edge Notch Tension (DENT) specimens with 4mm radius semicircular notches;
2. Single Edge Notch Bending (SENB) specimens with U-notches. In this case the notch depth is equal to 10 mm and three different values for the notch root radius have been used: 0.5, 1 and 2mm.

The experimental results clearly indicate that for notch root radii greater than a limit value, which depends on the clay content, the brittle failure of notched nanomodified components is a strength-controlled phenomenon.

All the results from specimens with the same clay content but with different values of the notch root radius (from 0.5mm to 4mm) were found to be characterized by the same critical value of the maximum principal stress, σ_t. Comparing the average critical values of σ_t allowed us to conclude that for the material systems and geometries investigated in this work, nanomodification has a detrimental effect on the strength of notched components. A final summary of the experimental results in terms of generalised (apparent) fracture toughness revealed that this behaviour is not influenced either by the notch root radius or the loading mode.

As a major conclusion of the present work, it can be stated that, even if nanoclays are suitable to improve the fracture toughness of polymeric systems, the same amelioration is not necessarily transferred to notched parts. Accordingly, in the engineering practice, particular care should be taken when using binary nanomodified resins for structural applications in the presence of notches or holes.

ACKNOWLEDGEMENTS

The authors greatly acknowledge the financial support to the activity by Veneto Nanotech, the Italian Cluster on Nanotechnologies and by Fondazione Cassa di Risparmio di Padova e Rovigo.

REFERENCES

[1] Fischer, H. (2003). Polymer nanocomposites: from fundamental research to specific applications. Materials Science and Engineering: C, 23(6), 763-772.

[2] Thostenson, E. T., Li, C., & Chou, T. W. (2005). Nanocomposites in context.Composites Science and Technology, 65(3), 491-516.

[3] Ajayan, P. M., Schadler, L. S., & Braun, P. V. (2006). Nanocomposite science and technology. John Wiley & Sons.

[4] Zappalorto, M., Salviato, M., & Quaresimin, M. (2012). A multiscale model to describe nanocomposite fracture toughness enhancement by the plastic yielding of nanovoids. Composites Science and Technology, 72(14), 1683-1691.

[5] Salviato, M., Zappalorto, M., & Quaresimin, M. (2013). Plastic shear bands and fracture toughness improvements of nanoparticle filled polymers: a multiscale analytical model. Composites Part A: Applied Science and Manufacturing, 48, 144-152.

[6] Zappalorto, M., Salviato, M., & Quaresimin, M. (2011). Influence of the interphase zone on the nanoparticle debonding stress. Composites Science and Technology, 72(1), 49-55.

[7] Sevostianov, I., & Kachanov, M. (2007). Effect of interphase layers on the overall elastic and conductive properties of matrix composites. Applications to nanosize inclusion. International Journal of Solids and Structures, 44(3), 1304-1315.

[8] Cho, J. W., & Paul, D. R. (2001). Nylon 6 nanocomposites by melt compounding. Polymer, 42(3), 1083-1094.

[9] Wang, L., Wang, K., Chen, L., Zhang, Y., & He, C. (2006). Preparation, morphology and thermal/mechanical properties of epoxy/nanoclay composite.Composites Part A: Applied Science and Manufacturing, 37(11), 1890-1896.

[10] Liu, T. X., Liu, Z. H., Ma, K. X., Shen, L., Zeng, K. Y., & He, C. B. (2003). Morphology, thermal and mechanical behavior of polyamide 6/layered-silicate nanocomposites. Composites science and technology, 63(3), 331-337.

[11] Dorigato, A., Pegoretti, A., & Quaresimin, M. (2011). Thermo-mechanical characterization of epoxy/clay nanocomposites as matrices for carbon/nanoclay/epoxy laminates. Materials Science and Engineering: A,528(19), 6324-6333.

[12] Quaresimin, M., Salviato, M., & Zappalorto, M. (2012). Fracture and interlaminar properties of clay-modified epoxies and their glass reinforced laminates. Engineering Fracture Mechanics, 81, 80-93.

[13] Lee, D. C., & Jang, L. W. (1996). Preparation and characterization of PMMA–clay hybrid composite by emulsion polymerization. Journal of Applied Polymer Science, 61(7), 1117-1122.

[14] Luo, J. J., & Daniel, I. M. (2003). Characterization and modeling of mechanical behavior of polymer/clay nanocomposites. Composites Science and Technology, 63(11), 1607-1616.

[15] Bharadwaj, R. K., Mehrabi, A. R., Hamilton, C., Trujillo, C., Murga, M., Fan, R., ... & Thompson, A. K. (2002). Structure–property relationships in cross-linked polyester–clay nanocomposites. Polymer, 43(13), 3699-3705.

[16] Wang, K., Chen, L., Wu, J., Toh, M. L., He, C., & Yee, A. F. (2005). Epoxy nanocomposites with highly exfoliated clay: mechanical properties and fracture mechanisms. Macromolecules, 38(3), 788-800.

[17] Quaresimin, M., Salviato, M., & Zappalorto, M. (2012). Strategies for the assessment of nanocomposite mechanical properties. Composites Part B: Engineering, 43(5), 2290-2297.

[18] Quaresimin, M., & Varley, R. J. (2008). Understanding the effect of nano-modifier addition upon the properties of fibre reinforced laminates. Composites Science and Technology, 68(3), 718-726.

[19] Xu, Y., & Hoa, S. V. (2008). Mechanical properties of carbon fiber reinforced epoxy/clay nanocomposites. Composites Science and Technology, 68(3), 854-861.

[20] Subramaniyan, A. K., & Sun, C. T. (2007). Toughening polymeric composites using nanoclay: crack tip scale effects on fracture toughness. Composites Part A: Applied Science and Manufacturing, 38(1), 34-43.

[21] Kornmann, X., Rees, M., Thomann, Y., Necola, A., Barbezat, M., & Thomann, R. (2005). Epoxy-layered silicate nanocomposites as matrix in glass fibre-reinforced composites. Composites Science and Technology, 65(14), 2259-2268.

[22] Becker, O., Varley, R., & Simon, G. (2002). Morphology, thermal relaxations and mechanical properties of layered silicate nanocomposites based upon high-functionality epoxy resins. Polymer, 43(16), 4365-4373.

[23] Liu, W., Hoa, S. V., & Pugh, M. (2005). Fracture toughness and water uptake of high-performance epoxy/nanoclay nanocomposites. Composites Science and Technology, 65(15), 2364-2373.

[24] Zerda, A. S., & Lesser, A. J. (2001). Intercalated clay nanocomposites: morphology, mechanics, and fracture behavior. Journal of Polymer Science Part B: Polymer Physics, 39(11), 1137-1146.

[25] Kornmann, X., Berglund, L. A., Thomann, R., Mulhaupt, R., & Finter, J. (2002). High performance epoxy-layered silicate nanocomposites. Polymer Engineering & Science, 42(9), 1815-1826.

[26] Zappalorto, M., Salviato, M., & Quaresimin, M. (2013). Mixed mode (I+ II) fracture toughness of polymer nanoclay nanocomposites. Engineering Fracture Mechanics, 111, 50-64.

[27] Ayatollahi, M. R., Shadlou, S., & Shokrieh, M. M. (2011). Mixed mode brittle fracture in epoxy/multi-walled carbon nanotube nanocomposites. Engineering Fracture Mechanics, 78(14), 2620-2632.

[28] Peterson, R. E., & Plunkett, R. (1975). Stress concentration factors. Journal of Applied Mechanics, 42, 248.

[29] ASTM D 5045. Standard Test Methods for Plane-Strain Fracture Toughness and Strain Energy Release Rate of Plastic Materials (1999).

[30] Moore, D. R., Williams, J. G., & Pavan, A. (2001). Fracture mechanics testing methods for polymers, adhesives and composites (Vol. 28). Elsevier.

[31] Atzori, B., & Lazzarin, P. (2001). Notch sensitivity and defect sensitivity under fatigue loading: two sides of the same medal. International Journal of Fracture,107(1), 1-8.

[32] Lazzarin, P., & Zambardi, R. (2001). A finite-volume-energy based approach to predict the static and fatigue behavior of components with sharp V-shaped notches. International Journal of Fracture, 112(3), 275-298.

[33] Leguillon, D. (2002). Strength or toughness? A criterion for crack onset at a notch. European Journal of Mechanics-A/Solids, 21(1), 61-72.

[34] Lazzarin, P., & Berto, F. (2005). Some expressions for the strain energy in a finite volume surrounding the root of blunt V-notches. International Journal of Fracture, 135(1-4), 161-185.

[35] Kullmer, G., & Richard, H. A. (2006). Influence of the root radius of crack-like notches on the fracture load of brittle components. Archive of Applied Mechanics, 76(11-12), 711-723.

[36] Seweryn, A. (1994). Brittle fracture criterion for structures with sharp notches.Engineering Fracture Mechanics, 47(5), 673-681.

[37] Seweryn, A., & Łukaszewicz, A. (2002). Verification of brittle fracture criteria for elements with V-shaped notches. Engineering Fracture Mechanics, 69(13), 1487-1510.

[38] Irwin, G. R. (1957). Analysis of stresses and strains near the end of a crack traversing a plate. J. appl. Mech.

[39] Gross, B., & Mendelson, A. (1972). Plane elastostatic analysis of V-notched plates. International Journal of Fracture Mechanics, 8(3), 267-276.

[40] Zappalorto, M., & Lazzarin, P. (2011). In-plane and out-of-plane stress field solutions for V-notches with end holes. International journal of fracture, 168(2), 167-180.

[41] Lazzarin, P., Zappalorto, M., & Berto, F. (2011). Generalised stress intensity factors for rounded notches in plates under in-plane shear loading. International journal of fracture, 170(2), 123-144.

[42] Gomez, F. J., Guinea, G. V., & Elices, M. (2006). Failure criteria for linear elastic materials with U-notches. International journal of fracture, 141(1-2), 99-113.

[43] Glinka, G. (1985). Calculation of inelastic notch-tip strain-stress histories under cyclic loading. Engineering Fracture Mechanics, 22(5), 839-854.

[44] Gómez, F. J., Elices, M., Berto, F., & Lazzarin, P. (2008). A generalised notch stress intensity factor for U-notched components loaded under mixed mode.Engineering Fracture Mechanics, 75(16), 4819-4833.

[45] Ayatollahi, M. R., & Torabi, A. R. (2010). Investigation of mixed mode brittle fracture in rounded-tip V-notched components. Engineering Fracture Mechanics, 77(16), 3087-3104.

[46] Ayatollahi, M. R., & Torabi, A. R. (2011). Failure assessment of notched polycrystalline graphite under tensile-shear loading. Materials Science and Engineering: A, 528(18), 5685-5695.

4 Advanced multifunctional polymer nanocomposites with enhanced mechanical and anti-microbial properties

KEYWORDS: A. Multifunctional nanocomposites; B. Epoxy resin; C. Antimicrobial activity; D. Reinforced laminates;

ABSTRACT
The main goal of the present chapter is to investigate the possibility to obtain multifunctional binary and ternary polymer nanocomposites with enhanced mechanical and anti-microbial properties. To this end a DGEBA-based epoxy resin is loaded using Montmorillonite clays and later used as matrix for glass fibre reinforced laminates. Both binary and ternary nanomodified specimens are manufactured and subjected to mechanical testing. An accurate analysis of the effect of nanomodification on the biological activity is carried out as well.

1. INTRODUCTION

The most recent advancements in polymer and composite science and technology allow the design of materials and structures at the nanometer scale, resulting in exciting accomplishments in the development of multi-functional materials with enhanced physical and mechanical properties for several fields of application [1-3].

Thanks to the complex physical interactions among constituents occurring at the atomic level, nanomodified polymers are provided with exceptionally enhanced properties even at low filler concentrations, making polymer nanocomposites a unique vector for functional properties.

Within this context, clay based nanocomposites are very promising new materials from the perspective of achieving high performances at a relative low cost. Nanoclays are silicate platelets with about 1nm of thickness and disposed in tactoids; commonly, a hybrid exfoliated and intercalated structure represents a trade-off between the capacity of obtaining the desired property enhancements and manufacturing complexity [4-11]. A complete exfoliation is, indeed, complicated to be obtained since it requires the separation of the platelets from the primary tactoids.

Due to their very high aspect ratio, nanoclay platelets are suitable to improve the tensile elastic modulus of polymeric systems [4-6], the matrix fracture toughness [11, 12] and, in principle, the strength, even if conflicting results have been reported [7–11].

As far as the possibility to transfer the improvements obtainable in the mechanical properties of binary nanocomposites to ternary fibre reinforced nanocomposites is concerned, the results reported up to now in the literature do not show a unique trend. Encouraging results were obtained by Becker et al. [13], who documented improvements in crack opening fracture toughness with low levels of clay addition and by Quaresimin and Varley [14], who reported "selective" improvements in the mode II toughness properties of carbon/clay-modified epoxy laminates. Differently, the investigations carried out by Timmerman et al. [15] and Quaresimin et al. [11] showed only limited improvements in the mechanical properties of clay modified composites compared to those produced with unmodified resins.

When using adequate surfactants, polymer loading through montmorillonite (MMT) nanoclays also offers exceptional improvements of anti-microbial properties [16-18], assisting in the achievement of self-decontaminating surfaces which are highly desirable for many fields of application, such as composite parts in the medical field (external prostheses or sterilised equipments and tables).

Quaternary ammonium compounds (QACs) have great antibacterial activity thanks to the positive charge of the amine which is attracted and interact with the negatively charged cell surfaces of bacteria [17, 18]. The concept of polymeric spacer is commonly used when describing QACs activity: more precisely, the agent is supposed to adsorb and penetrate into the bacterial cell thanks to a sufficiently long alkyl chain which should allow it to reach gradually the cytoplasmic membrane and kill the bacteria by destabilizing and destroying the phospholipid bilayer.

An alternative mechanism proposed to explain the antimicrobial activity of these compounds is known as the contact-killing via the phospholipid sponge effect which consist of an absorption and removal of such negative molecules from cell membranes thus leading bacteria to death [19-22].

This concept is reconsidered in this work, where the preliminary results of a project aimed at designing, manufacturing and testing advanced multifunctional polymer nanocomposites with enhanced mechanical and anti-microbial properties are presented. In more details, binary and ternary nanocomposite specimens are manufactured using a DGEBA-resin reinforced with octadecylamine surface-modified montmorillonite (MMT).

By one side, this particular functionalisation is proved to be very effective in terms of anti-microbial properties. On the other side clay-loading assists in the improvement of the polymer toughness. Eventually, the capability of translating the improved resin properties to the fibre reinforced composite is studied as well.

2. MATERIALS AND SPECIMENS MANUFACTURING

In this work, a diglycidyl ether of bisphenol A (DGEBA, Elan-tech EC157) epoxy with the mixture of cycloapliphatic amines Elan-TechW 152LR (supplied by Elantas) was used as polymer matrix. Nanomer I.30E (montmorillonite clay with 25-30%wt octadecylamine surfactant, supplied by Sigma-Aldrich) and a 350g/m^2 balanced twill of glass fibres supplied by G.Angeloni were used as nanofiller and microsize reinforcement, respectively.

The presence of amine groups with carbon chains on clay surfaces ensures compatibility between the epoxy resin and the nanoreinforcement and, at the same time, add amine groups in excess with respect to the stoichiometric ratio, giving a contribution to the development of anti-microbial properties. Indeed, Kubo et al. [17] reported how amine groups are capable to modify the ph of the material and might affect antibacterial activities.

Dog-Bone (DB) specimens and Compact Tension (CT) specimens were manufactured with the nanomodified epoxy resin (Figure 1a-b), while Double Cantilever Beam (DCB) specimens as well as Inter-Laminar Shear Strength (ILSS) specimens were obtained from the laminates.

The above mentioned samples were manufactured according to the following steps:

1. Nanoclays were dispersed in the DGEBA resin by means of shear mixing and sonication. The shear mixing was carried out with a DISPERMAT TU shear blender from VMA-GETZMANN with a 70mm diameter blade (about 1800rpm for 40 minutes). Then, the blend was sonicated with a HIELSCHER UP 200s sonicator using a 40mm diameter sonotrode (amplitude 160W and duty cycle 1) for 10 minutes, in order to improve the clay dispersion. After the sonication, the hardener was added and a further shear mixing at 300rpm for 5 minutes was performed.
2. Degassing was carried out for removing the air trapped within the blend as a consequence of the shear mixing. To this end a low vacuum pump was used to

reach a low pressure within the resin pot and, at the same time, mechanical shaking of the blend was performed. After 30 minutes the composite was poured in silicone moulds to manufacture binary nanocomposite samples.

3. Differently, glass fibre reinforced laminates were produced by means of room temperature vacuum infusion of the nanomodified resin into a vacuum bag where 16 layers of glass fibre ply were layered. An Aluminium film 15μm thick was used to create the pre-crack for the DCB specimens.
4. After 3 days of curing at room temperature, demoulding of the specimens was carried out. Finally, the specimens were polished and for ct specimens manual tapping was carried out. Filler weight fractions of 1% and 3% have been used to modify the polymer resin.

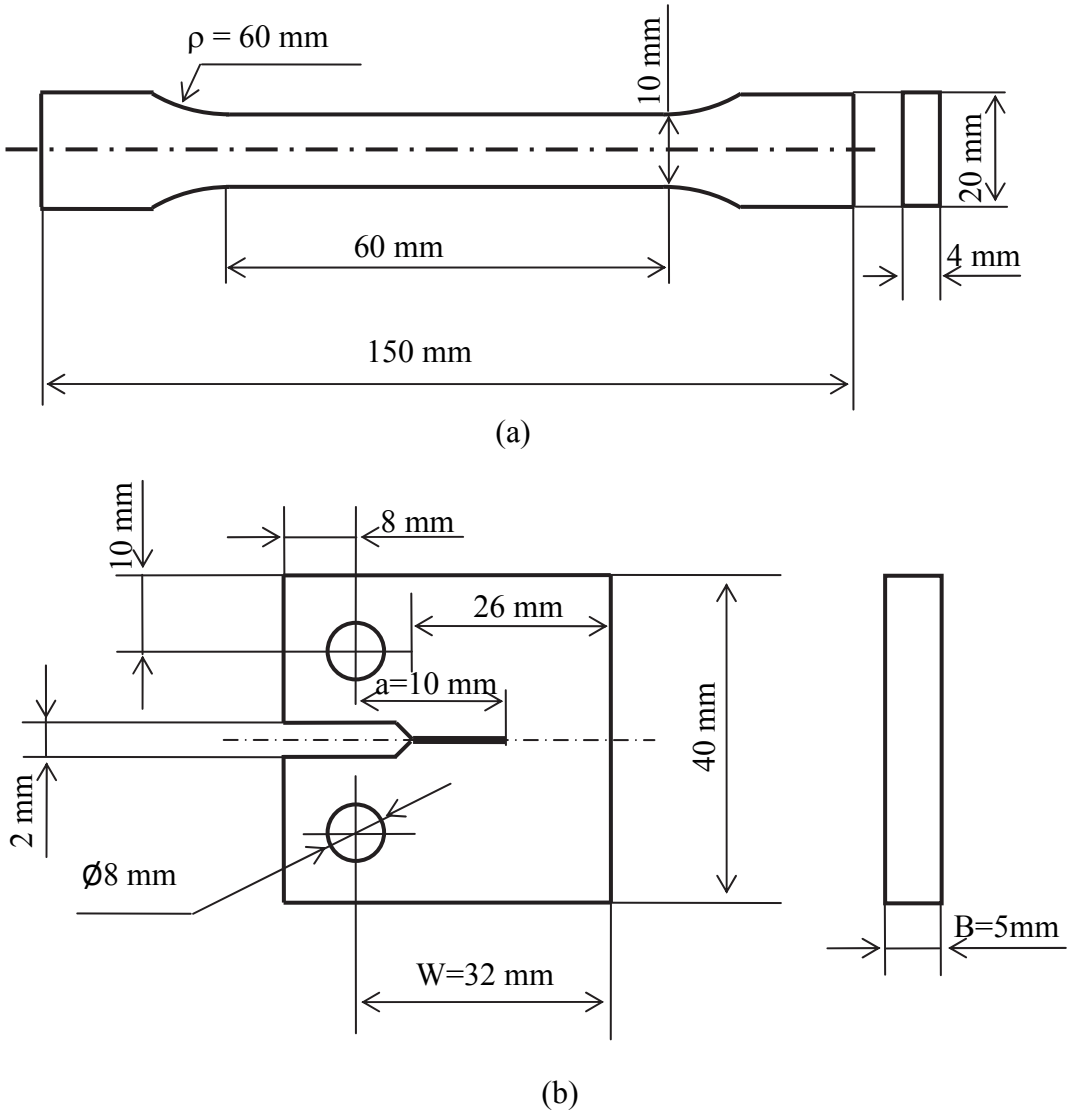

Figure 1. (a) A Dog-Bone (DB) specimen and (b) a Compact Tension (CT) specimen used in the mechanical tests.

3. BINARY NANOCOMPOSITES

3.1 Morphological and chemical characterization

A chemical characterization of the samples made of nanomodified polymer was carried out through FTIR spectroscopy using a thermo electron Nicolet Nexus 5700 with smart performer single-bounce ATR accessory. Results shown in Figure 2 make it evident that the characteristic peaks of montmorillonite were too low to be identified (-OH stretching mode of Al-OH or Si-OH at 3626 cm^{-1} and the band associate with the bending in plane vibration of the -OH from water at 1634cm^{-1}).

Moreover, high magnification TEM images showed a partially intercalated structure for the nanoclay (Figure 3).

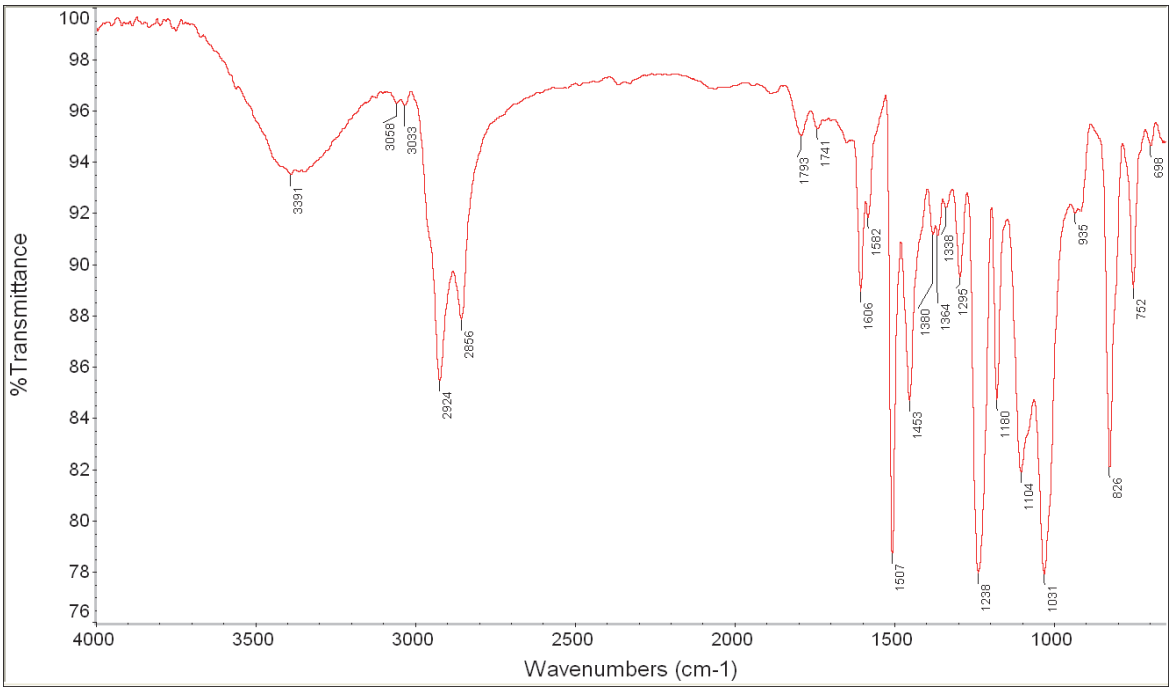

Figure 2. FTIR spectrum in ATR of a sample of epoxy resin containing 3%wt of clay loading.

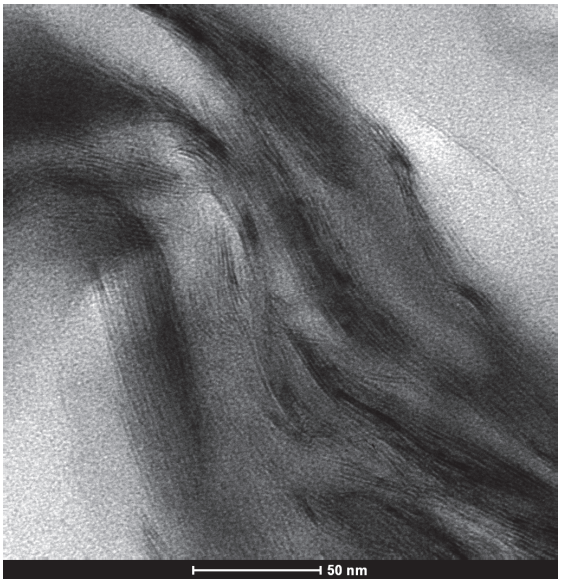

Figure 3. TEM micrograph for a nanocomposite containing 3%wt of clay loading.

3.2. Tensile tests and results

Tensile tests on DB specimens were carried out with the aim to determine the failure stress, σ_R, the elastic modulus, E, and the strain to failure, ε_R, of neat and nanomodified epoxy resins.

A MTS809 servo-hydraulic machine equipped by a 2.5kN load cell was used, with crosshead speed equal to 2mm/min. Accurate strain measurements were obtained by using a MTS 632.29F-30 extensometer. The specimen geometry is shown in Figure 1a and complies with the ISO 527-2 suggestions [23]. Three specimens were tested for each clay content, failure taking place in the gauge length of the specimens.

The effect of the weight content of nanoclay on the nanocomposite tensile properties is shown in Figure 5 in terms of average values. In particular a modulus of 3.2 GPa was measured for the unmodified epoxy resin and a maximum modulus of 3.3 GPa was measured, for the epoxy polymer with 3%wt of nanoclay, with negligible increase with respect to the unmodified epoxy resin.

Figure 4 makes it also evident that the nanocomposite strength and strain to failure are monotonously decreased while increasing clay loading, in agreement with results reported by other authors [11,12].

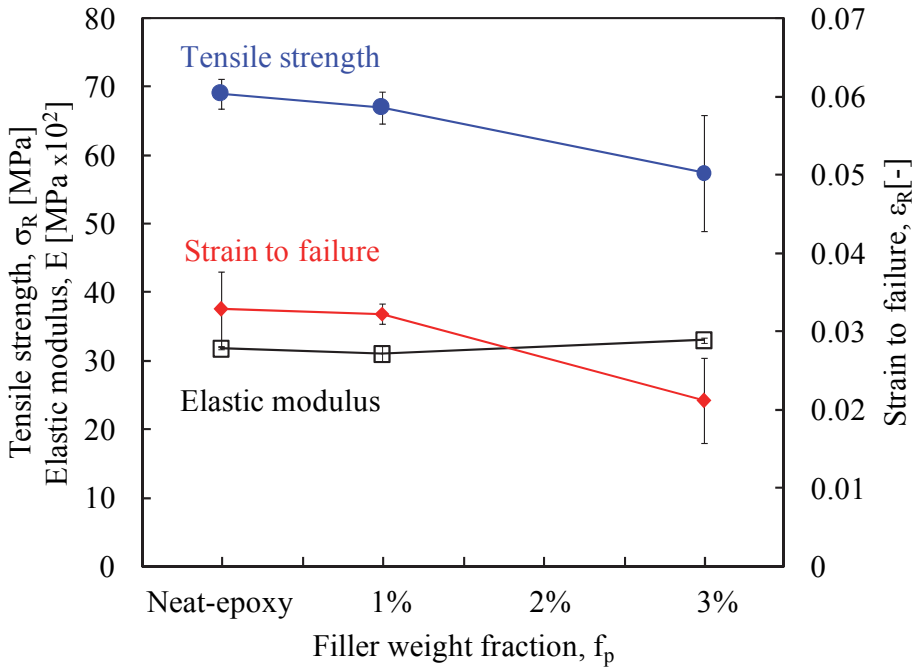

Figure 4. Effect of the nanomodification of the epoxy resin evaluated from tensile tests.

3.3 Mode I Fracture Tests

In agreement with the ASTM D5045-99 suggestions [24], fracture tests were carried out on CT specimens of which the geometry is shown in Figure 1b. After demoulding, specimens were pre-cracked by manual tapping, obtaining artificial short cracks. Then 10mm long cracks (double the specimen width) were obtained by applying some zero-to-tension fatigue cycles.

Samples were tested using a MTS858 servo-hydraulic machine equipped with a 2.5kN load cell and experimental results were re-arranged according to the following expression to compute the Mode I fracture toughness [24]:

$$K_{Ic} = \frac{P_{cr}}{B\,W^{0.5}}\, f\left(\frac{a}{W}\right) \tag{1}$$

where P_{cr} is the critical load, B, a and W are defined in Figure 1b, and f(a/W) can be assessed as [8]:

$$f\left(\frac{a}{W}\right) = \frac{\left(2+\frac{a}{W}\right)\left[0.886+4.64\frac{a}{W}-13.32\left(\frac{a}{W}\right)^2+14.72\left(\frac{a}{W}\right)^3-5.6\left(\frac{a}{W}\right)^4\right]}{\left(1-\frac{a}{W}\right)^{1.5}} \tag{2}$$

with $0.2 < \frac{a}{W} < 0.8$.

Three values of K_{Ic} have been obtained for each material configuration and results, in terms of average values, are reported in Figure 5.

Different from tensile properties, the mode I fracture toughness of the epoxy resin has been enhanced by nanomodification: the K_{Ic} of 0.96MPa·$m^{0.5}$ of the neat-epoxy is increased to 1.23MPa·$m^{0.5}$ (about +30%) with a filler weight fraction of 3% of nanoclay. The improvement is even more significant when considering the already high toughness of the neat resin.

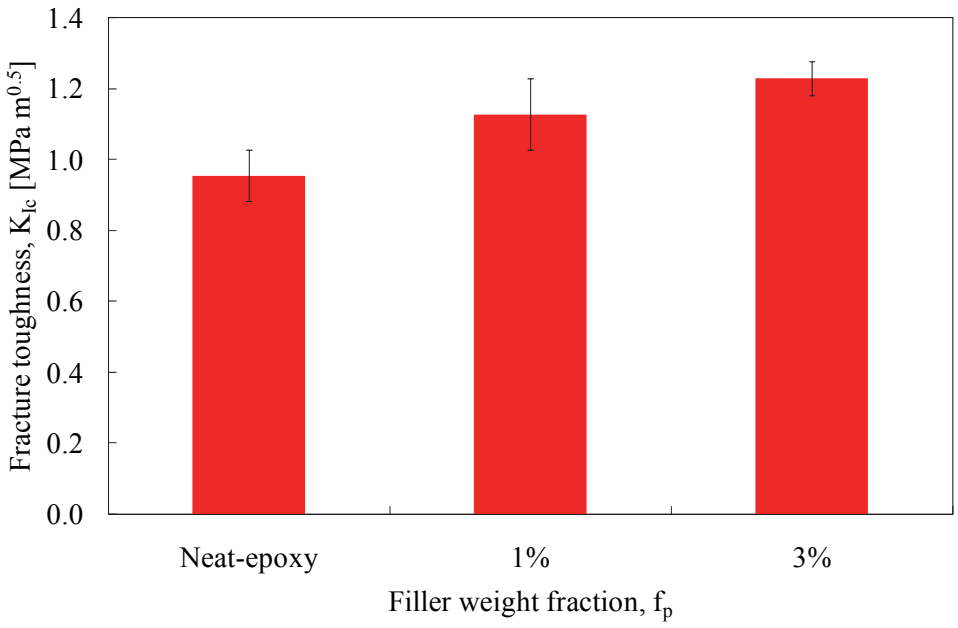

Figure 5. Effect of the nanomodification of the epoxy resin evaluated from CT tests.

3.4 Morphological analysis of the fracture surfaces

A morphological analysis of the fracture surfaces of nanomodified CT specimens with 3wt% of clay content was carried out by means of a Quanta400 FEI scanning electron microscope and are shown in Figure 6. It is evident that nanoclays developed a micrometric clustered structure, with agglomerates up to a size of some μm. Moreover, a significant roughness is evident on the fracture surface, caused by pronounced crack deflections and cluster ruptures. Such a kind of fracture surface is typical of intercalated platelets [11, 12].

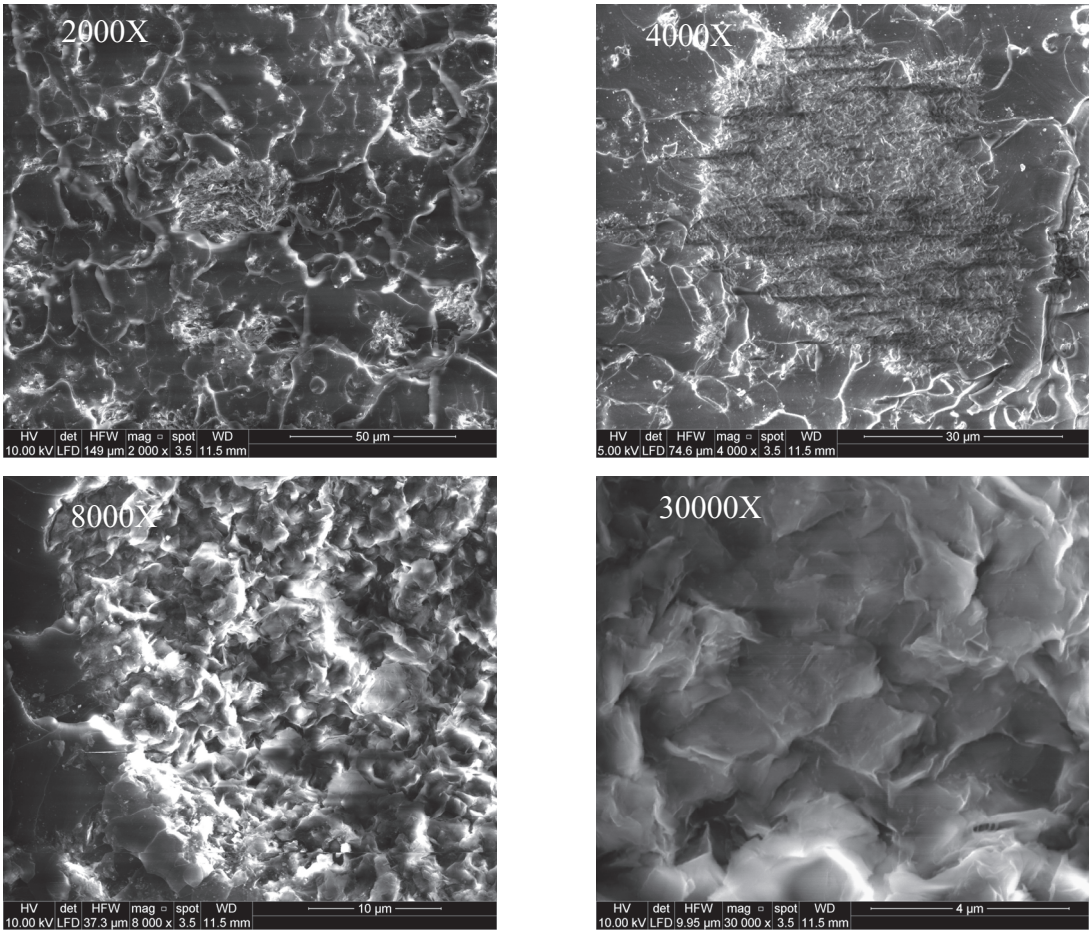

Figure 6. SEM images of the fracture surface of CT specimens with 3wt% of clay content.

3.4. Evaluation of the biological activity

Besides the improvements in polymer toughness, polymer loading through MMT nanoclays also offers great potential in terms of anti-microbial properties [16-18], thus assisting in the achievement of self-decontaminating surfaces.

In the present work, the antibacterial activity was evaluated against E.coli ATCC 8739 and S.Aureus ATCC 6538P selected as examples of gram-negative and gram-positive bacteria, respectively. Bacteria and culture media were provided by VWR International PBI SrL.

Initially, the Minimum Inhibitory Concentration (MIC) of Nanomer I.30E was determined by a broth dilution method, as recommended in [25]. To this end, Nanomer I.30E was diluted in Tryptic Soy Broth (TSB) gradually and the bacteria was added to achieve a bacterial concentration of 1-2x10^5UFC/mL. MIC was read after 24h of incubation at 37°C by comparing the turbidity with respect to standard samples of MMT. MIC was determined in the range 62.5-125.0ppm only for *S.Aureus*, but not clearly for

E.Coli. Thus a different procedure was carried out improving the direct contact between Nanomer I.30E and cells.

Bacterial suspensions containing $5x10^6$CFU/mL were distributed on 20mL plate count Agar (PCA) in Petri capsules and water suspensions (20μL) containing different amounts of Nanomer I.30E (in the range 46-100000ppm) were added. The results are reported in Table 1 where it can be observed that for *E.Coli* MIC value was in the range 1563-3125ppm and for *S. Aureus* in the range 91-181ppm, indicating a significantly higher antimicrobial activity against *S.Aureus* as previously reported for ammonium quaternary salts bearing long aliphatic chains [22].

Subsequently, the antibacterial activity of the surfaces of nanomodified specimens was evaluated using unbroken CT specimens (see Figure 1b). The tested samples ($4cm^2$) were submitted for 24 h to a sterilizing UV irradiation, coated ($25\mu L/cm^2$) with 100μL of bacteria in a Tryptic Soy Broth suspension (1:500) containing 10^6-10^7 cells and incubated 24h at 37°C. The bacteria were recovered by adding 10mL of soybean casein digest with lecithin and polysorbate neutralizer broth (SCDLP: 17.0g of casein peptone, 3.0g of soybean peptone, 5.0 of sodium chloride, 2.5g of sodium hydrogen phosphate, 2.5g of D-glucose, 1.0g of lecitine and 7.0g of Tween 80 in 1000mL of deionized water) according to the ISO 22196 suggestions [26]. The viable bacteria were enumerated by performing successive 10-fold serial dilutions in phosphate buffered physiological saline (34g/l di KH_2PO_4 diluted 1:800 in physiological solution) of the 10mL suspension recovered from the test specimen. Samples of 1mL of each dilution were put into sterilized Petri dishes, together with 15mL of a plate count agar. The suspensions were gently swirled to disperse the bacteria and incubated at 35°C for 40h. All the platings were performed in duplicate. After incubation, the number of colonies of each dilution was counted and the mean values of the counts below 300 UFC/mL were reported. The data have been compared with reference samples.

The antimicrobial activity of the nanocomposite containing different amounts of clay was established by comparing the initial number of UFC of E.coli and S. Aureus to the final number of bacterial colonies after contact. The antibacterial activity was very high (Table 2), in particular against S.Aureus, and it was shown to be dependent from the clay amount; in the case of 3%wt of clay addition the killing percentage is close to 88%. Representative photographs of the test discs on the agar plates are shown in Figure 7,

where the antimicrobial activity of samples with different clay content is compared as well.

MMTNH4+ [mg/L]	ESCHERICHIA COLI	STRAPHILOCOCCUS AUREUS
100.000	–	–
50.000	–	–
25.000	–	–
12.500	–	–
6.250	–	–
3.125	–	–
1563	+	–
782	+	–
361	+	–
181	+	–
91	+	+
46	+	+

Table 1. MIC of Nanomer I.30E against E.Coli and S. Aureus, where "–" stands for inhibited growth while "+" means non-inhibited growth.

	E.Coli		S.Aureus	
Filler %wt	UFC/25μL	% Kill	UFC/25μL	% Kill
Base resin	8.5×10^6	-	1.4×10^6	-
1%	7.5×10^6	11.8	2.5×10^5	82.1
3%	4.3×10^5	94.9	1.7×10^5	87.9

Table 2. Antimicrobial activity of specimens made of neat resin and nanomodified polymer.

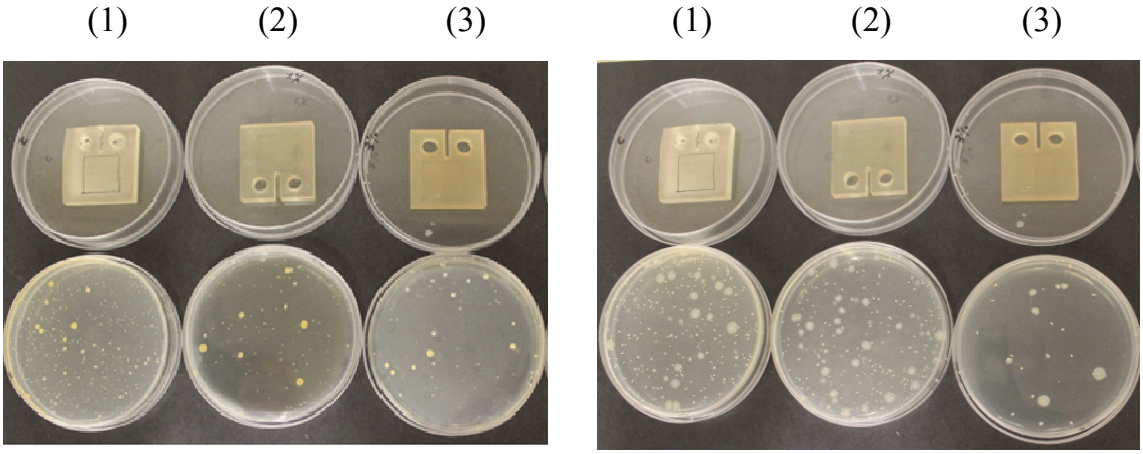

Figure 7. Images of agar-plates from antimicrobial tests on neat and nanomodified polymers. (a) against S.Aureus and (b) against E.coli. (1) neat polymer; (2) 1%wt of I30E; (3) 3%wt of I30E.

4. TERNARY NANOCOMPOSITES: NANOMODIFIED LAMINATES

4.1 Mechanical testing and results

For ternary (nanomodified) laminates, the matrix toughness improvement itself is the most interesting and promising result, the interlaminar fracture behaviour of long fibre-reinforced composites being a weak matrix dominated property. In the previous section it was proved that nanomodified epoxy resin exhibits higher fracture properties with respect to the neat resin. In this section, the capability of translating the improved mechanical properties of the resin to fibre reinforced composites is analysed by discussing the laminate interlaminar properties evaluated through ILSS and DCB tests.

DCB tests were carried out following the guidelines reported in ASTM D5528 [27]. For each composite 3 specimens were tested and the crack propagation was monitored by means of a travelling stereoscope. The crosshead speed was set to 0.5mm/min. The resulting critical energy release rate, G_{Ic}, was evaluated by means of the modified compliance calibration method (MCC) and the initiation values were measured according to the 5% offset method. The results are reported in Figures 8 and 9 where it is evident that the nanomodified laminates exhibit a comparable interlaminar fracture toughness, with respect to the base laminates, both in terms of crack initiation and propagation.

In addition, ILSS tests were carried out according to the ASTM D2344 suggestions [28]. The specimen thickness was 4mm and the span was 16mm. The crosshead speed was set at 1mm/min and five specimens were tested for each material configuration. During the

tests all specimens failed by delamination. The results, reported in Figure 10, show that the interlaminar shear strength exhibits a slight reduction with the increase of the nanoclay content.

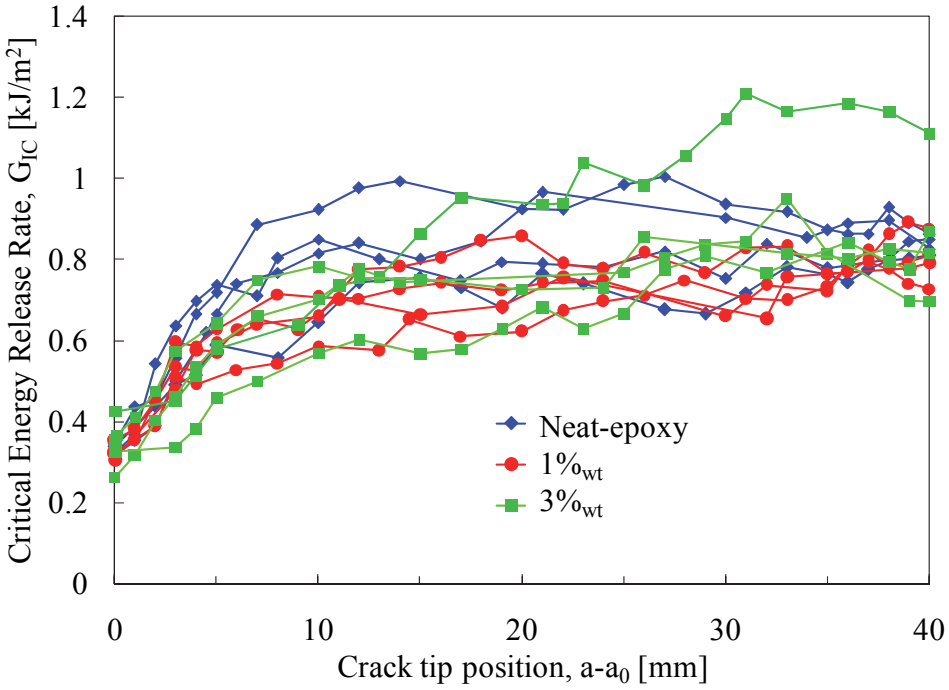

Figure 8. R-curves obtained from the DCB tests.

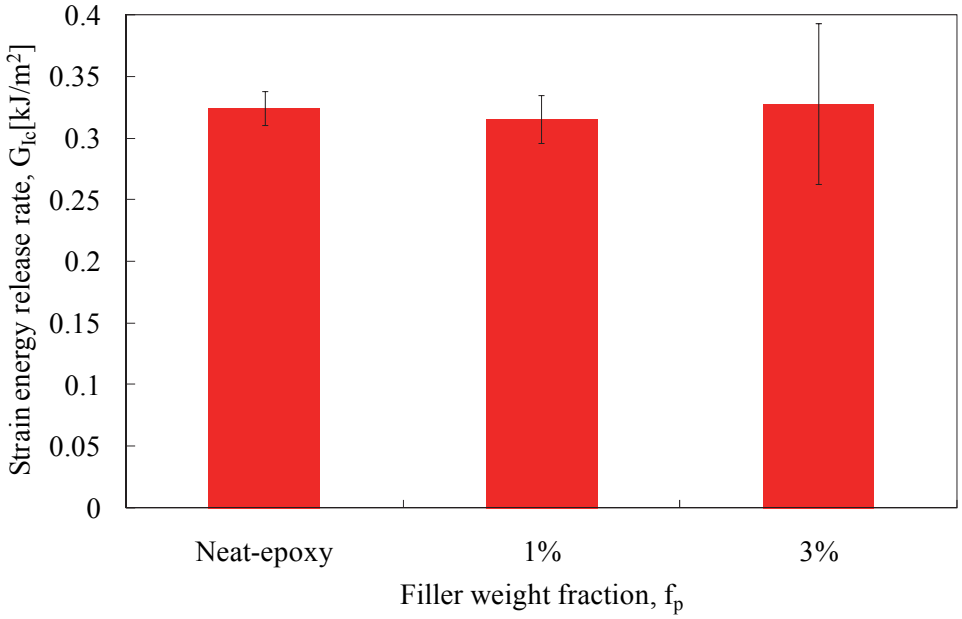

Figure 9. Initiation values of the R-curves from DCB tests.

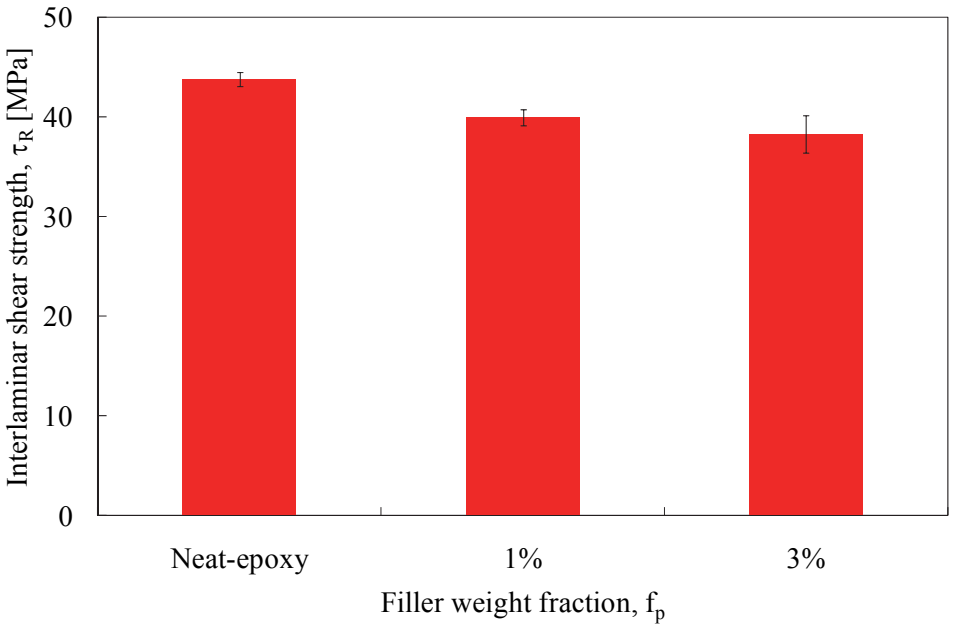

Figure 10. Laminate interlaminar shear strength obtained from ILSS tests.

4.2. Evaluation of the biological activity

As for binary nanocomposites, the antibacterial activity of nanomodified laminates was evaluated against E.coli ATCC 8739 and S.Aureus, ATCC 6538P. To this end the same standardized procedure presented in section 3.4 was followed, in agreement with the ISO 22196 suggestions [26]. In this case, the 4cm^2 tested samples were directly cut from DBC specimens.

Quantitative results are reported in Table 3 and representative photographs of test discs on the agar plates are shown in Figure 11 where the antimicrobial activity of samples with different clay content is presented.

Comparing Tables 2 and 3 it can be noted that the antimicrobial activity is higher in the case of nanomodified laminates with respect to nanomodified polymers, the killing percentage rising up to 97%.

	E.Coli		S.Aureus	
Filler %wt	UFC/25µL	% Kill	UFC/25µL	% Kill
Base resin	1.9 x10^7	-	2.8 x10^7	-
1%	7.6 x10^6	60.0	3.5 x10^6	87.5
3%	6.1 x10^5	96.8	1.7 x10^6	94.0

Table 3. Antimicrobial activity of neat and nanomodified laminates.

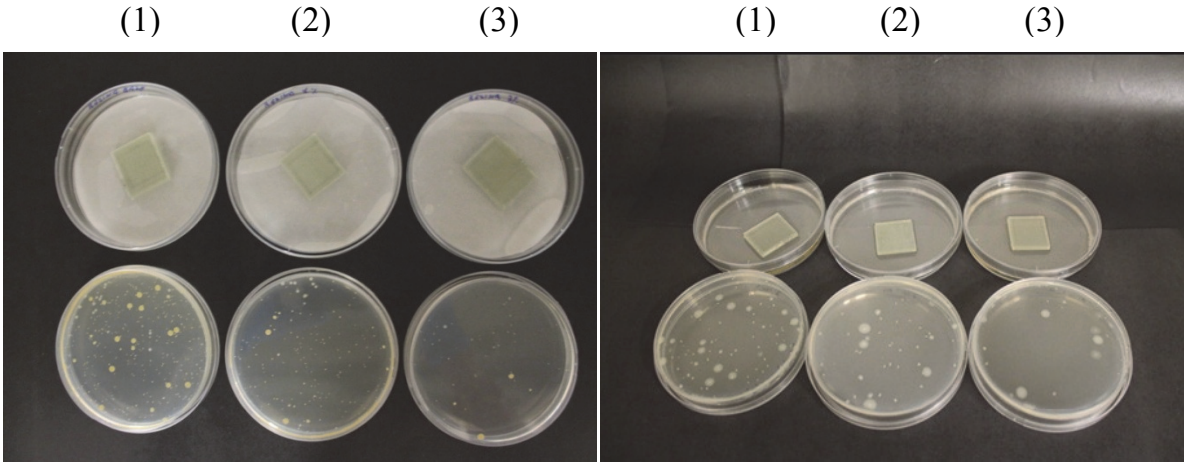

Figure 11. Images of agar-plates from antimicrobial tests on neat and nanomodified laminates. (a) against S.Aureus and (b) against E.coli. (1) neat polymer; (2) 1%wt of I30E; (3) 3%wt of I30E.

5. CONCLUSIONS

In this work the possibility to obtain binary and ternary polymer nanocomposites with enhanced mechanical and anti-microbial properties was investigated. To this end a DGEBA-based epoxy resin was loaded using montmorillonite clays and later used as matrix for glass reinforced laminates. Both binary and ternary nanomodified specimens were manufactured and subjected to mechanical testing. Moreover an accurate analysis of the effect of nanomodification on the biological activity was carried out.

The relevant results can be summarised as follows:

1. As far as binary nanocomposites are concerned, modification of the polymer resin with Nanomer I.30E enhanced the polymer fracture toughness (+30%). At the same time a considerably increase of the antimicrobial activity against E.coli ATCC 8739 and S.Aureus ATCC 6538P was obtained, with killing percentage close to 88%.
2. Moving to ternary nanocomposites, results indicated that nanomodification is less effective in terms of mechanical properties, nanomodified laminates exhibiting only a slightly improved, or almost comparable, interlaminar fracture toughness, with respect to the base ones. Differently, the antimicrobial activity is considerably enhanced, with a killing percentage of 94%. In particular the antimicrobial property of the ternary nanocomposite with respect to E.Coli results of the same order of magnitude of the binary one.

Further analyses need be carried out, introducing the post-curing treatment in the specimen manufacturing.

ACKNOWLEDGMENTS
The authors acknowledge the financial support to the activity by Veneto Nanotech, the Italian cluster of Nanotechnology, and by CARIVERONA Foundation, (within the frame "Contributo di Fondazione Cariverona a valere sui finanziamenti alla ricerca scientifica e tecnologica per l'anno 2012").

REFERENCES

[1] Fischer, H. (2003). Polymer nanocomposites: from fundamental research to specific applications. Materials Science and Engineering: C, 23(6), 763-772.

[2] Thostenson, E. T., Li, C., & Chou, T. W. (2005). Nanocomposites in context.Composites Science and Technology, 65(3), 491-516.

[3] Ajayan, P. M., Schadler, L. S., & Braun, P. V. (2006). Nanocomposite science and technology. John Wiley & Sons.

[4] Cho, J. W., & Paul, D. R. (2001). Nylon 6 nanocomposites by melt compounding. Polymer, 42(3), 1083-1094.

[5] Wang, L., Wang, K., Chen, L., Zhang, Y., & He, C. (2006). Preparation, morphology and thermal/mechanical properties of epoxy/nanoclay composite.Composites Part A: Applied Science and Manufacturing, 37(11), 1890-1896.

[6] Liu, T. X., Liu, Z. H., Ma, K. X., Shen, L., Zeng, K. Y., & He, C. B. (2003). Morphology, thermal and mechanical behavior of polyamide 6/layered-silicate nanocomposites. Composites science and technology, 63(3), 331-337.

[7] Lee, D. C., & Jang, L. W. (1996). Preparation and characterization of PMMA–clay hybrid composite by emulsion polymerization. Journal of Applied Polymer Science, 61(7), 1117-1122.

[8] Luo, J. J., & Daniel, I. M. (2003). Characterization and modeling of mechanical behavior of polymer/clay nanocomposites. Composites Science and Technology, 63(11), 1607-1616.

[9] Bharadwaj, R. K., Mehrabi, A. R., Hamilton, C., Trujillo, C., Murga, M., Fan, R., ... & Thompson, A. K. (2002). Structure–property relationships in cross-linked polyester–clay nanocomposites. Polymer, 43(13), 3699-3705.

[10] Wang, K., Chen, L., Wu, J., Toh, M. L., He, C., & Yee, A. F. (2005). Epoxy nanocomposites with highly exfoliated clay: mechanical properties and fracture mechanisms. Macromolecules, 38(3), 788-800.

[11] Quaresimin, M., Salviato, M., & Zappalorto, M. (2012). Fracture and interlaminar properties of clay-modified epoxies and their glass reinforced laminates. Engineering Fracture Mechanics, 81, 80-93.

[12] Zappalorto, M., Salviato, M., & Quaresimin, M. (2013). Mixed mode (I+ II) fracture toughness of polymer nanoclay nanocomposites. Engineering Fracture

Mechanics, 111, 50-64.

[13] Becker, O., Varley, R. J., & Simon, G. P. (2003). Use of layered silicates to supplementarily toughen high performance epoxy-carbon fiber composites.Journal of materials science letters, 22(20), 1411-1414.

[14] Quaresimin, M., & Varley, R. J. (2008). Understanding the effect of nano-modifier addition upon the properties of fibre reinforced laminates. Composites Science and Technology, 68(3), 718-726.

[15] Timmerman, J. F., Hayes, B. S., & Seferis, J. C. (2002). Nanoclay reinforcement effects on the cryogenic microcracking of carbon fiber/epoxy composites. Composites Science and Technology, 62(9), 1249-1258.

[16] Roy, B., Bharali, P., Konwar, B. K., & Karak, N. (2014). Modified hyperbranched epoxy/clay nanocomposites: A study on thermal, antimicrobial and biodegradation properties. International Journal of Materials Research,105(3), 296-307.

[17] Kubo, T., Yasuda, K., Tominaga, Y., Otsuka, K., & Hosoya, K. (2013). Antibacterial activities effectuated by co-continuous epoxy-based polymer materials. Colloids and Surfaces B: Biointerfaces, 107, 53-58.

[18] Moore, S. L., & Payne, D. N. (2004). Types of antimicrobial agents. Russell Hugo & Ayliffe's Principles and Practice of Disinfection Preservation & Sterilization, 8-97.

[19] Mondrzyk, A., Fischer, J., & Ritter, H. (2014). Antibacterial materials: structure–bioactivity relationship of epoxy–amine resins containing quaternary ammonium compounds covalently attached. Polymer International.

[20] Timofeeva, L., & Kleshcheva, N. (2011). Antimicrobial polymers: mechanism of action, factors of activity, and applications. Applied microbiology and biotechnology, 89(3), 475-492.

[21] Gozzelino, G., Lisanti, C., & Beneventi, S. (2013). Quaternary ammonium monomers for UV crosslinked antibacterial surfaces. Colloids and Surfaces A: Physicochemical and Engineering Aspects, 430, 21-28.

[22] Harney, M. B., Pant, R. R., Fulmer, P. A., & Wynne, J. H. (2008). Surface self-concentrating amphiphilic quaternary ammonium biocides as coating additives.ACS applied materials & interfaces, 1(1), 39-41.

[23] ISO 527-2: Plastics. Determination of tensile properties (2012).

[24] ASTM D5045. Standard test methods for plane-strain fracture toughness and strain energy release rate of plastic materials (1999).

[25] NCCLS. Methods for dilution antimicrobial susceptibility tests for bacteria that grow aerobically: approved standard, 5th ed. (2000).

[26] ISO 22196. Measurement of antibacterial activity on plastics and other non-porous surfaces (2011).

[27] ASTM D5528-13. Standard test method for mode I interlaminar fracture toughness of unidirectional fiber-reinforced polymer matrix composites (2013).

[28] ASTM D2344. Standard test method for short beam strength of polymer matrix composite materials and their laminates (2005).

MODELLING

5 Influence of interphase and filler distribution on the elastic properties of nanoparticle filled polymers

KEYWORDS: A. Nanoparticles; B. Nanocomposites; C. Interphase; D. Elastic properties

ABSTRACT
The assessment of nanocomposite mechanical properties is a challenging task. Their hierarchical structure, spanning from nano to macro length-scales, urges to account for the characteristic phenomena of each length-scale and to bridge their effects from the smaller scale to the macroscale.
In the present chapter two different approaches for the estimation of the elastic modulus of a nanoparticle filled polymer are proposed and compared. Both models account for the emergence of an interphase layer embedding the nanoparticle, with mechanical properties different from those of the matrix.

1. INTRODUCTION

One of the most interesting features characterizing nanocomposite material is that they offer outstanding improvements of mechanical and physical properties at very low filler concentrations, thus assisting in the achievement of high-level performances across various engineering applications.

In nanomodified polymers, as the filler size is decreased to the nanoscale, intra- and supra-molecular interactions lead to the emergence of an interphase zone whose properties differ from those of both constituents and whose thickness may be comparable to the particle size. Sevostianov and Kachanov [1] showed that the effect of such interphase on the overall mechanical properties can be substantial, depending on the ratio of the interphase thickness to the particle size and the variability of the properties across the interface thickness.

Moreover other complexities which may arise in the material configuration, such as macromolecular chain entanglement or imperfect bonding, can be accounted for through the “apparent” elastic properties of the interphase.

In this chapter two different approaches for the estimation of the elastic modulus of a nanoparticle filled polymer are analyzed and compared. Both of them account for the emergence of an interphase layer embedding the nanoparticle, with mechanical properties different from those of the matrix.

The first method makes use of Hashin and Shtrikman's micromechanical solution [2] within a two step-analysis and provides an analytical estimation of the elastic modulus of the nanocomposites, explicitly accounting for the size and properties of the interphase.

The second approach makes a combined use of the Voronoi cell concept and of the finite element method. This approach, initially proposed by Davy and Guild [3] for microparticle reinforced polymers, is based on the construction of a FE axisymmetrical cell of which the size depends on the nanoparticle radius and on the filler volume fraction and provides a numerical estimation of the global stiffness of the studied system.

Relevant results are discussed and compare with the aim to shown the influence of all the involved parameters.

2. A NANOSTRUCTURAL MODEL BASED ON HASHIN AND SHTRIKMAN'S SOLUTION

By using variational principles in the linear theory of elasticity, Hashin and Shtrikman [2] provided the upper and lower bounds for the effective elastic moduli, K* and G*, of an isotropic composite material comprising a matrix (m) and a filler (p):

$$K_m + \frac{f_p\left(K_p - K_m\right)}{1+(1-f_p)R_m\left(K_p - K_m\right)} \le K^* \le K_p + \frac{(1-f_p)\left(K_m - K_p\right)}{1+f_p R_p\left(K_m - K_p\right)} \tag{1a}$$

$$G_m + \frac{f_p\left(G_p - G_m\right)}{1+(1-f_p)Q_m\left(G_p - G_m\right)} \le G^* \le G_p + \frac{(1-f_p)\left(G_m - G_p\right)}{1+f_p Q_p\left(G_m - G_p\right)} \tag{1b}$$

where:

$$R_k = \frac{3}{3K_k + 4G_k}, \quad Q_i = \frac{6\left(K_k + 2G_k\right)}{5G_k\left(3K_k + 4G_k\right)} \quad k = m, p \tag{2}$$

f_p is the filler volume fraction and subscripts m and p refers to the matrix and the filler, respectively.

Eqs. (1) can be easily extended to account for the presence of a spherical interphase layer embedding the nanoparticle, with elastic properties different from those of the matrix, by using a two-step analysis.

Under the hypothesis of isolated particles, namely low volume fractions, and perfectly bonded surface (Figure 1a), each particle and the surrounding interphase material can be

changed for an "*equivalent homogeneous spherical particle (EHP)*" of radius a=r_0+t, being r_0 the radius of the original nanoparticles and t the interphase thickness (Figure 1b).

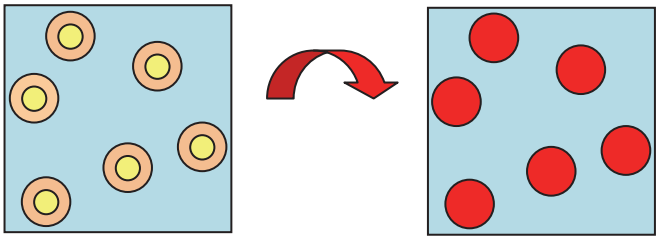

Figure 1. Conversion of the three-phase nanocomposite into an equivalent two-phase material.

Then, as a first step, the elastic properties of the *EHP*, K' and G', can be thought of as the lower bound of the effective elastic moduli of a two phase material constituted by the interphase and the nanoparticle only, which can be estimated according to Eqs. (1):

$$K' = K_i\left\{1+\frac{\left(\frac{r_0}{a}\right)^3\left(\frac{K_p}{K_i}-1\right)}{1+\left[1-\left(\frac{r_0}{a}\right)^3\right]\frac{1+\nu_i}{3(1-\nu_i)}\left(\frac{K_p}{K_i}-1\right)}\right\}$$

$$G' = G_i\left\{1+\frac{\left(\frac{r_0}{a}\right)^3\left(\frac{G_p}{G_i}-1\right)}{1+\left[1-\left(\frac{r_0}{a}\right)^3\right]\frac{8-10\nu_i}{15(1-\nu_i)}\left(\frac{G_p}{G_i}-1\right)}\right\} \quad (3)$$

As a second step, the elastic properties of the nanocomposite, K_C and G_C, can be assessed through the lower bound of the effective elastic moduli of the two phase material constituted by the matrix and the *EHP*:

$$K_C = K_m\left\{1+\frac{f_p\left(\frac{a}{r_0}\right)^3\left(\frac{K'}{K_m}-1\right)}{1+\left[1-f_p\left(\frac{a}{r_0}\right)^3\right]\frac{1+\nu_m}{3(1-\nu_m)}\left(\frac{K'}{K_m}-1\right)}\right\} \quad (4a)$$

$$G_C = G_m\left\{1+\frac{f_p\left(\frac{a}{r_0}\right)^3\left(\frac{G'}{G_m}-1\right)}{1+\left[1-f_p\left(\frac{a}{r_0}\right)^3\right]\frac{8-10\nu_m}{15(1-\nu_m)}\left(\frac{G'}{G_m}-1\right)}\right\} \quad (4b)$$

Finally the modulus of elasticity in tension of the nanocomposite, E_C, can be determined as:

$$E_C = \frac{9K_C G_C}{3K_C + G_C} \tag{5}$$

The validity of Eqs. (4a) and (4b) is hampered by the condition $f_p\left(\frac{a}{r_0}\right)^3 < 1$, providing the following limitation on the interphase thickness t:

$$t < r_0 \frac{1-\sqrt[3]{f_p}}{\sqrt[3]{f_p}} \tag{6}$$

It is worth mentioning here that a "two-step" analysis using Hashin's solution has also been proposed by Dorigato *et al.* [4] with the aim to take into account agglomeration effects arising in nanocomposites. However in the first step of their analysis, Dorigato et al. [4] suggested to use the upper bound Eq. (1) instead of the lower one, as proposed in the present work.

3 A FE APPROACH BASED ON THE VORONOI CELL

The Voronoi cell approximation was developed by Davy and Guild [3] with the aim to determine the stiffening effects due to spherical particles within a matrix using finite element analysis, under the hypothesis of homogeneous Poisson process of particles, with a further correction to account for the non-overlapping of particles. The Voronoi cell surrounding each particle is defined as the set of points belonging to the space which is regarded as the domain of the distribution, characterized by being closer to the center of the particle belonging to that cell than to every other center of particle in the material [3] (Figure 2a). Generally speaking, this cell can be much irregular; in order to overcome this Davy and Guild [3] proposed to reshape it into a cylinder with the same volume. This approximation is consistent with the nature of the stress state around a spherical particle under uniaxial loading [5, 6]. The size of the equivalent cylinder is defined by the following averaged radius (Figure 2b):

$$\overline{R} = \sqrt[3]{\frac{2}{3f_p}}\, r_0 \tag{7}$$

Where r_0 is the radius of the spherical filler and f_p the volume fraction.

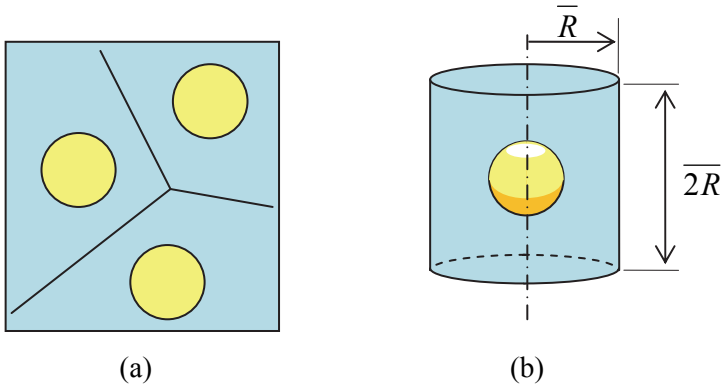

Figure 2. (a) Schematic representation of Voronoi's cells surrounding particles in a 2D space. (b)The equivalent Voronoi's cell proposed by Davy and Guild [5].

The method proposed by Davy and Guild is modified here to account for an interphase layer embedding the nanoparticle, with elastic properties different from those of the matrix (see Figure *3*a). Such a region is assumed to be homogeneous, with uniform elastic properties. By doing so, the outer interphase radius, $t+r_0$, should always be lower than $\overline{R}$, so that the following condition on the on the interphase thickness holds :

$$t \le r_0\left(1-\sqrt[3]{\frac{2}{3f_p}}\right) \tag{8}$$

The equivalent Voronoi cell can be used within a finite element analysis with the aim to determine the elastic modulus of the nanocomposite by simply evaluating the global stiffness of the cell. The polar symmetry of the analyzed system allows one to use axi-symmetric plane elements for the finite element analysis. With reference to Figure 3b, symmetric boundary conditions can be used, along *AB*, further reducing the complexity of the analysis. An example of the mesh used in the FE models is shown in Figure 3c.
The boundary conditions applied to the cell are shown in Figure 3 and can be summarized as follows:

1. all nodes along BC are constrained to the same displacement u_x;
2. all nodes along DC are constrained to the same displacement u_y;
3. a constant stress $\overline{\sigma}$ is finally applied along DC.

Accordingly, the averaged stiffness of the FE cell can be calculated as follows:

$$\overline{E}=\frac{\sigma}{\varepsilon}=\frac{\sigma}{\delta\overline{R}^{-1}} \tag{9}$$

where δ is the u_y displacement of the nodes along *DC*.

In addition a statistical correction, (E_{corr}) related to particle dispersion, can be introduced. The elastic modulus of the nanocomposite can be finally estimated according to the following expression:

$$\frac{1}{E_c} = \frac{1}{\overline{E}} + \frac{1}{E_{corr}} \qquad \frac{1}{E_{corr}} = \frac{1}{2}\left(\frac{\overline{R}^3}{r_0^3}\right)\left(\frac{R^3}{r_0^3 E}\right)^{II} CV(f_P) \tag{10a-b}$$

The second order differential term in Eqs. (10 a-b), $\left(\frac{R^3}{r_0^3 E}\right)^{II}$, can be approximated, using the finite difference method, as:

$$\left(\frac{R^3}{r_0^3 E}\right)^{II} = \left(\frac{R_1^3}{r_0^3 E_1} + \frac{R_2^3}{r_0^3 E_2} - 2\frac{\overline{R}^3}{r_0^3 \overline{E}}\right)\Big/\Delta^2 \tag{11}$$

where E_1 and E_2 are the averaged Young modulus associated to cells of radius R_1 and R_2:

$$\frac{R_{1,2}^3}{r_0^3} = \frac{\overline{R}^3}{r_0^3} \pm \Delta \tag{12}$$

Being Δ the step size (convenient values of Δ are listed in Table 1).

The coefficient of variation, *CV*, accounting for particle statistical distribution can be calculated as follows:

$$CV(f_p) = \left[\left(f_p^{\,2}/1.1108\right)\left(1 - 2\int_0^1 u^{-3} e^{\left(-k\left(u^{-1}+3u^{\frac{1}{3}}-4\right)\right)} du\right)\right] - 1 \tag{13}$$

where k can be obtained from the following equation:

$$\frac{1-f_p}{f_p} = \int_0^1 u^{-2} e^{\left(-k\left(u^{-1}+3u^{\frac{1}{3}}-4\right)\right)} du \tag{14}$$

f_P	Δ	CV	f_P	Δ	CV
0.02	8	0.705579	0.1	1	0.4652
0.04	6	0.632405	0.2	0.6	0.27647
0.06	4	0.569664	0.3	0.4	0.14935
0.08	2	0.514471	0.4	0.2	0.061194

Table 1.Values for CV and Δ, as a function of f_P, to be used in Eq. (10) and Eq. (11).

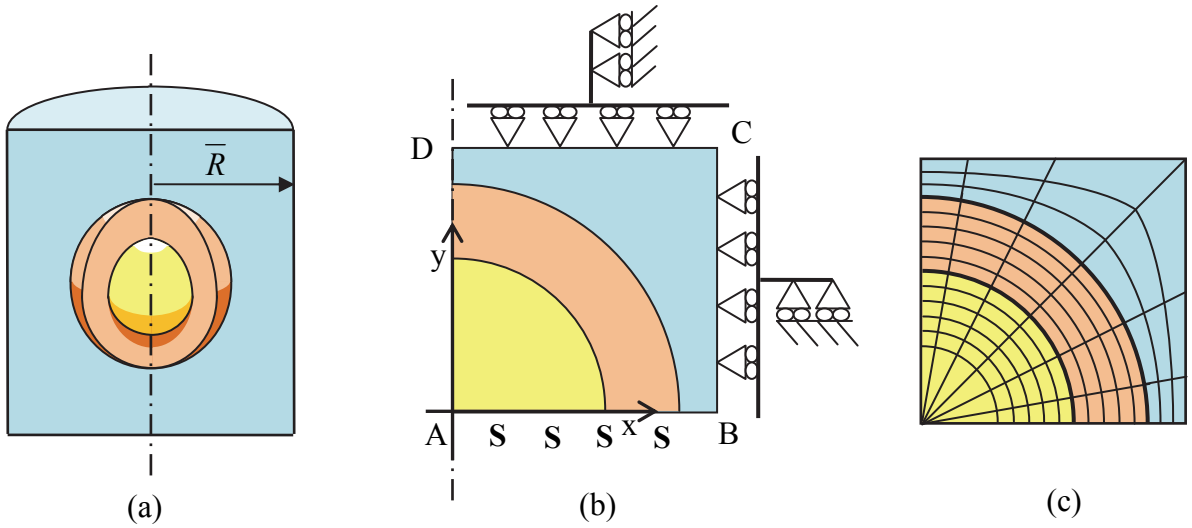

Figure 3. (a) The equivalent Voronoi cell proposed to account for an interphase layer. (b) Geometry and boundary conditions of the axis-symmetric cell used in the FE calculations. (c) Example of the mesh used in the FE analyses.

5. RESULTS AND DISCUSSION

The aim of this section is to compare the results which can be obtained with the model proposed.

Figure 4 shows the values of the normalized elastic modulus, E_c/ E_m, where E_m is the Young modulus of the polymer matrix, versus the nanoparticle radius. The effect of the interphase thickness and of the nanoparticle size is evident. For a given value of t, the smaller the particle size the higher the overall elastic modulus. Conversely, as the nanoparticle size increases, the overall elastic modulus asymptotically decreases. This effect is due to the reduced influence of the interphase for larger nanoparticles. It is also evident that beyond particle radii greater that about 70nm, independently of the interphase thickness, the nanocomposite elastic modulus tends towards the same constant value.

Differently, Figure 5 shows the effect of the elastic properties of the interphase on the normalised elastic modulus of the nanocomposite. It is evident that as the interphase elastic stiffness increases the nanocomposite elastic modulus increases, while for softer interphases the nanocomposite stiffness is lower than that of the matrix.

Figures 4 and 5 also show that the results obtained by using the two analyzed method are in good agreement as far as conditions given by Eq. (6) and Eq. (8) are guaranteed.

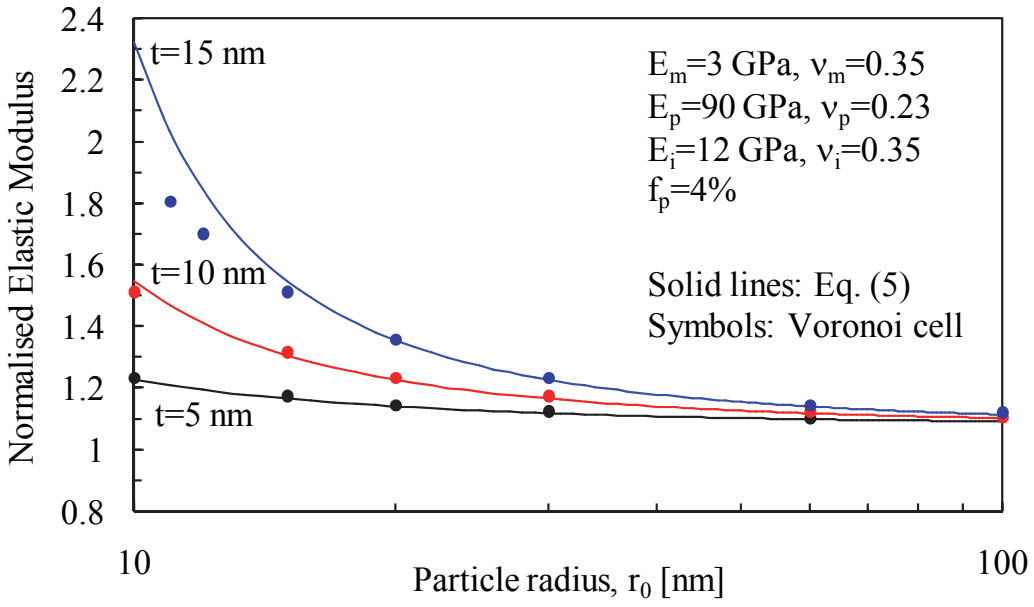

Figure 4. Effect of the particle radius and of the interphase thickness on the normalized nanocomposite elastic modulus. Comparison between Eq. (5) and Eq. (10a).

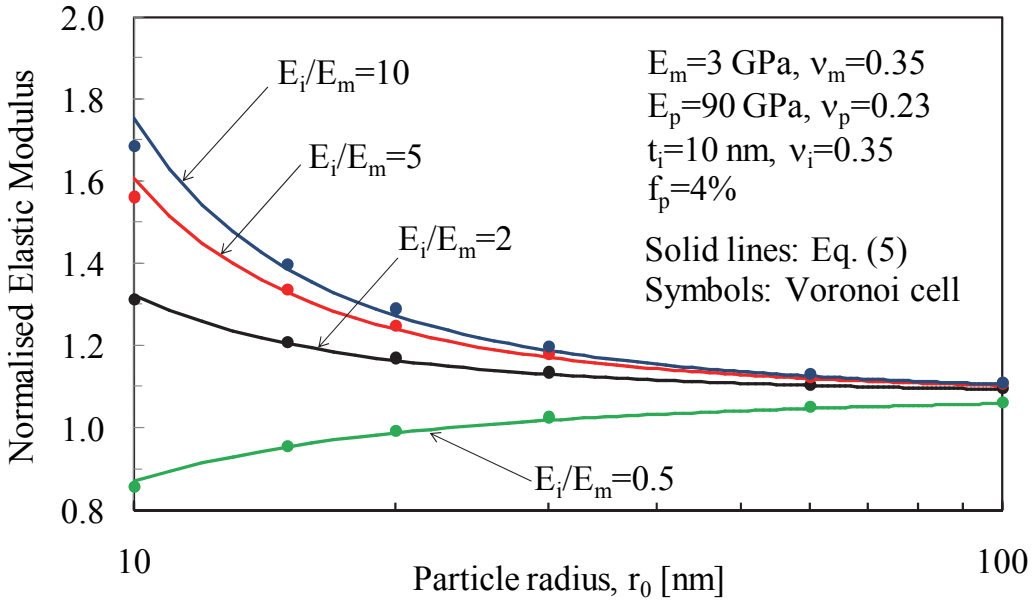

Figure 5. Effect of the particle radius and of the E_i/E_m ratio on the normalized nanocomposite elastic modulus. Comparison between Eq. (5) and Eq. (10a).

Finally Figure 6 shows the normalized elastic modulus of the nanocomposite versus the nanofiller volume fraction for different interphase thickness. It is evident that, for a given

value of f_p, the thicker the interphase layer, the higher the overall elastic modulus. Moreover, it is evident that both methods predict an elastic modulus monotonically increasing as a function of the nanoparticle volume fraction. This trend disagrees with the behaviour of "*stiffness leveling*" exhibited by the experimental data which is universally acknowledged to be due to aggregation effects arising at higher volume fractions and which are, by hypothesis, neglected by the models proposed in the previous sections.

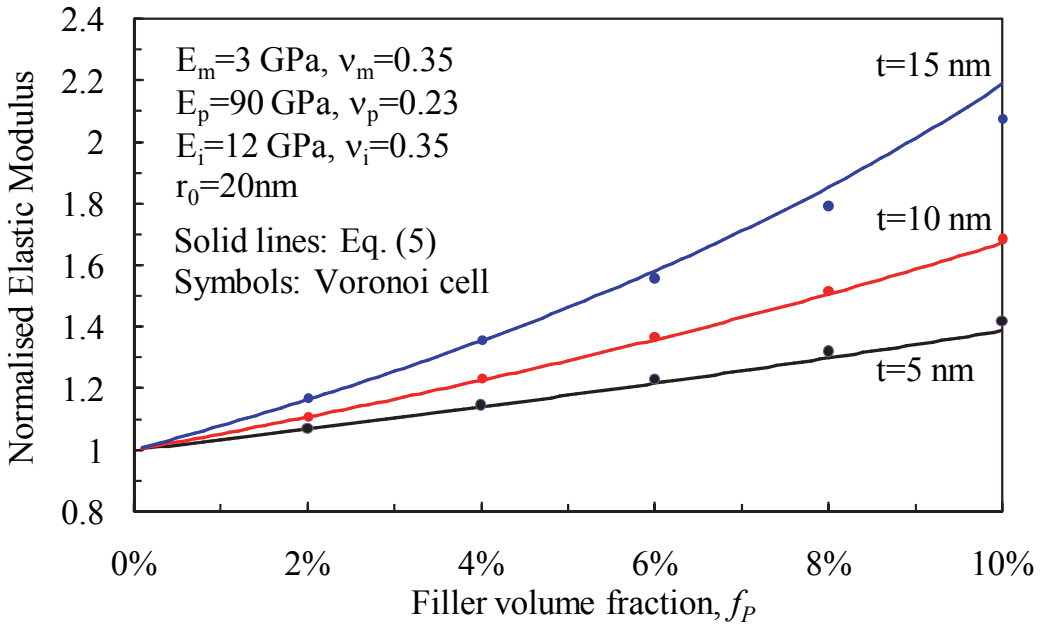

Figure 6. Effect of the filler volume fraction and of the interphase thickness on the normalized nanocomposite elastic modulus. Comparison between Eq. (5) and Eq. (10a).

6. CONCLUSIONS

In this work two different approaches for the estimation of the elastic modulus of a nanoparticle filled polymer are analyzed and compared. Both the proposed models account for the emergence of an interphase layer embedding the nanoparticle, with mechanical properties different from those of the matrix. It has been shown that both models are able to seize the effect of the interphase thickness and elastic properties. Moreover the models are able to account for the nanoparticle size, the smaller the particle radius the higher the overall elastic modulus.

ACKNOWLEDGEMENTS
The financial support to the activity by Veneto Nanotech, the Italian cluster of Nanotechnology, is greatly acknowledged.

REFERENCES

[1] Sevostianov, I., & Kachanov, M. (2007). Effect of interphase layers on the overall elastic and conductive properties of matrix composites. Applications to nanosize inclusion. International Journal of Solids and Structures, 44(3), 1304-1315.

[2] Hashin, Z., & Shtrikman, S. (1963). A variational approach to the theory of the elastic behaviour of multiphase materials. Journal of the Mechanics and Physics of Solids, 11(2), 127-140.

[3] Davy, P. J., & Guild, F. J. (1988). The distribution of interparticle distance and its application in finite-element modelling of composite materials. Proceedings of the Royal Society of London. A. Mathematical and Physical Sciences,418(1854), 95-112.

[4] Dorigato, A., Dzenis, Y., & Pegoretti, A. (2011). Nanofiller aggregation as reinforcing mechanism in nanocomposites. Procedia Engineering, 10, 894-899.

[5] Goodier, J. N. (1933). Concentration of stress around spherical and cylindrical inclusions and flaws. J. appl. Mech, 55(7), 39-44.

[6] Zappalorto, M., Salviato, M., & Quaresimin, M. (2012). Stress distributions around rigid nanoparticles. International Journal of Fracture, 176(1), 105-112.

[7] Chen, C. H., Jian, J. Y., & Yen, F. S. (2009). Preparation and characterization of epoxy/γ-aluminum oxide nanocomposites. Composites Part A: Applied Science and Manufacturing, 40(4), 463-468.

[8] Salviato, M., Pontefisso, A., Zappalorto, M., Santi, M., De Rossi, N., & Quaresimin, M. FRACTURE THOUGHNESS OF NANOMODIFIED EPOXY RESINS AND GLASS REINFORCED LAMINATES. Proceedings of the 15th European Conference on Composite Materials.

6 An efficient RVE formulation for the analysis of the elastic properties of spherical nanoparticle reinforced polymers

KEYWORDS: A. RVE; B. Nanocomposites; C. Interphase; D. Elastic properties;

ABSTRACT
Based on the use of Ripley function, a new algorithm for the generation of three-dimensional Representative Volume Elements (RVEs), easy to be meshed and imported in a FE code, is developed. The presence of an interphase zone, surrounding the nanofiller, of different mechanical properties with respect to the polymer matrix is accounted for. The basic features and potentialities of the tool are discussed by referring to a Complete Spatial Random Distribution. Moreover the effect of the material morphology on the overall interphase amount and on the elastic properties of polymer/nanoparticle nanocomposites are analysed.
Eventually, a computational analysis is carried out to study the effects of the interphase thickness and properties on the elastic properties of nanocomposites.

1. INTRODUCTION

Nanomodification, meant as the addition of nanofillers to polymer matrices, has recently emerged as an extremely promising technology to manufacture multi-functional materials through the designing of structures at the nanoscale. Surely, the most appealing feature of nanocomposite materials, when compared to more conventional micro-sized filler reinforced polymers, is that they offer outstanding improvements of physical and mechanical properties at very low concentrations. This assists in the achievement of high-level performances across various engineering applications and makes the use of nanomodified fibre–reinforced composites a smart solution.

Among the different types of nanofillers, the use of spherical nanoparticles allows to strengthen and toughen polymer resins as shown in some recent papers [1-5].

The mechanical properties of epoxy resins filled with spherical silica nanoparticles was investigated by Chen et al. [1] and Ma et al. [2] who obtained substantial improvements of the tensile modulus and the fracture toughness. Within this context, the nanoparticle size effect was analysed by Liang and Pearson [3] and Dittanet et al. [4] who found significant improvements of the Young's modulus and the fracture toughness, almost independently of the particle size. Different from the above mentioned works where a

clear size effect was absent, Zamanian et al. [5] showed that the mechanical properties of an epoxy resin were largely improved by the addition of silica nanoparticles with different size, the better improvements being obtained with the smaller nanoparticles.

However the understanding of the relation between the nanostructure and the overall mechanical behaviour of nanocomposites is essential in the development and design of such materials.

It is widely acknowledged that in nanocomposite materials the molecular structure of the polymer matrix is significantly altered at the particle/matrix interface, giving rise to an interphase zone comparable in size with that of the nanoparticle. This perturbed region, characterised by physical and mechanical properties different from those of the constituents, is created by interactions between components at the atomistic level and allows to explain the properties and the mechanisms exhibited at the upper scales. With the aim to account for molecular aspects into continuum-based methods, some authors have recently included into micromechanics tools the presence of an interphase with peculiar size and properties, thus accounting for nanofillers/polymer molecular interactions implicitly (see [6-18] and references reported therein). This new class of modeling tools, which allows one to simulate these features on length and time scales currently inaccessible by discrete numerical methods (such as Molecular Dynamics, MD) have been classified as "nanostructural models" [19]. However most of them still keep on being based on the concept of Eshelby dilute solution or Mori Tanaka theorem, being, in this way, unable to accurately seize the effect of the actual material morphology as well as filler-to-filler mechanical interactions. This is the reason why, with concern to the prediction of the mechanical response of nanofilled polymers, further efforts have been devoted in the recent literature to develop numerical approaches able to include non-regular filler distribution and agglomeration effects.

Within this topic, worth of mention is the work by Peng *et al.* [20] where a computational-analytical model, accounting for particle clustering effects, has been presented. A program code was used by the authors for the automatic generation of two-dimensional multiparticle unit cells on the basis of the "grid method" algorithm.

Differently, Mortazavi *et al.* [21], carried out a bulk of three-dimensional Finite Element Analyses to investigate the interphase effects on the elastic modulus and thermal conductivity of polymers loaded with randomly oriented or unidirectional nanofillers. These authors studied the combined effects of fillers geometry and volume fraction,

interphase thickness and properties, using the hard-core method to avoid intersection or contact between nanoparticles.

3D periodic Finite Element (FE) simulations were carried out also by Pahlavanpour *et al.* [22] on polymer clay nanocomposites; the effect of the interphase was taken into account in a two-step homogenization approach and a simplified procedure to guide the definition of the RVE was presented. The same authors also developed a one- and two-step homogenization models for predicting the stiffness of Polymer–Clay Nanocomposites (PCN) with aligned particles, of which the results were compared to 3D FE analyses where the PCN layered microstructure was explicitly simulated [23]. Approaches based on the FE method have been employed also to understand the effect of filler characteristics on the mechanical properties of CNT reinforced polymers (see for example, Bhuiyan *et al.* [24] and Joshi and Upadhyay [25]), while Marcadon *et al.* [26] carried out a comparison between Molecular Dynamics and micromechanical approaches to analyse the particle size effect on the mechanical behaviour of polymer nanocomposites.

In the present work, a new computational approach for the analysis of polymer-spherical particle nanocomposites is developed.

Making use of Ripley function, an efficient procedure for the generation of three-dimensional unit cell models, easy to be meshed and imported in a FE code, is developed. Particular attention is paid to the interphase zone surrounding the nanoparticles, which, due to inter and supra-molecular interactions, might be characterised by mechanical and physical properties different from those of the constituents. The basic features and potentialities of the tool are discussed by referring to a Complete Spatial Random Distribution (CSRD). Moreover the developed tool is used to analyse the effect of the material structure on the overall interphase volume fraction and on the elastic properties of the nanocomposite, by comparing the results from the generated RVEs to those obtained by a regular distribution. Eventually, the solid models created are used in combination with a FE code in order to carry out a computational study on the effects of the interphase thickness and properties on the overall elastic properties of the nanocomposite.

2. INTRODUCTORY REMARKS

Nanocomposite materials are characterised by a hierarchical structure, which includes the nano, the micro and the macro length-scales. A successful prediction of the mechanical properties of these materials thus requires models able to account for the phenomena peculiar of each length-scale and to bridge their effects from the nanoscale to the macroscale.

Within the classical Continuum Mechanics theory, the macroscale is commonly ragarded as an amount of material over which all the mechanical quantities are averaged values [27], representative of the overall material behaviour. This definition inherently contains the concept of a material point. However, moving from the macroscale to the microscale, the concept of "material point" is substituted by the *Representative Volume Element (*RVE), to be thought of as sufficiently small to be regarded, mathematically, as an infinitesimal volume of the macroscale. At the same time it has to be, by definition, large enough to be statistically representative of the properties of the material system, being it built with the real material microconstituents and microstructures. Defining a Volume Element (VE) as a volume containing a certain number of reinforcements, the RVE is a VE for which increasing the number of represented heterogeneities does not alter the computed effective properties.

Besides the macro and the micro length scales, when dealing with nanocomposites, the nano length scale is relevant as well and represents a single unit cell of those compounding the micro-scale system, thus accounting for the material morphology at the nanoscale.

Different from traditional microsized composites, it has to be considered that in nanoscale materials the surface effects become significant [28], due to the high surface/volume ratio and, for this reason, the amount of interphase volume might represent a large part of the matrix.

Experimental observations [29-32] and Molecular Dynamics simulations [33-37] allow to state that the mechanical properties of the interphase zone surrounding a nano-reinforcement are different from those of the polymer matrix and the nanofiller. Very recently, the present authors [17-18, 38-40] have proven that such properties highly affect the mechanical behaviour of nanocomposites. Unfortunately, even if some hypotheses have been made [20], the data available so far in the literature about the interphase zone

are not enough to formulate a reliable law of variation of its properties across the thickness and its size [6].

Thus, according to a large number of papers in the previous literature [6, 17-18, 33- 34, 38-40], in this work it is assumed that a through-the-thickness average is representative of the overall property distribution within the interphase, so that the interphase is supposed to be homogeneous and isotropic. Moreover, the interphase thickness is approximately assumed to be an inherent characteristic of the filler and polymer matrix materials and, as far as the effective properties are concerned, the continuum mechanics approach is used to characterise its mechanical behaviour [6, 21, 38-40]. In the light of this, the system under investigation at the nanoscale, shown in Figure 1, is constituted by:

1. a spherical nanoparticle of radius r_0;
2. a shell-shaped interphase of external radius a, thickness t ($a = r_0 + t$), and uniform properties;
3. a zone of bulk matrix embedding the interphase.

The interphase properties and size can be computed by means of MD simulations [33-37], which provide, as outputs, the radial extension of the interphase as well as the elastic properties averaged through the thickness.

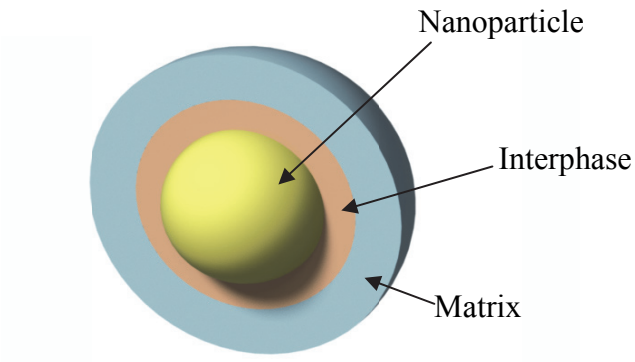

Figure 1. Description of the system under analysis at the nanoscale: nanoparticle of radius r_0, interphase region of thickness t both embedded within the bulk matrix.

3. FORMULATION OF RVES WITH A PRESCRIBED DISTRIBUTION OF SPHERICAL NANOPARTICLES: THEORETICAL ASPECTS

In this section a new procedure to create RVEs with a random distribution of spherical nanoparticles is briefly presented and discussed. The material is regarded as undamaged and composed by three homogeneous phases (spherical particles, polymer matrix and interphase zone).

Particles are constrained to have inter-centre distances greater than the sum of their radii, thus preventing particle merging in the FE modelling. However, close enough particles are allowed to share their interphase (see Figure 2). This allows the model to calculate the effective amount of interphase developed in the RVE, as a function of the interphase thickness, the filler volume fraction and the particle distribution.

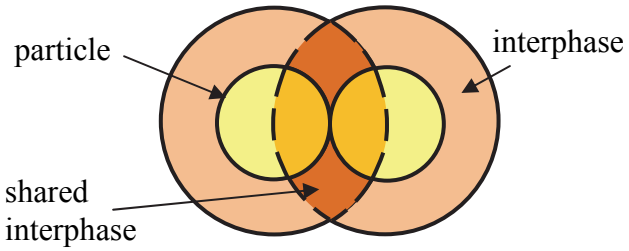

Figure 2. Schematic of non-overlapping particles sharing the interphase zone.

The developed numerical approach is based on an algorithm which generates particles distributed within the polymer matrix according to a prescribed distribution.

The developed approach requires as inputs the number of particles to be included in the RVE, n_p, the nanoparticle radius r_0, the interphase thickness, t, and filler volume fraction, f_p. These input data suffice to define a spatial domain containing all the particle centres, being it defined as a cube with edge length C:

$$C = \sqrt[3]{\frac{4}{3}\pi\frac{n_p}{f_p}}\, r_0 \tag{1}$$

The Cartesian coordinates of each particle centre are initially created using a random number generator, which produces values in the domain $]r_0+t;\ C-(r_0+t)[$, so that all particles are fully contained within the RVE. This choice has been made in order to guarantee an easier meshing process. Indeed in a 3D model the intersection between a particle and a face of the RVE would create a sharp angle which represents a critical zone

to be meshed, especially in a three-dimensional model where this critical zone is developed along a curved edge.

For each newly generated triad of coordinates, the algorithm automatically verifies that its distance from all other previously defined centres is greater than $2r_0$, in order to avoid overlapping particles; if this condition is not verified, the triad is rejected and new coordinates are generated. This process is iterated until the number of created centres equates n_p.

The next step of the algorithm consists is determining the Ripley function for the obtained distribution. The Ripley function, K(h) which is a powerful statistical evaluator, able to investigate the presence of repulsion or aggregation between events at several length-scale, considering the distance between each event from each other [41-42].

λ being the intensity of the distribution, function K is defined as [42]:

$$K(h) = \lambda^{-1} \cdot \varepsilon(h),\ h \geq 0 \tag{2a}$$

where $\varepsilon(h)$ is the average number of extra events within distance h of an arbitrary event.

In the engineering practice, K can be estimated according to the following expression [42]:

$$\hat{K}(h) = \hat{\lambda}^{-1} \sum_{i=1}^{n_p} \sum_{j=1}^{n_p} \frac{I\left(\left\|P_i - P_j\right\| \leq h\right)}{n_p} \qquad \text{with } h > 0 \text{ and } i \neq j \tag{2b}$$

where:

- h is the variable representing the distance of analysis.
- P_i are the coordinates of the n_p particle centres.
- $||P_i-P_j||$ is the distance between the centres of two particles (i and j), calculated considering spatial periodicity of particle positions within the RVE. This allows, according to Cressie [42] to inherently compute K(h) including corrections for edge effects.
- I is a step function equal to 1, if the argument is true, or 0 if it is false.
- $\hat{\lambda}$ is the estimation of the distribution intensity given by the number of particles within the RVE divided by the volume of the RVE, assuming the stationarity of the process [42].

The K(h) for the obtained pattern of nanoparticles, which should represent an "hard core process", allows to evaluate the following parameter:

$$P_Z \equiv \sqrt[3]{\frac{\hat{K}(h)}{K_{OB}(h)}} = \sqrt[3]{\frac{\hat{\lambda}^{-1}\sum_{i=1}^{n_p}\sum_{j=1}^{n_p}\frac{I\left(\left\|P_i - P_j\right\| \le h\right)}{n_p}}{K_{OB}(h)}} \qquad \text{with } h > 0 \text{ and } i \neq j \tag{3}$$

where $K_{OB}(h)$ is the K(h) for the target (desired) distribution.

Function P_Z allows to check whether, within a spatial interval, the given nanoparticle pattern is representative, within a given tolerance, of the desired distribution (P_Z=1). If this condition is verified, the obtained distribution is accepted.

If not, the distribution is further modified and forced to respect such a condition by applying iteratively to each particle the following formula:

$$\vec{u}_j = \sum_{i=1}^{n_p}\vec{u}_{ij} = \sum_{i=1}^{n_p}\left[\frac{F}{\left\|P_i - P_j\right\|^k}\frac{P_i - P_j}{\left\|P_i - P_j\right\|}I\left(\left\|P_i - P_j\right\| < q\right)\right] \qquad \text{with } i \neq j \tag{4}$$

Eq. (4) defines the movement of a particle, by superimposing the interaction vectors, $\vec{u}_{ij}$ between j-th particle and the surrounding ones. Each of these vectors, $\vec{u}_{ij}$, can be decomposed into the following terms:

1. $I\left(\left\|P_i - P_j\right\| < q\right)$ is a step function, equating 1 whenever the distance between particle centres, $\left\|P_i - P_j\right\|$, is lower than q, 0 otherwise. Accordingly it gives a cut-off for the particle-to-particle interactions, by defining an interaction radius, q (see Figure 3a). Optimum values for q depend on the target function;
2. the term $F/\left\|P_i - P_j\right\|^k$ is a scalar quantity giving the intensity of the interaction vector through an appropriate scale factor F and the distance between particles, $\left\|P_i - P_j\right\|$ raised to the k-th power. Parameters F and k are scalar quantities to be appropriately chosen depending on the target function (considering that the smaller the value of F, the smoother the evolution of the system is);
3. The term $P_i - P_j/\left\|P_i - P_j\right\|$ defines the direction of the interaction vector, being the unit vector linking the centres of the considered particles (see Figure 3b). This term transforms the scalar term $F/\left\|P_i - P_j\right\|^k$ into a vector;

4. Finally, the summation defines the sum of the interacting vectors for each particle and allows to evaluate the final displacement of the particle, $\vec{u}_j$ (see Figure 3c). The constraint $i \neq j$ means that particle self interactions are not considered.

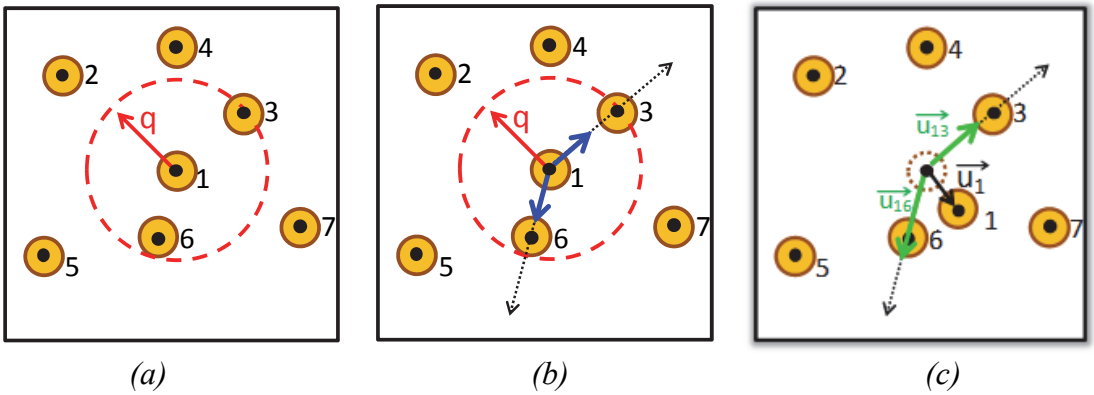

Figure 3. Graphical explanation of Eq. (4). (a) Definition of an interactive radius of length q around the j-th particle centre (j=1); (b) Definition of the unit vectors linking the j-th particle with the interacting particles. (c) Determination of the displacement vector $\vec{u}_i$ to be applied to the j-th particle centre.

This algorithm is applied iteratively to each particle of the RVE until P_Z=1 within a given tolerance. Values of F, k and q are chosen, within reason, in order to guarantee the desired degree of accuracy and might essentially depends on the target distribution.

The virtual distribution so obtained can be easily converted into a solid model using a commercial solid modeller (see, for example, Figure 4).

A flow chart of the complete developed algorithm is shown in Figure 5. It is also worth mentioning here that a similar approach has been used by Rintoul and Torquato [43], who used the Radial Distribution Function to reconstruct bi-dimensional particle distributions.

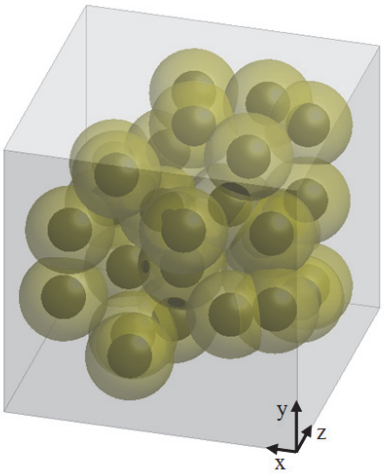

Figure 4. Example of the solid model with a complete random distribution of particles.

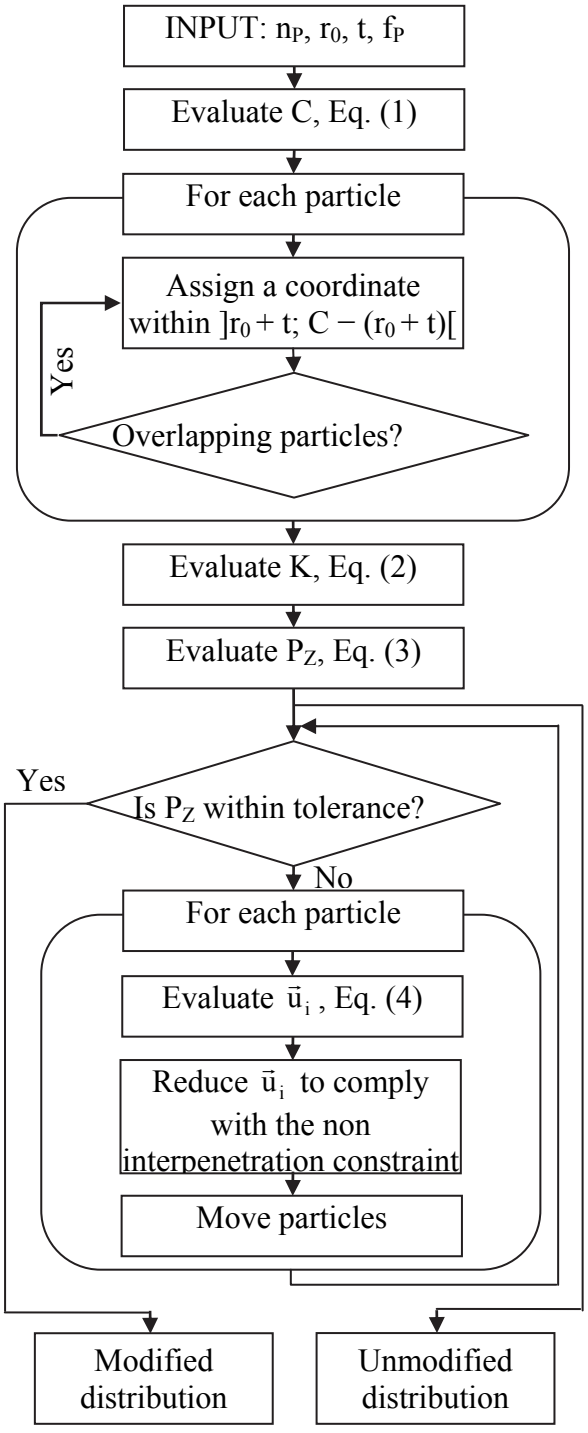

Figure 5. Flow chart of the developed algorithm.

4. ANALYSIS OF NANOPARTICLE REINFORCED POLYMERS: RESULTS AND DISCUSSION

4.1 Preliminary remarks

In order to successfully apply the developed algorithm to nanocomposites, it has be accounted for that the mechanical properties of polymer/spherical particle nanocomposites, especially the fracture toughness and the strength, might strongly depend on the filler morphology which, in turn, is influenced by several factors, such as the chemical nature of the constituents and the manufacturing processes employed. Unfortunately, as far as the authors are aware, in the literature there are no sound relationships correlating manufacturing parameters and chemical/physical properties of constituents to material morphology.

Accordingly, in order to explore the features and the efficacy of the developed algorithm, in this work we have chosen the Complete Spatial Random Distribution (CSRD) as a reference distribution, even if, in principle, the developed algorithm should allow to "reproduce" a convenient filler distribution by simply changing the reference value for the K(h) function.

The CSRD has the capability "to characterize the absence of structure in the data and it could be used as null hypothesis in a statistical test to look for spatial structure in the distribution" [42] and is characterized by $K(h) = \frac{4}{3}\pi h^3$. Accordingly, in the subsequent analysis the evaluator P_Z will be computed as:

$$P_Z \equiv \sqrt[3]{\frac{\hat{\lambda}^{-1}\sum_{i=1}^{n_p}\sum_{j=1}^{n_p}\frac{I\left(\left\|P_i - P_j\right\| \le h\right)}{n_p}}{\frac{4}{3}\pi h^3}} \qquad \text{with } h > 0 \text{ and } i \neq j \tag{5}$$

As far as Eq. (4) is concerned, the optimum value for q, F and k for a CSRD were found to be 5, 1 and 1, respectively. Moreover, an acceptance tolerance of 10% has been used for Pz. This value offered a reasonably computational cost to gain convergence (usually a hundred of iterations).

An example of application of the algorithm is shown in Figure 6, where the statistical analysis of two different particle centre distributions is presented. In particular:

1. the first one is simply obtained by using the random number generator, without any correction by Eq. (4): such a kind of distribution will be named here "unmodified" (black line).

2. the second one is instead obtained by applying iteratively Eq. (4) to each particle of the previous distribution: such a kind of distribution will be name here "modified" (red line).

The dotted lines identify the tolerance used with respect to the CSRD condition. It is evident that the modification of the distribution according to Eq. (4) allows to better match, within a given strict tolerance, the CRSD hypothesis. In addition, Figure 6 shows five unmodified distributions, with n_p = 10, 20, 30, 60 and 100 where P_Z is out of a prescribed tolerance. It is evident that increasing the number of particles, n_p, the distribution tends, slowly, toward a CSRD condition.

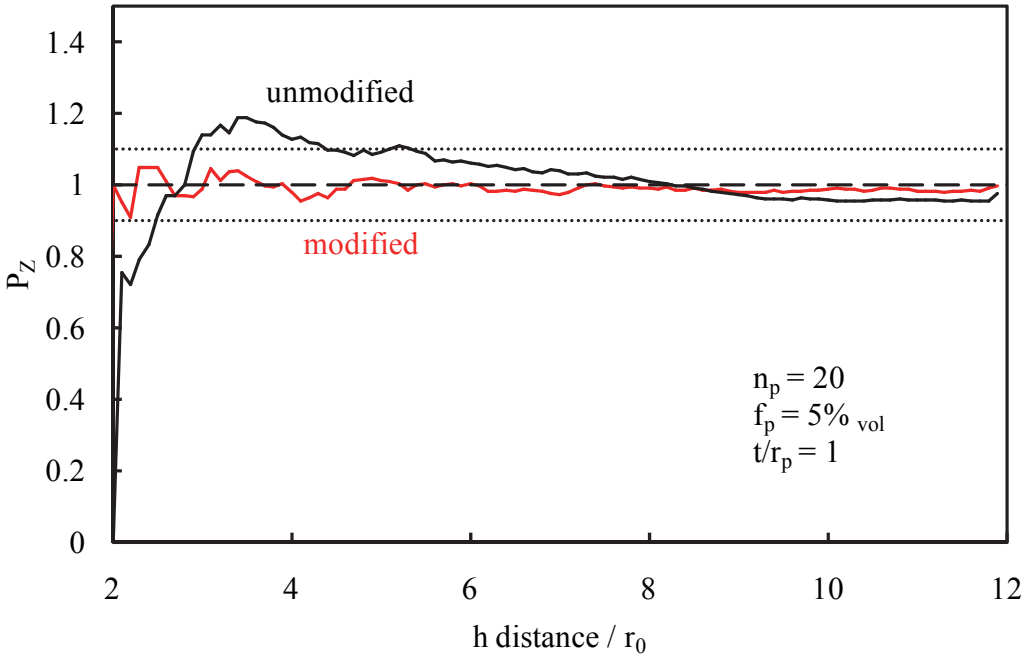

Figure 6. Example of analysis through Ripley function and comparison between a modified and an unmodified distribution.

4.2 Effect of the filler distribution on the interphase volume fraction

One of the basic assumption of the present analysis is the absence of overlapping particles. However, it might happen that some non-overlapping particles are so close to share part of the interphase (see Figure 7). Accordingly, it is expected that, in the presence of a complete random distribution, the actual interphase volume fraction, f_i, is lower than that associated to a regular distribution (cubic array of non-overlapping particles). These quantities can be determined as in Eqs. (6), the latter representing the regular distribution:

$$f_i = \frac{\text{Interphase volume within the VE}}{\text{Total volume of the VE}} \qquad f_i^{REG} = \left[\left(\frac{a}{r_0}\right)^3 - 1\right] f_p \qquad \text{(6a-b)}$$

Since it has been proven that the interphase properties highly affect the mechanical properties of nanocomposites [17-18, 38-40], the correct estimation of the overall amount of interphase within the material becomes essential. Under the hypothesis that the interphase thickness is, approximately, an inherent characteristic of the analysed system (filler type and polymer matrix), the RVE generator developed in the present work has been used to create several distributions with the aim to determine the overall interphase volume fraction, fi within the VEs, given by Eq. (6a) and to compare them with the results given by Eq. (6b).

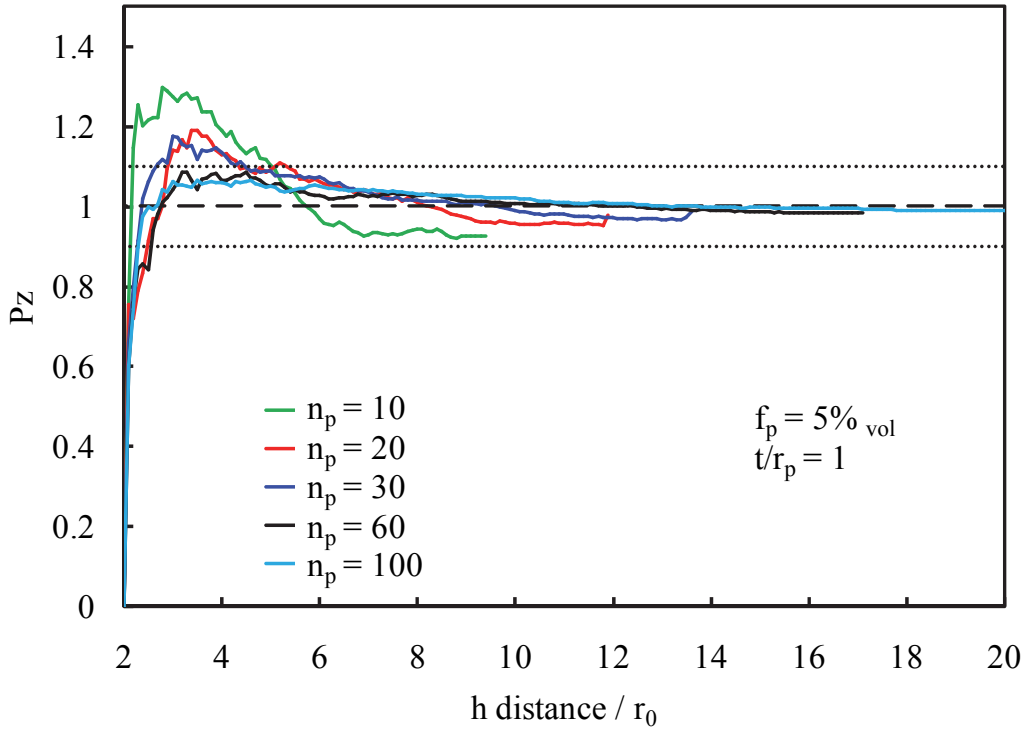

Figure 7. Example of analysis through Ripley function of five unmodified distributions.

To this end a nanocomposite material with f_p=0.05 and 0.1, r_0=10nm and t=10nm has been considered, and VEs with n_p=10, 20, 30 and 60 have been generated. For each value of n_p 5 different VEs have been built, and results are provided in terms of mean values and standard deviations in Figure 9. It is evident that the nanoparticle distribution affects the interphase volume fraction, a CSR distribution resulting in a strong reduction of f_i (about 20% for f_p=0.05, up to 45% when f_p=0.1). Figure 8 gives a more comprehensive overview of this effect; the interphase reduction is shown to increase, as expected, while

increasing the interphase thickness t and the nanoparticle volume fraction. At the same time, Figures 9 make it also evident the efficiency of the developed algorithm: indeed, as far as the modified distributions are concerned, the results in terms of f_i are almost independent of the number of particles. Unmodified distributions are characterised, instead, by higher standard deviations and require a lot more particles to obtain a stabilized mean value. This result agrees with those shown in Figures 6 and 7, where distributions have been analyzed through Ripley function.

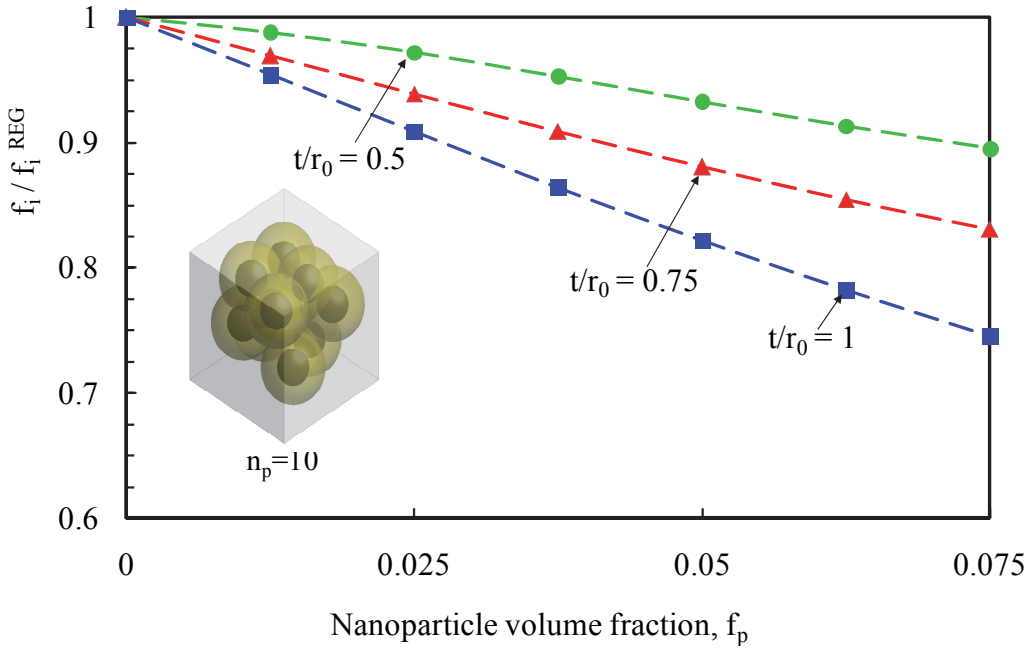

Figure 8. Interphase volume fraction for modified CSRs distribution versus the nanoparticle volume fraction and the interphase size.

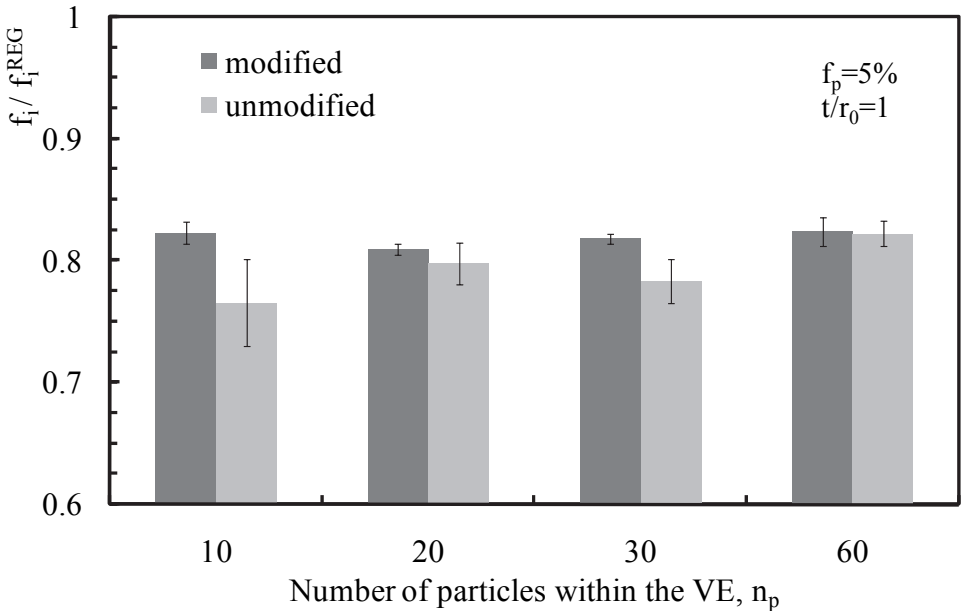

(a)

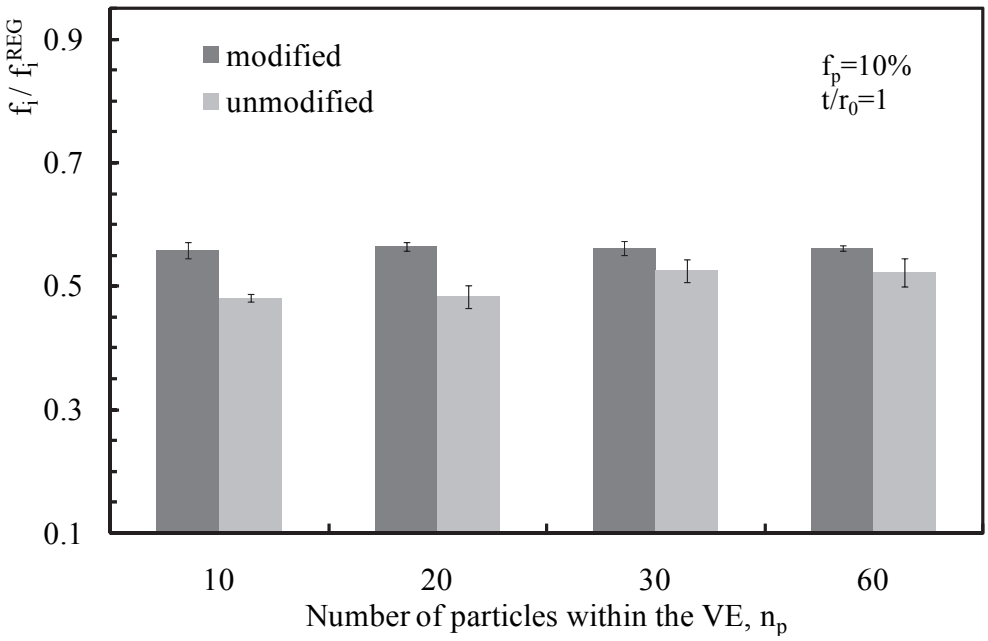

(b)

Figure 9. Interphase volume fraction versus the number of particles of the VEs. Comparison between regular distribution, unmodified and modified CSR distributions. f_p=5% (a), f_p=10% (b)

4.3 Effect of the filler distribution on the nanocomposite elastic properties

The VEs created in the previous section have been meshed in order to determine the elastic properties of the nanocomposite material. All the analyses have been carried out with the Ansys Workbench code, release 14.5, using 10-node thetrahedron elements (SOLID 187 in Ansys). The used mesh pattern was an unstructured tetrahedral mesh (see Figure 10).

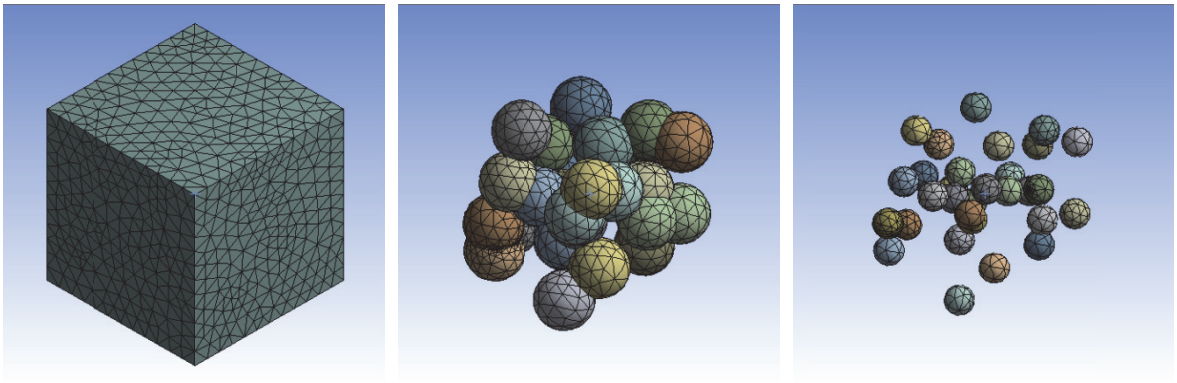

(a) *(b)* *(c)*

Figure 10. Example of VEs meshing: complete VE (a) , interphase zone (b), particles (c).

The optimal meshing parameters have been chosen on the basis of a preliminary sensitivity analysis according to which about $1400*n_p$ elements per RVE have been proven enough to reach a stable convergence.

In addition to CSRDs, RVEs with a regular distribution (cubic array of 8 particles) have been created as well. The following material properties have been used:

1. Matrix: elastic modulus, $E_m = 3000MPa$, Poisson's ratio, $\nu_m = 0.35$, typical of a DGEBA resin.
2. Particle: elastic modulus, $E_p = 70000MPa$, Poisson's ratio, $\nu_p = 0.17$, typical of a silica nanoparticle.
3. Interphase: elastic modulus, $E_i = 6000MPa$, Poisson's ratio, $\nu_i = 0.25$.

With reference to the coordinate system shown in Figure 4, the following boundary conditions have been applied to the analysed VEs, where i, k = x, y, z:

1. All nodes on the faces with i = 0 are constrained ($u_i=0$).
2. All nodes with i=C ($i \neq k$) are forced to have the same displacement u_i.
3. A constant displacement in the k direction, u_k, is finally applied to all nodes on the face k=C ($k \neq i$).

These boundary conditions result in a zero normal average stress in the i direction, thus allowing to determine the longitudinal elastic modulus in the k direction, without stiffening caused by transversal constraints and do not give rise to edge effects, symmetry conditions being applied to the RVE edges. For each VE three analyses have been carried out (with k = x, y, z) so that the elastic moduli in the x, y and z direction have been determined.

It is worth mentioning here that the proposed boundary conditions differs from the more conventional periodic boundary conditions, of which the implementation often hampers the possibility to use automatic/free meshing, requiring a correspondence between nodes on the opposite faces of the RVE. Accordingly, in order to avoid the need of an "intelligent" meshing of RVEs, which might be particularly time consuming for 3D domains, in this work we have adopted the set of boundary conditions explained above.

Results of FE analyses are shown in Figure 11. It has to be noted that, for the studied system, the elastic modulus of the nanocomposite is only slightly affected by the particle distribution. This is clear comparing the results from CSRD distributions to those related to the regular distribution, the difference being within 10%. Another proof can be given by comparing Figure 7 and Figure 11, where it is evident that the differences in the interphase content between modified and unmodified distributions have a very limited effect on the value of the elastic modulus. This effect is particularly emphasised by the fact that, in the results shown in Figure 11, the interphase is only moderately stiffer than the matrix ($E_i = 2E_m$). However it has also to be mentioned that other mechanical properties, such as the fracture toughness, can be largely affected by the interphase content, and limited variation in f_i can produce substantial changes in G_{IC} (see for example [38-40]).

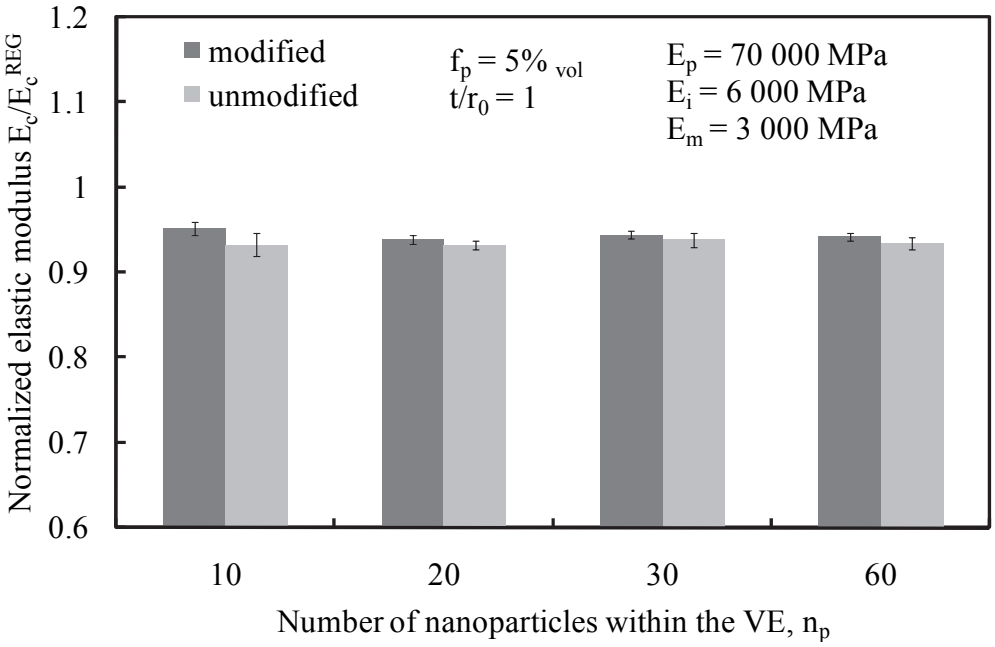

Figure 11. Normalized elastic modulus. Comparison between unmodified and modified CSR distributions.

4.3. Effect of the interphase thickness and elastic properties

The RVEs with r_0 = 10nm and n_p = 10 used in the previous sections have been employed to study the effect of the interphase elastic properties and size on the overall elastic properties of the nanocomposite. In particular, the effect of the interphase to matrix elastic properties ratio, E_i/E_m, for a constant interphase thickness t = 5nm, is shown in Figure 12, considering different volume fractions. It is evident that when the interphase is softer than the matrix ($E_i/E_m = 0.5$), the reinforcement due to the addition of nanofillers is almost cancelled by the low interphase properties. On the other hand, a stiffer interphase ($E_i/E_m > 1$) results in a more pronounced increase for the nanocomposite elastic modulus.

Figure 13 shows the effect of the interphase thickness, E_i/E_m being constant and equal to 2; results clearly indicate that the increase of the interphase thickness gives an enhanced stiffening effect.

These results, which agree with those recently discussed by other authors (see [17-18, 20-21] and references reported therein), clearly prove the importance of the interphase properties and size for the correct assessment of the mechanical properties of polymer/nanoparticle nanocomposites.

It is finally worth mentioning that the deviation from linearity exhibited by the nanocomposite elastic properties, as evident from Figures 12 and 13, is due to the stiffening effect of the interphase.

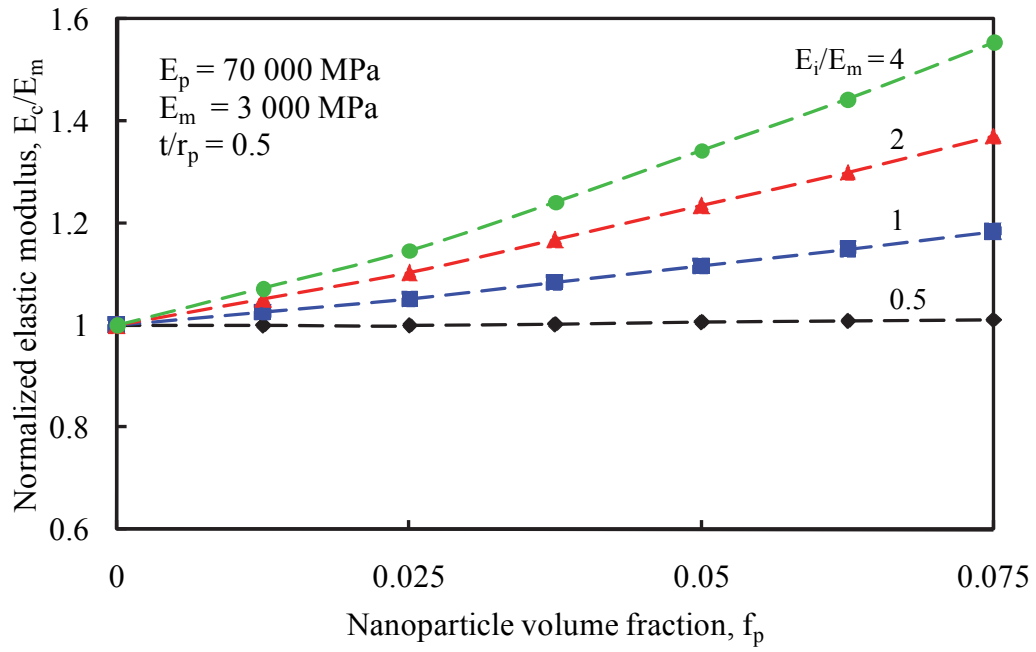

Figure 12. Nanocomposite normalized elastic modulus, E_c/E_m, versus the nanoparticle volume fraction (CSRD). Different E_i/E_m ratios. The data point are averaged values.

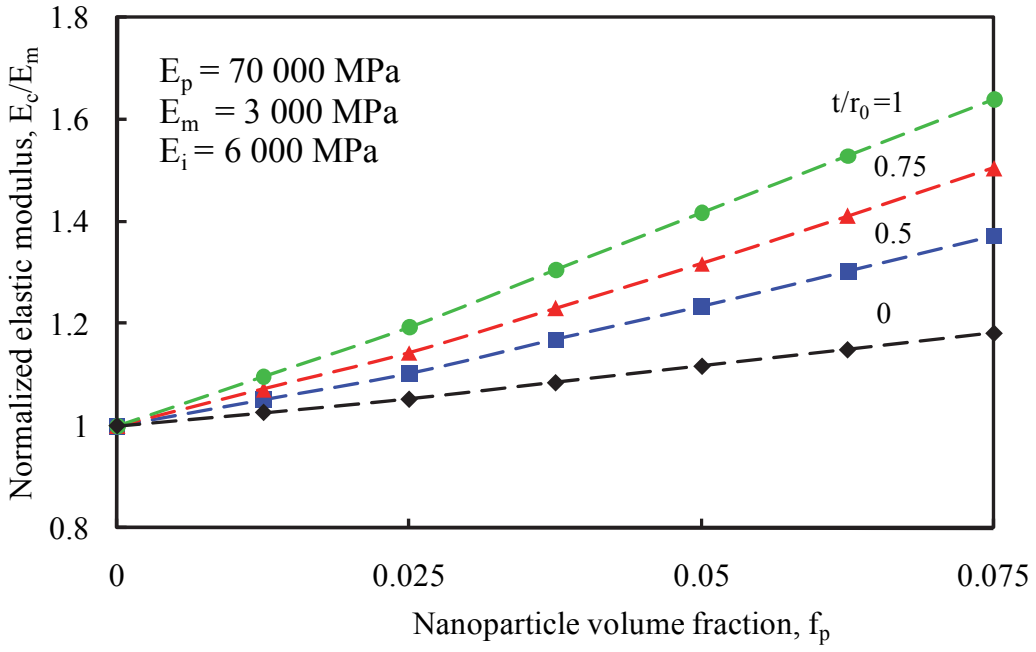

Figure 13. Nanocomposite normalized elastic modulus, E_c/E_m, versus the nanoparticle volume fraction and the interphase size (CSRD). The data point are averaged values.

5. CONCLUSIONS

Based on the use of Ripley function, in this work a new algorithm for the generation of three-dimensional Representative Volume Elements (RVEs) has been presented. The presence of an interphase zone, surrounding the nanofiller, of different mechanical properties with respect to the matrix has been accounted for. The basic features and potentialities of the tool are discussed by referring to a Complete Spatial Random Distribution (CSRD). It is found that the developed approach is extremely efficient, by a computational point of view, the results in terms of the actual interphase volume fraction and nanocomposite elastic properties being almost independent of the number of particles used in the RVE. The developed numerical procedure has then been used to prove the substantial effect of the material structure on the overall interphase amount and the elastic properties of polymer/nanoparticle nanocomposites.

ACKNOWLEDGEMENTS
The authors acknowledge the financial support to the activity by Veneto Nanotech, the Italian cluster of Nanotechnology and by CARIVERONA Foundation, (within the frame "Contributo di Fondazione Cariverona a valere sui finanziamenti alla ricerca scientifica e tecnologica per l'anno 2012").

REFERENCES

[1] Chen, C., Justice, R. S., Schaefer, D. W., & Baur, J. W. (2008). Highly dispersed nanosilica–epoxy resins with enhanced mechanical properties.Polymer, 49(17), 3805-3815.

[2] Ma, J., Mo, M. S., Du, X. S., Rosso, P., Friedrich, K., & Kuan, H. C. (2008). Effect of inorganic nanoparticles on mechanical property, fracture toughness and toughening mechanism of two epoxy systems. Polymer, 49(16), 3510-3523.

[3] Liang, Y. L., & Pearson, R. A. (2009). Toughening mechanisms in epoxy–silica nanocomposites (ESNs). Polymer, 50(20), 4895-4905.

[4] Dittanet, P., & Pearson, R. A. (2012). Effect of silica nanoparticle size on toughening mechanisms of filled epoxy. Polymer, 53(9), 1890-1905.

[5] Zamanian, M., Mortezaei, M., Salehnia, B., & Jam, J. E. (2013). Fracture toughness of epoxy polymer modified with nanosilica particles: Particle size effect. Engineering Fracture Mechanics, 97, 193-206.

[6] Sevostianov, I., & Kachanov, M. (2007). Effect of interphase layers on the overall elastic and conductive properties of matrix composites. Applications to nanosize inclusion. International Journal of Solids and Structures, 44(3), 1304-1315.

[7] Wang, H. W., Zhou, H. W., Peng, R. D., & Mishnaevsky Jr, L. (2011). Nanoreinforced polymer composites: 3D FEM modeling with effective interface concept. Composites Science and Technology, 71(7), 980-988.

[8] Li, Y., Waas, A. M., & Arruda, E. M. (2011). A closed-form, hierarchical, multi-interphase model for composites—Derivation, verification and application to nanocomposites. Journal of the Mechanics and Physics of Solids, 59(1), 43-63.

[9] Mercier, S., Molinari, A., & El Mouden, M. (2000). Thermal conductivity of composite material with coated inclusions: Applications to tetragonal array of spheroids. Journal of Applied Physics, 87(7), 3511-3519.

[10] Boutaleb, S., Zaïri, F., Mesbah, A., Naït-Abdelaziz, M., Gloaguen, J. M., Boukharouba, T., & Lefebvre, J. M. (2009). Micromechanics-based modelling of stiffness and yield stress for silica/polymer nanocomposites. International Journal of Solids and Structures, 46(7), 1716-1726.

[11] Brisard, S., Dormieux, L., & Kondo, D. (2010). Hashin–Shtrikman bounds on the shear modulus of a nanocomposite with spherical inclusions and interface effects. Computational Materials Science, 50(2), 403-410.

[12] Pontefisso, A., Zappalorto, M., & Quaresimin, M. (2013). Influence of interphase and filler distribution on the elastic properties of nanoparticle filled polymers. Mechanics Research Communications, 52, 92-94.

[13] Anoukou, K., Zaïri, F., Naït-Abdelaziz, M., Zaoui, A., Messager, T., & Gloaguen, J. M. (2011). On the overall elastic moduli of polymer–clay nanocomposite materials using a self-consistent approach. Part I: Theory.Composites science and technology, 71(2), 197-205.

[14] Anoukou, K., Zaoui, A., Zaïri, F., Naït-Abdelaziz, M., & Gloaguen, J. M. (2013). Molecular dynamics study of the polymer clay nanocomposites (PCNs): Elastic constants and basal spacing predictions. Computational Materials Science, 77, 417-423.

[15] Salviato, M., Zappalorto, M., & Quaresimin, M. (2011). The effect of surface stresses on the critical debonding stress around nanoparticles. International journal of fracture, 172(1), 97-103.

[16] Zappalorto, M., Salviato, M., & Quaresimin, M. (2012). Stress distributions around rigid nanoparticles. International Journal of Fracture, 176(1), 105-112.

[17] Zappalorto, M., Salviato, M., & Quaresimin, M. (2011). Influence of the interphase zone on the nanoparticle debonding stress. Composites Science and Technology, 72(1), 49-55.

[18] Salviato, M., Zappalorto, M., & Quaresimin, M. (2013). Nanoparticle debonding strength: a comprehensive study on interfacial effects. International Journal of Solids and Structures, 50(20), 3225-3232.

[19] Quaresimin, M., Salviato, M., & Zappalorto, M. (2012). Strategies for the assessment of nanocomposite mechanical properties. Composites Part B: Engineering, 43(5), 2290-2297.

[20] Peng, R. D., Zhou, H. W., Wang, H. W., & Mishnaevsky Jr, L. (2012). Modeling of nano-reinforced polymer composites: Microstructure effect on Young's modulus. Computational Materials Science, 60, 19-31.

[21] Mortazavi, B., Bardon, J., & Ahzi, S. (2013). Interphase effect on the elastic and thermal conductivity response of polymer nanocomposite materials: 3D finite element study. Computational Materials Science, 69, 100-106.

[22] Pahlavanpour, M., Moussaddy, H., Ghossein, E., Hubert, P., & Lévesque, M. (2013). Prediction of elastic properties in polymer–clay nanocomposites: Analytical homogenization methods and 3D finite element modeling.Computational Materials Science, 79, 206-215.

[23] Pahlavanpour, M., Hubert, P., & Lévesque, M. (2014). Numerical and analytical modeling of the stiffness of Polymer–Clay Nanocomposites with aligned particles: One-and two-step methods. Computational Materials Science, 82, 122-130.

[24] Bhuiyan, M. A., Pucha, R. V., Worthy, J., Karevan, M., & Kalaitzidou, K. (2013). Understanding the effect of CNT characteristics on the tensile modulus of CNT reinforced polypropylene using finite element analysis. Computational Materials Science, 79, 368-376.

[25] Joshi, P., & Upadhyay, S. H. (2014). Evaluation of elastic properties of multi walled carbon nanotube reinforced composite. Computational Materials Science, 81, 332-338.

[26] Marcadon, V., Brown, D., Hervé, E., Mélé, P., Albérola, N. D., & Zaoui, A. (2013). Confrontation between Molecular Dynamics and micromechanical approaches to investigate particle size effects on the mechanical behaviour of polymer nanocomposites. Computational Materials Science, 79, 495-505.

[27] Timoshenko, S. P., Goodier, J. N., & Abramson, H. N. (1970). Theory of elasticity. Journal of Applied Mechanics, 37, 888.

[28] Ajayan, P. M., Schadler, L. S., & Braun, P. V. (2006). Nanocomposite science and technology. John Wiley & Sons.

[29] Zammarano, M., Maupin, P. H., Sung, L. P., Gilman, J. W., McCarthy, E. D., Kim, Y. S., & Fox, D. M. (2011). Revealing the interface in polymer nanocomposites. ACS nano, 5(4), 3391-3399.

[30] Berriot, J., Lequeux, F., Monnerie, L., Montes, H., Long, D., & Sotta, P. (2002). Filler–elastomer interaction in model filled rubbers, a ^{1}H NMR study. Journal of Non-Crystalline Solids, 307, 719-724.

[31] Berriot, J., Martin, F., Montes, H., Monnerie, L., & Sotta, P. (2003). Reinforcement of model filled elastomers: characterization of the cross-linking density at the filler–elastomer interface by ^{1}H NMR measurements. Polymer, 44(5), 1437-1447.

[32] Watcharotone, S., Wood, C. D., Friedrich, R., Chen, X., Qiao, R., Putz, K., & Brinson, L. C. (2011). Interfacial and substrate effects on local elastic properties of polymers using coupled experiments and modeling of nanoindentation. Advanced Engineering Materials, 13(5), 400-404.

[33] Odegard, G. M., Clancy, T. C., & Gates, T. S. (2005). Modeling of the mechanical properties of nanoparticle/polymer composites. Polymer, 46(2), 553-562.

[34] Valavala, P. K., & Odegard, G. M. (2005). Modeling techniques for determination of mechanical properties of polymer nanocomposites. Rev. Adv. Mater. Sci, 9, 34-44.

[35] Zeng, Q. H., Yu, A. B., & Lu, G. Q. (2008). Multiscale modeling and simulation of polymer nanocomposites. Progress in Polymer Science, 33(2), 191-269.

[36] Yu, S., Yang, S., & Cho, M. (2009). Multi-scale modeling of cross-linked epoxy nanocomposites. Polymer, 50(3), 945-952.

[37] Starr, F. W., Douglas, J. F., & Glotzer, S. C. (2003). Origin of particle clustering in a simulated polymer nanocomposite and its impact on rheology.The Journal of chemical physics, 119(3), 1777-1788.

[38] Zappalorto, M., Salviato, M., & Quaresimin, M. (2012). A multiscale model to describe nanocomposite fracture toughness enhancement by the plastic yielding of nanovoids. Composites Science and Technology, 72(14), 1683-1691.

[39] Salviato, M., Zappalorto, M., & Quaresimin, M. (2013). Plastic shear bands and fracture toughness improvements of nanoparticle filled polymers: a multiscale analytical model. Composites Part A: Applied Science and Manufacturing, 48, 144-152.

[40] Quaresimin, M., Salviato, M., & Zappalorto, M. (2014). A multi-scale and multi-mechanism approach for the fracture toughness assessment of polymer nanocomposites. Composites Science and Technology, 91, 16-21.

[41] Ripley, B. D. (1977). Modelling spatial patterns. Journal of the Royal Statistical Society. Series B (Methodological), 172-212.

[42] Cressie, N. (1992). Statistics for spatial data. Terra Nova, 4(5), 613-617.

[43] Rintoul, M. D., & Torquato, S. (1997). Reconstruction of the structure of dispersions. Journal of Colloid and Interface Science, 186(2), 467-476.

7 Study of the Random Sequential Absorption algorithm in the generation of nanoplatelet Volume Elements

KEYWORDS: A. RSA algorithm; B. Statistical analysis; C. Nanoplatelets;

ABSTRACT
In this chapter, the study of the Random Sequential Absorption (RSA) algorithm in the generation of nanoplatelet Volume Elements (VEs) has been carried out. The effect of the algorithm input parameters on the reinforcement distribution is studied through the implementation of statistical tools, showing that the platelet distribution is systematically affected by these parameters. The consequence is that the parametric study of the VE input parameters may be biased by hidden differences in the filler distribution. Finally, the same statistical tools used in the analysis are implemented in a modified RSA algorithm to overcome this issue.

1. INTRODUCTION

In the past decades polymer nanocomposites surprised the scientific community with outstanding improvements of polymer functional [1, 2] and mechanical [3, 4] properties. Nowadays thousands of scientific publications per year testify the huge interest in this research area.

Many materials have been created and tested using several type of nanoreinforcements, which can be classified as a function of their geometry: spherical (e.g. alumina nanoparticles), rod-like (e.g. CNTs) and platelet-like (e.g. nanoclays). Focussing on nanoplatelets, many authors showed their capability in increasing the matrix tensile properties [5], fracture toughness [6], barrier [7] and antibacterial properties [8]. However the same authors presented also the complexity involved in processing these materials and the need of better understanding their behaviour in order to employ them effectively [9].

Several research papers have been published on computational modelling of nanoplatelet reinforced composites [10-13] in an attempt to shed light on the mechanisms involved within these materials.

Ma et al. [10] propose a FE simulation on nanoclay-epoxy nanocomposites to study their impact behaviour. In particular they implement a Random Sequential Absorption (RSA)

algorithm to create 2D Volume Elements (VEs) of the material and to perform damaging analyses taking into account the reinforcement-matrix traction-separation law.

Hbaieb et al. [11] model the stiffness of polymer/clay nanocomposites. They create 2D and 3D VEs with aligned and randomly oriented platelets, through a RSA algorithm, and perform a comparison with the Mori-Tanaka model.

Dai and Mishnaevsky [12] study the damaging evolution in nanoclay reinforced epoxy. They create 2D and 3D VEs of aligned or randomly oriented platelets, obtained with a RSA algorithm, and perform XFEM simulations of the initiation and propagation of the damage.

What emerges from the analysis of the literature is that the RSA algorithm is the most common approach in nanoplatelet VE generation. This is reasonably due to the easiness of its implementation added to the soundness of its statistical base. However, when dealing with nanoplatelets, the randomness inherently possessed by the RSA algorithm is biased. In fact this emerges in [13], where Cricrì et al. study the prediction of the stiffness constants of a nanocomposite, using a periodic 3D-FEM model. After obtaining statistical parameters of the reinforcement orientation through TEM analyses of the material, they implement a RSA algorithm able to take into account those parameters in the construction of 3D models. In their analyses, they highlight the link between the VE size (in terms of number of platelets) an the possibility for it to display isotropic structural characteristics. In doing so, they remark the connection existing between the input parameters for the VE generation and the reinforcement distribution resulting from the RSA algorithm.

In the following work, three statistical indexes are defined to study the platelet distribution within VEs. Then a RSA algorithm is implemented to generate VEs of different aspect ratios, filler volume fraction and number of platelets, proving the existence of a systematic effect of the input parameters on these VEs. Finally a way to overcome this issue when using RSA approaches is proposed.

2. STATISTICAL TOOLS

2.1. Analysis of the platelet orientation distribution

The platelet distribution is defined in terms of centre positions and platelet orientations. Considering that in this study hexagonal platelets have been used, the platelet shape results in a quasi-transversal-isotropic behaviour, allowing the use of the sole unit vector orthogonal to the platelet plane, $\vec{n}$, as orientation descriptor. This parameter is studied within the frame of the statistical analysis of axial data through the definition of an

orientation matrix [T] [14]. Expressing, for each platelet i, $\vec{n}$ as $\vec{n}_i = < x_i, y_i, z_i >$, [T] is evaluated as:

$$[T] = \begin{bmatrix} \sum_i x_i^2 & \sum_i x_i y_i & \sum_i x_i z_i \\ \sum_i x_i y_i & \sum_i y_i^2 & \sum_i y_i z_i \\ \sum_i x_i z_i & \sum_i y_i z_i & \sum_i z_i^2 \end{bmatrix} \quad (1)$$

Solving the eigenproblem associated to [T] it is possible to obtain 3 eigenvalues and 3 eigenvectors which give information about the preferred orientation of $\vec{n}_i$ within the VE. Eigenvalues have been defined as v_1, v_2, v_3 with $v_1 \geq v_2 \geq v_3$.

To evaluate the effects of the input parameters on the VE filler configuration, it seems reasonable to assume an isotropic distribution of platelet orientations as a reference. If the eigenvalues are equal, the distribution is uniform (which means isotropic), therefore in this paper the ratio v_3/v_1 has been assumed as an index of anisotropy: a value of one means uniform distribution, while decreasing values identify a higher anisotropy. The second eigenvalue is not considered in the following analysis for brevity.

Alongside the analysis by means of eigenvalues, a qualitative analysis of the distribution was carried out by means of a graphical representation of $\vec{n}_i$. Each unit vector can be plotted as a point on a sphere of radius 1, assuming a common origin for each vector. Considering that in the case of platelets only the axis is of consequence (i.e. $\vec{n}_i \equiv -\vec{n}_i$) all data have been reformulated with negative z coordinate: in this way all the points belong only to the lower hemisphere, which simplifies the plotting. The representation implemented is a Wulff stereographic projection [14] which is an equal-angle projection obtained projecting each point on the middle plane of the sphere (i.e. the plane which connects the lower and the upper hemisphere) not through rays parallel to the sphere axis, as in the case of orthographic projections, but with rays linking the points with the pole in the positive hemisphere. This projection results in a view akin to watching the lower hemisphere as a physical object in the real world.

2.2.Analysis of the platelet centre distribution

In order to study the particle centre distribution, Ripley function, K, has been employed [15] and the comparison between the VE K-function and the K-function of a Complete Spatial Random Distribution (CSRD), which is assumed as reference distribution, has been performed through the function P_z [16].

λ being the intensity of the distribution, function K is defined as [17]:

$$K(h) = \lambda^{-1} \cdot \varepsilon(h),\ h \geq 0 \tag{2a}$$

where $\varepsilon(h)$ is the average number of extra events within distance h of an arbitrary event. In the engineering practice, K can be estimated according to the following expression [17]:

$$\hat{K}(h) = \hat{\lambda}^{-1} \sum_{i=1}^{n_p} \sum_{j=1}^{n_p} \frac{I\left(\left\|P_i - P_j\right\| \leq h\right)}{n_p} \qquad \text{with } h > 0 \text{ and } i \neq j \tag{2b}$$

where:

- h is the variable representing the distance of analysis.
- P_i are the coordinates of the n_p platelet centres.
- $||P_i-P_j||$ is the distance between the centres of two platelets (i and j), calculated considering spatial periodicity of reinforcement positions within the VE. This allows, according to Cressie [17], to inherently compute K(h) including corrections for edge effects.
- I is a step function equal to 1, if the argument is true, or 0 if it is false.
- $\hat{\lambda}$ is the estimation of the distribution intensity given by the number of platelets within the VE divided by the volume of the VE, assuming the stationarity of the process [17].

In case of CSRD in a tridimensional space, Ripley function assumes a value of $K(h) = \frac{4}{3}\pi h^3$ [17].

Function P_Z allows a comparison between K functions and it is expressed as:

$$P_Z \equiv \sqrt[3]{\frac{\hat{K}(h)}{K_{OB}(h)}} \qquad \text{with } h > 0 \text{ and } i \neq j \tag{3}$$

In this case $K_{OB}(h)$ is $K(h) = \frac{4}{3}\pi h^3$, thus the final expression of P_Z is:

$$P_Z \equiv \sqrt[3]{\frac{\hat{\lambda}^{-1} \sum_{i=1}^{n_p} \sum_{j=1}^{n_p} \frac{I\left(\left\|P_i - P_j\right\| \leq h\right)}{n_p}}{\frac{4}{3}\pi h^3}} \qquad \text{with } h > 0 \text{ and } i \neq j \tag{4}$$

3. RVE-GENERATOR ALGORITHM

The generation of a VE is based on a software which implements a Random Sequential Absorption (RSA) approach. The RSA method is based on the definition of a domain in which platelets are generated sequentially with random coordinates and orientation, and each time a new platelet is created a check is performed to verify that no platelet-overlapping with already generated platelets is detected. If it is so, the platelet is retained ("absorbed") in the VE; otherwise it is discarded. The algorithm is iterated until the desired amount of platelets are placed in the VE. Considering that the domain is defined as an input, for each newly placed platelet the filler volume fraction, f_v, increases. In the case of the VEs developed in this study, the domain is a cube of edge length C with periodicity between opposite faces. In this way a platelet may cross a face and the amount of filler within the VE is not affected. This geometric periodicity is mandatory in the VE generation, because the placement of high aspect ratio reinforcements would otherwise require a significantly bigger domain.

The developed algorithm is able to manage platelets of several shapes, but in the present analysis only hexagonal platelets have been considered: this geometry seems a good compromise between the most used shapes in the literature (i.e. square and circle). In addition, platelets are constrained to have the same size and are generated independently, both in terms of centres coordinates and orientation: this means that no intercalation is enforced "ab initio". Finally, it seems convenient for the reader to point out that the software has been developed within the Object Oriented and Multi-threading paradigms, which enabled to manage the complexity of the routines involved in the checking of platelet-overlapping and to contain the time required to the software to carry out the VE generation.

The obtained VE is post-processed to obtain the orientation matrix [T] and the eigenvalues. Moreover a routine imports the VE within a CAD software , which allows a visual inspection of the VE. The overall procedure is reported in Figure 1.

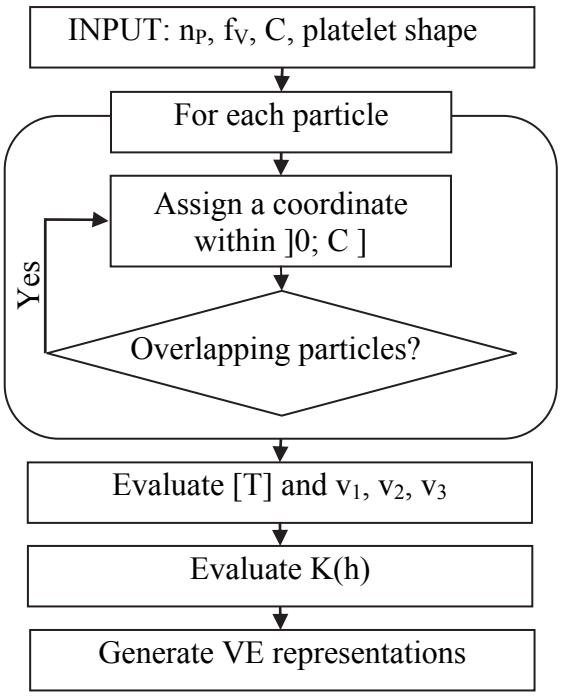

Figure 1. Diagram of the overall procedure in RVE generation an analysis

4. ANALYSIS AND RESULTS

Three statistical indicators have been obtained for each VE:

1. An index of average isotropy of platelet orientation, evaluated as v_3/v_1, which highlights the presence of a preferable orientation within the VE.
2. An index of local anisotropy which is evaluated again as v_3/v_1, but as a function of the distance from a platelet centre. This index is calculated for each platelet of the VE and than averaged.
3. An index of the distribution of the platelet centres, P_z. This index is evaluated as a function of the distance from the platelet centre.

These indicators have been employed to study the effects of the algorithm input parameters on the platelet distribution within the VE. These input parameters are:

1. The filler volume fraction, f_v, calculated as the ratio between platelets overall volume and the volume of the domain (C^3).
2. The platelet aspect ratio, AR, evaluated as the ratio between the diameter of the circle circumscribed the platelet and the its thickness.
3. The number of particles within the VE, n_p.

It must be point out that, due to the way in which the algorithm generates new platelets, each time a new one is retained, f_v rises. Taking advantage on this, the VE realizations at different f_v are obtained from the same VE saving its data history at steps of $f_v = 0.5\%$.

4.1. Global isotropy

In Figure 2 the effect of the aspect ratio on the overall VE isotropy has been studied. The analysis has been carried out at AR = 50 and 100 up to $f_v = 3\%$, and at AR = 200 up to only $f_v = 1.5\%$ due to the high computational cost required to generate the VE. For the same reason while AR = 50, 100 and 200 have a scatter band representing the standard deviation on v_3/v_1 of 3 different realizations, a single VE at AR = 1000 $f_v = 0.5\%$ has been generated. n_p at $f_v = 3\%$ is 60. Considering $f_v = 0.5\%$ wide scatter bands can be seen. This seems reasonable due to the low number of platelets placed in each VE ($n_p = 10$), thus resulting in a low statistical representativeness of the single VE. The global trends highlights that, for the same n_p and f_v, higher is the aspect ratio lower is v_3/v_1. This is particularly visible at $f_v = 3\%$ where a relatively small difference in AR results in a significant difference in the isotropy index.

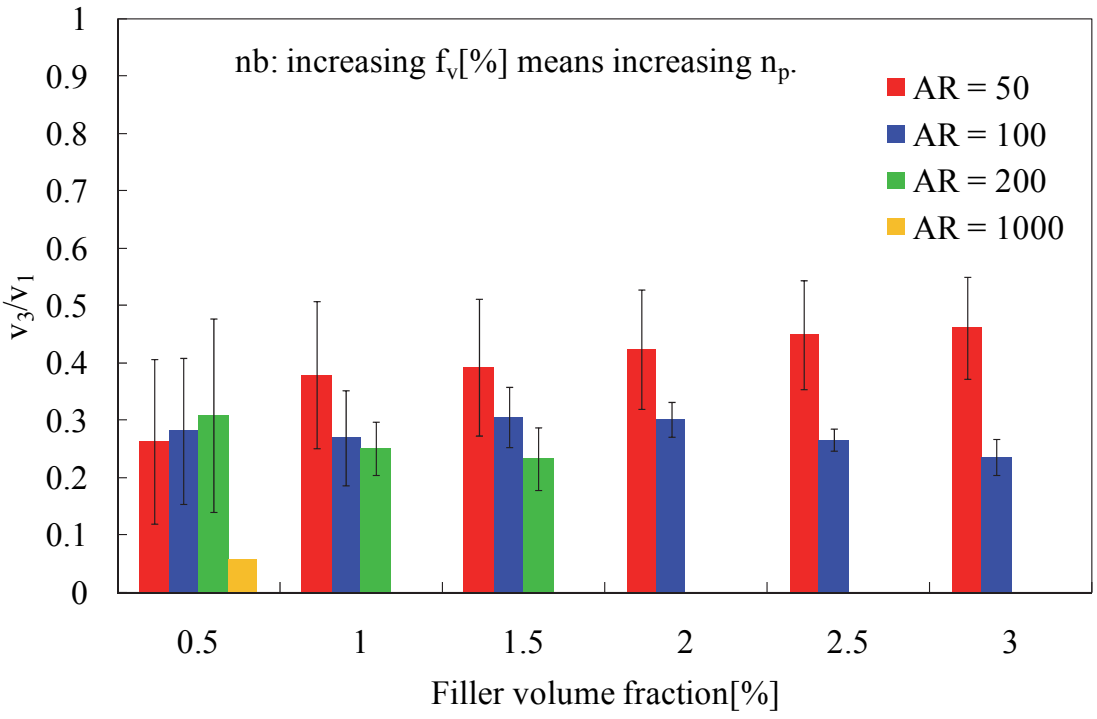

Figure 2. Effect of the aspect ratio (AR) on the overall VE isotropy.

To gain a better understanding of this difference, the reader is encouraged to see Figure 3 where the distributions are reported with Wulff projections.

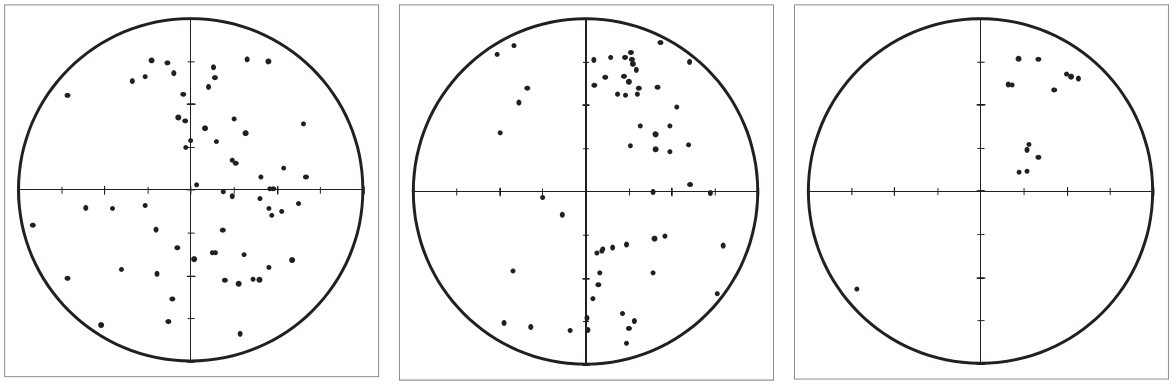

(a) (b) (c)

Figure 3. Wulff projections of some VEs considered in Figure 2: (a) AR = 50, f_v = 3%, (b) AR = 100, f_v = 3%, (c) AR = 1000, f_v = 0.5%.

A comparison between Figure 3-a and Figure 3-b shows quite clearly that the distribution of platelet orientations is different for different ARs: while Figure 3-a seems qualitatively homogeneous, it is not the case of Figure 3-b, where the distribution seems bi-modal. Figure 3-c instead shows a distribution which is significantly polarized.

In Figure 4 the orthogonal projection of the solid model plotted in Figure 3-b is reported, as an attempt to give the better comprehension of the egenvalue values as possible. The existence of a favourite orientation is clear: while in the front view it is possible to see through the VE, in the other directions it is not. Moreover it must be considered that the eigenvalues are linked to the directions of the eigenvectors which do not coincide with the projection coordinate system, therefore the projections on x, y and z directions attenuates the perceived anisotropy effect.

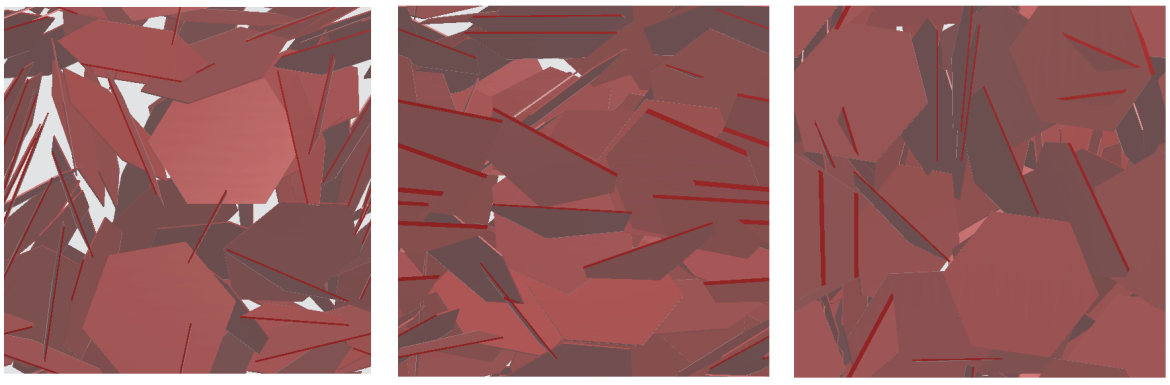

Front *Right side* *Top*

Figure 4. 3 orthogonal projections of the solid model of Figure 3-b VE.

The global isotropy index has also been used to study the effect of the number of particles on the VE platelet distribution. The results of the analysis are reported in Figure 5 for VEs of different size but with the same aspect ratio (AR = 50).

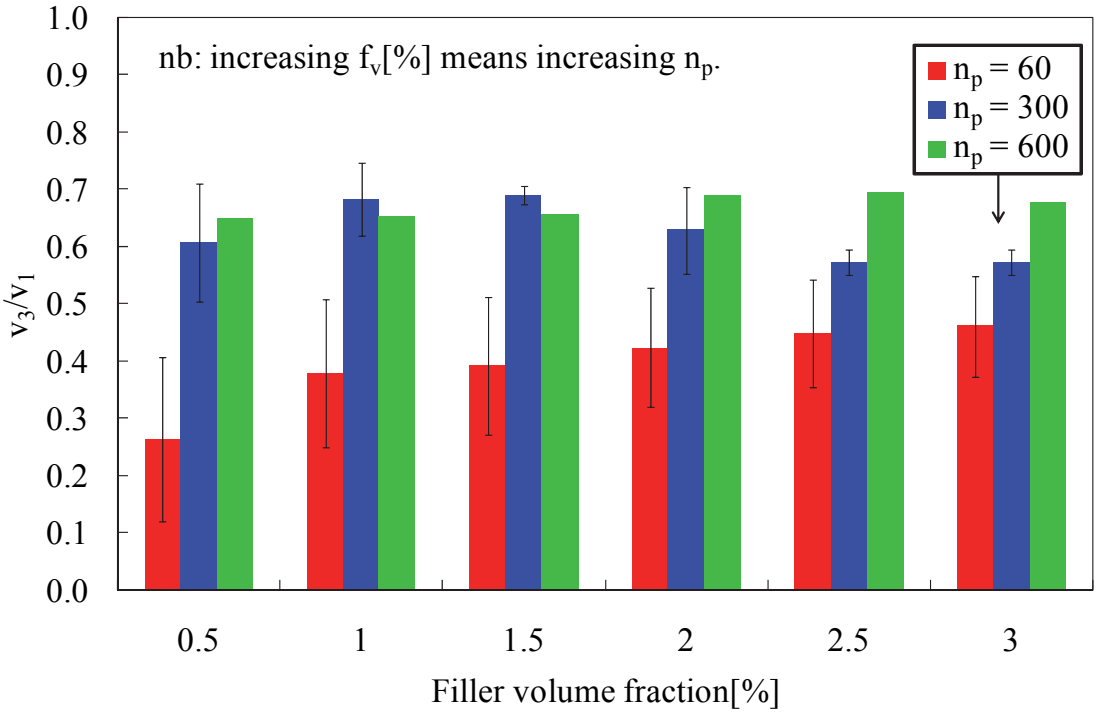

Figure 5. Effect of the VE size on the overall VE isotropy, with AR = 50. In the legend n_p is reported for each series at f_v = 3%.

The analysis has been carried out with AR = 50 to reduce the computational resources required to perform the analysis. Again the scatter band is relative to 3 simulation runs for each series, beside the case n_p = 600 where only one realization has been performed.

The increasing in n_p results in an overall higher isotropy and in the reduction of the scatter bands. Considering that the increase in n_p results in a higher statistical representativeness, the reduction of the scatter bands is reasonable. Differently, the increase in the v_3/v_1 ratio suggests the existence of a "scale-effect" in the VE: bigger is the VE, higher is the isotropy index. This can be explained by an averaging process of local anisotropies: one platelet affects the way in which the algorithm puts new platelets around itself (i.e. nearer is the new platelet to the older one, more parallel they must be), however if the initial VE is sufficiently big the initial platelets are not affected from each other and if they have a globally isotropic distribution the local effects on following placed platelets are compensated. This hypothesis can be verified through the study of the second statistical indicator, which allows the study of local anisotropies.

4.2. Local isotropy

Using the second statistical indicator, the study of the local anisotropy in the platelet distribution has been carried out. The results of this analysis are reported in Figure 6 and 7, for a f_v of 3% and 0.5% respectively. All series are averaged values of the second statistical indicator considering 3 VE realizations, beside the one with black dots which is only one VE realization, due to the high computational cost. The distance of analysis spans from zero up to the VE edge length: this introduce an aliasing effects for distances greater than half VE edge length but gives a perception of the size of the VE in comparison with the platelet size.

All curves show the same shape:

1. From 0 to about half platelet width the value of v_3/v_1 is about 0. This means that locally there is a preferred orientation.
2. From half platelet width to about half VE edge length there is a steady increase in v_3/v_1, which means that farther from the platelet centre there is the "averaging process of local anisotropies" explained before.
3. From about half VE edge length up to the full edge length the value of the second statistical indicator is stable, reasonably due to the inclusion in the analysis of platelet aliases. These stable values agree with the values of the first statistical indicator previously reported in Figure 2 and 5, as it is expected.

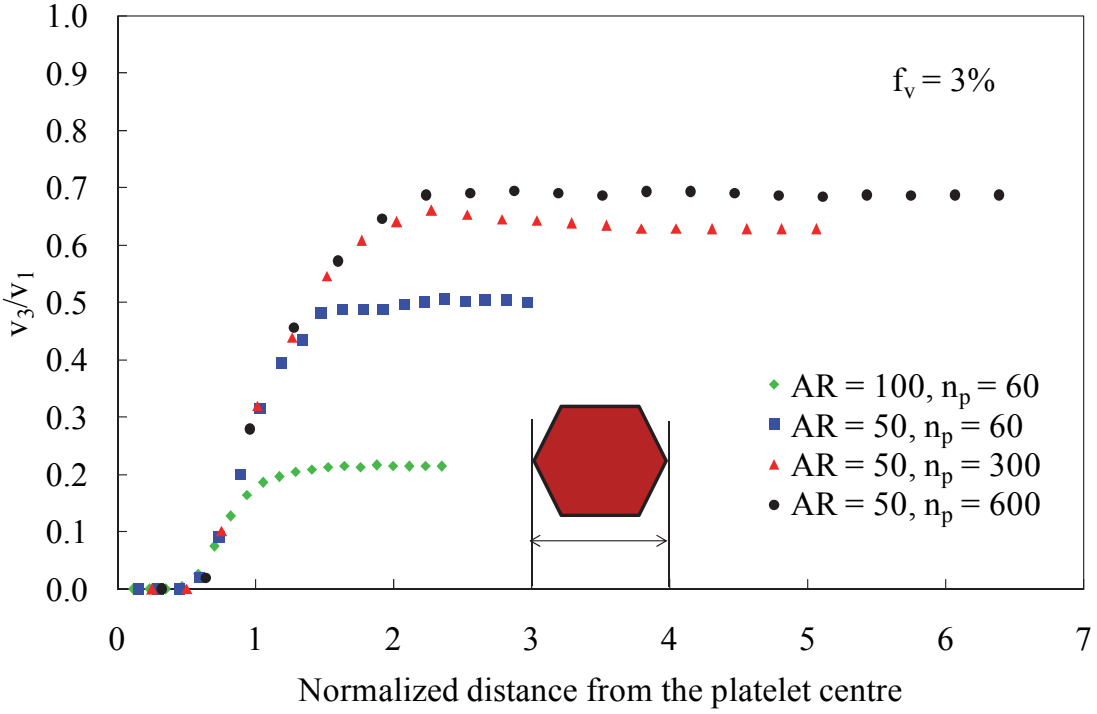

Figure. 6. Second statistical indicator trend with different VE input parameters. The distance from the platelet centre is normalized against the width of the platelet.

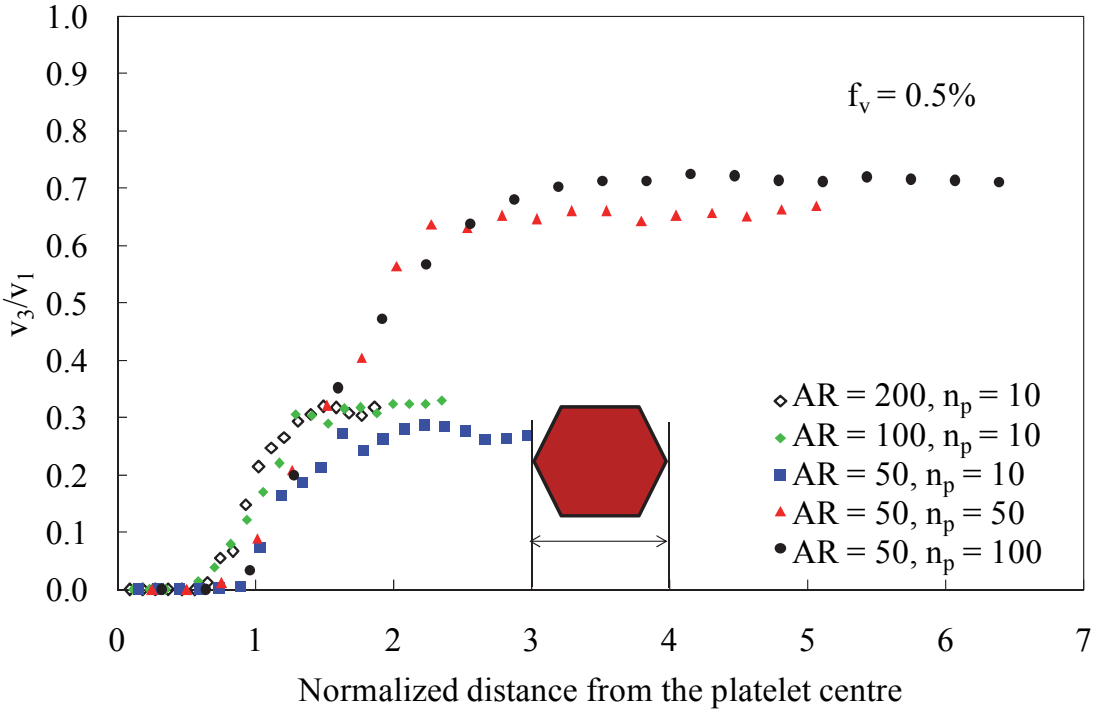

Figure 7. Second statistical indicator trend with different VE input parameters.

4.3. Platelet centre distribution

Finally the distribution of the platelet centres has been considered using function P_Z. In Figure 8 the values of P_Z within 3 VEs, obtained with the parameters reported in the figure, are plotted.

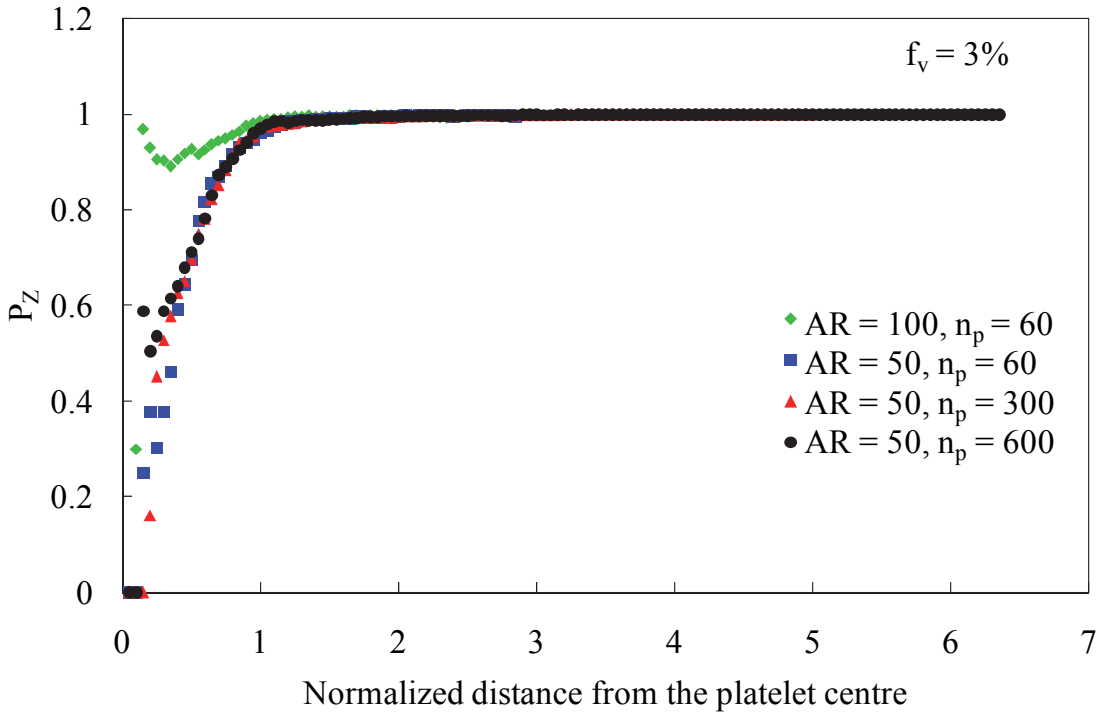

Figure 8. Trend of the function P_Z calculated at different AR.

The data show a generalized regularization at short distances, which means that few particles are actually stacked. This is also an indicator of platelet exfoliation, which agrees with the way in which the algorithm operates (i.e. generating platelets independently). Increasing the AR it seems that more intercalation takes place, considering that the distribution is more alike a random one. This is reasonably due to the correlation existing among the input parameters and the way in which the RSA algorithm operates.

In Figure 9 the same analysis of Figure 8 has been performed, but with f_v = 0.5%. In this case more dispersion is observed in the data, but again it is clear that at short range there is regularization in the distribution of platelet centres.

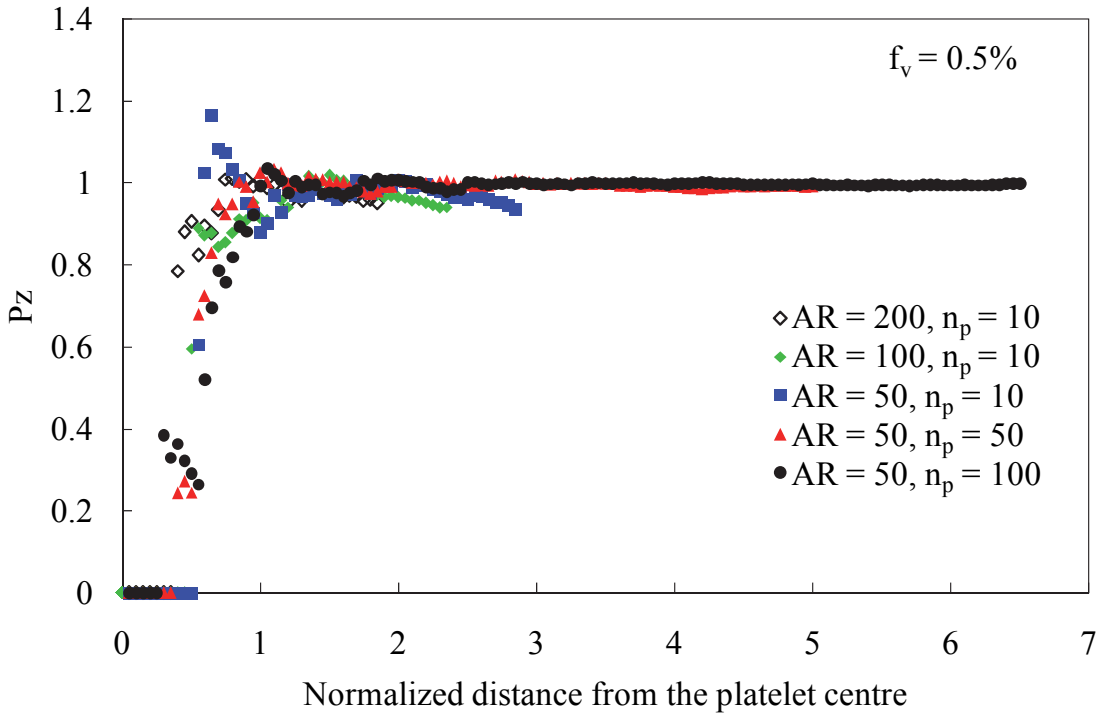

Figure 9. Trend of the function P_Z calculated at different AR.

5. DISCUSSION OF THE RESULTS

The analysis reported above highlighted the strong influence of the input parameters on the platelet distribution: differences of the aspect ratio, the number of platelets or the VE size resulted in different configurations for the reinforcement distribution. The most important consequence is that the properties displayed by VEs obtained with different input parameters may hide the effect of a different reinforcement distribution. The origin of these systemic differences may be due a combination of factors, such as the sequential nature of the algorithm, for which every new platelet depends on every other already generated, and the finite size of the VE, which affects the distribution of platelets of high AR. However, the same statistical tools which allow the analysis of the filler configuration may offer a solution to remove the effect of the input parameters: the RSA algorithm can be modified to perform the statistical analysis at run-time and new constraints can be defined on this analysis. In particular, it is possible to reject platelets which result in values of P_Z or v_3/v_1 ratios outside a prescribed tolerance – $K(h)_{OB}$ becomes an input of the algorithm, as well as the target value for v_3/v_1. This new algorithm is reported in Figure 10.

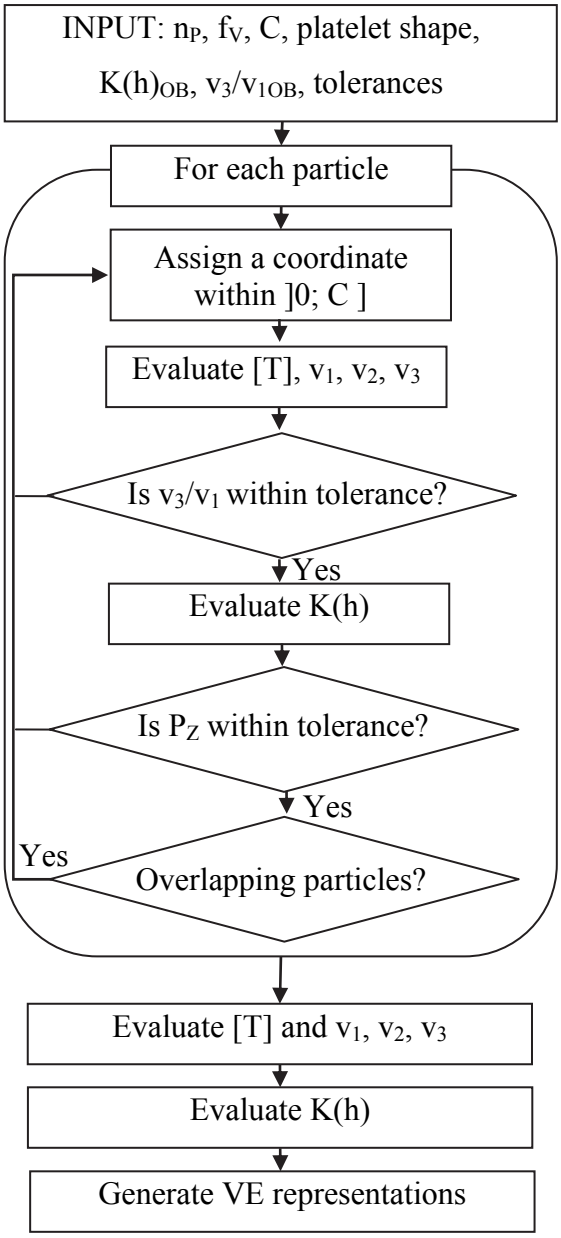

Figure 10. Diagram of the modified RSA algorithm.

This new approach results in two relevant advantages:

1. It is possible to generate VEs which display a consistent reinforcement distribution, thus solving the dependency on the input parameters;
2. It is possible to define a target distribution through experimental or theoretical analyses and use this modified RSA algorithm to reproduce this particular reinforcement configuration.

The proposed approach has been implemented in order to verify its feasibility. 3 VEs have been generated with AR = 50 and n_p = 60 at f_v = 3% and their global index of anisotropy is reported in Figure 11, where a comparison with the output of the standard algorithm for 3 AR = 50, n_p = 60 at f_v = 3% distributions and 3 AR = 50, n_p = 300 at f_v = 3% ones is reported. In this case an acceptance threshold of $v_3/v_1 > 0.5$ has been set.

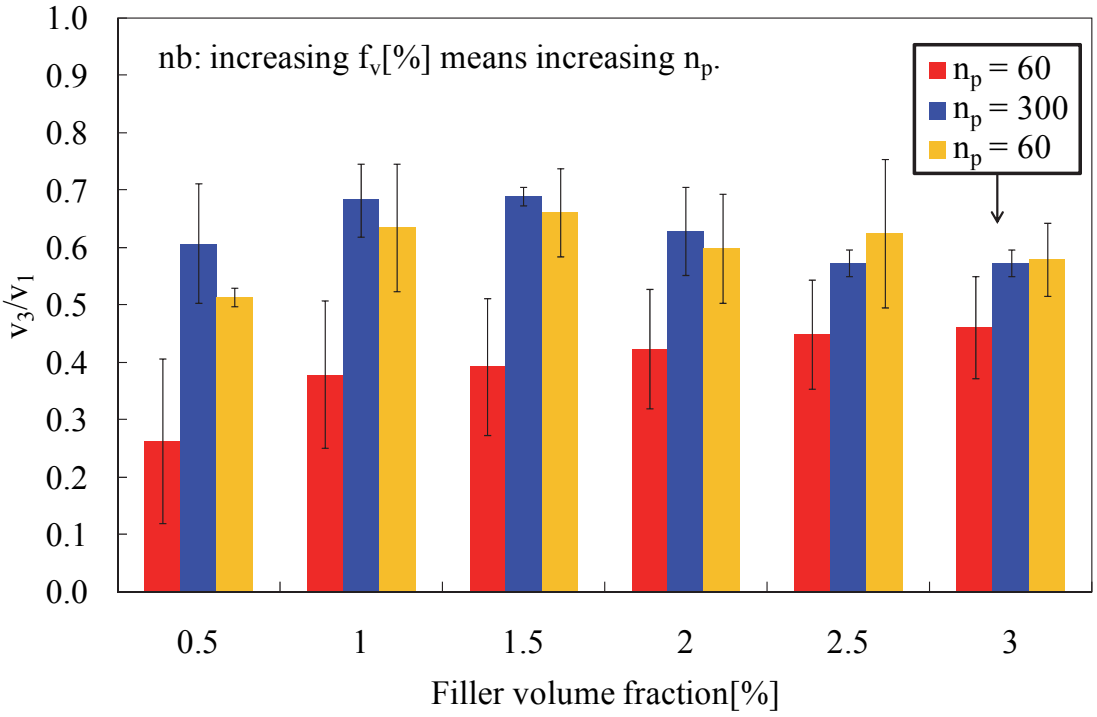

Figure 11. Effect of the aspect ratio (AR) on the overall VE isotropy. In yellow is the series obtained from the modified RSA algorithm.

This simple constraint allows the generation of VEs with a value of v_3/v_1 more similar to the one displayed by bigger VEs obtained with the classical algorithm. Moreover the new series of VEs displays a stabilized index of anisotropy even at f_v = 0.5%, differently from the older one.

However, the specific way in which the constraints on the platelet distribution are enforced depends heavily on the target VE parameters: when there are few platelets the statistical indexes needs to be relaxed or shifted. For instance, when there are just 2 platelets v_3 is 0, by definition, and a constraint may be enforced on v_2/v_1, instead. Another example regards the obtaining of high v_3/v_1 indexes with high AR: higher is the AR, more difficult is to place platelets which satisfy that constraint, and within a small VE it may be geometrically impossible.

6. CONCLUSIONS

In this chapter, the study of the Random Sequential Absorption algorithm in the generation of nanoplatelet volume elements has been carried out. The effect of the algorithm input parameters on the reinforcement distribution is studied through the implementation of statistical tools, showing that the platelet distribution is systematically affected by these parameters. The consequence is that the parametric study of the VE input parameters may be biased by hidden differences in the filler distribution. Finally, the same statistical tools used in the analysis are implemented in a modified RSA algorithm to remove the effects of the input parameters on the filler morphology.

REFERENCES

[1] Gilman, J. W., Kashiwagi, T., & Lichtenhan, J. D. (1997). Nanocomposites: a revolutionary new flame retardant approach. Sampe Journal, 33, 40-46.

[2] Giannelis, E. P. (1996). Polymer layered silicate nanocomposites. Advanced materials, 8(1), 29-35.

[3] Tjong, S. C. (2006). Structural and mechanical properties of polymer nanocomposites. Materials Science and Engineering: R: Reports, 53(3), 73-197.

[4] Becker, O., Varley, R., & Simon, G. (2002). Morphology, thermal relaxations and mechanical properties of layered silicate nanocomposites based upon high-functionality epoxy resins. Polymer, 43(16), 4365-4373.

[5] Kim, H., Abdala, A. A., & Macosko, C. W. (2010). Graphene/polymer nanocomposites. Macromolecules, 43(16), 6515-6530.

[6] Zappalorto, M., Salviato, M., & Quaresimin, M. (2013). Mixed mode (I+ II) fracture toughness of polymer nanoclay nanocomposites. Engineering Fracture Mechanics, 111, 50-64.

[7] Rhim, J. W., Hong, S. I., & Ha, C. S. (2009). Tensile, water vapor barrier and antimicrobial properties of PLA/nanoclay composite films. LWT-Food Science and Technology, 42(2), 612-617.

[8] Roy B., Bharali P., Konwar B., Karak N.: Modified hyperbranched epoxy/clay nanocomposites: A study on thermal, antimicrobial and biodegradation properties. International Journal of Materials Research, 105, 296-307 (2014)

[9] Zappalorto, M., Salviato, M., Pontefisso, A., & Quaresimin, M. (2013). Notch effect in clay-modified epoxy: a new perspective on nanocomposite properties. Composite Interfaces, 20(6), 405-419.

[10] Ma, Z. D., Sun, C., Cui, Y., Liu, Y., Hulbert, G. M., Raju, B., & Rostam-Abadi, F. (2010). Simulation and Test of Nanocomposites for Application in the Army. ARMY TANK AUTOMOTIVE RESEARCH DEVELOPMENT AND ENGINEERING CENTER WARREN MI.

[11] Hbaieb, K., Wang, Q. X., Chia, Y. H. J., & Cotterell, B. (2007). Modelling stiffness of polymer/clay nanocomposites. Polymer, 48(3), 901-909.

[12] DAI, Gaoming; MISHNAEVSKY JR, Leon. Damage evolution in nanoclay-reinforced polymers: A three-dimensional computational study. Composites Science and Technology, 2013, 74: 67-77.

[13] Cricrì, G., Garofalo, E., Naddeo, F., & Incarnato, L. (2012). Stiffness constants prediction of nanocomposites using a periodic 3D-FEM model. Journal of Polymer Science Part B: Polymer Physics, 50(3), 207-220.

[14] Fisher N.I., Lewis T., Embleton B.J.J. Statistical analysis of spherical data. Cambridge University Press, 1978.

[15] Ripley, B. D. (1977). Modelling spatial patterns. Journal of the Royal Statistical Society. Series B (Methodological), 172-212

[16] Pontefisso, A., Zappalorto, M., & Quaresimin, M. (2015). An efficient RVE formulation for the analysis of the elastic properties of spherical nanoparticle reinforced polymers. Computational Materials Science, 96, 319-326.

[17] Cressie, N. (1993). Statistics for Spatial Data: Wiley Series in Probability and Statistics.

APPENDIX

A1 Molecular dynamics simulation of nanoscale interactions in epoxy nanocomposites

KEYWORDS: A. Molecular dynamics; B. Epoxy resins; C. Nanoclay; D. Elastic properties;

ABSTRACT
In the following chapter the research activity carry out to develop a framework for the analysis of nanoscale interactions in epoxy nanocomposite materials is reported. The steps needed to analyse the elastic properties of epoxy resins are explained, using LAMMPS as molecular dynamics simulation software. Then it follows the explanation of the procedure which is being developed by the author to generate volume elements of epoxy-nanoclay nanocomposites and the difficulties found.

1. INTRODUCTION

The research activity on polymer nanocomposite materials started at the beginning of '90s and in about 25 years it grew relentlessly up to thousands of publications per year. This growth has been fostered by the stunning properties displayed by these materials, both in terms of functional properties and mechanical ones [1-3]. In order to handle their properties, multiscale approaches have been developed and the need of tackling interactions at the nanoscale and beyond emerged [4, 5]. In terms of nanoscale simulation tools, FEA fails to cope with the atomic scale, where continuum mechanics hypotheses prove to be unrealistic. Thus, different simulation techniques are employed, such as Molecular Dynamics (MD) simulations, where atoms interacts through the integration of Newton's law associated to an interacting potential [6].

In 2005 Odegard *et al.* [7] carried out MD simulations on a nanosilica reinforced polymer; the results, in terms of predicted elastic properties, highlighted how in nanocomposite materials the stunning surface over volume ratio induces the generation of an interphase between the nanoreinforcement and the matrix, with a size comparable to the filler dimension. The overall extension of this interphase with respect to other phases depends on the absolute size of the reinforcement, thus resulting in size effects within the material. Its mechanical properties are a function of the chemical and mechanical interactions between the nanoreinforcement and the matrix and, as such, depend heavily on the surfactant used to compatibilize the organic polymer with the inorganic

reinforcement. In order to incorporate the interphase in continuum-based micromechanics, Odegard *et al.* resolved to consider an effective interphase, characterized by homogeneous properties and constant thickness, hence setting the foundation for a hierarchical multiscale approach.

Since then, many researchers used the concept of an effective interphase, both in analytical and computational models: Wang et al. [8], for instance, developed a FE method to perform a parametric study on the effects of particle size, distribution and interphase properties in the overall elastic properties of a nanomodified polymer; another example can be found in [4] where the authors developed a multi-scale and multi-mechanism approach for the assessment of the fracture toughness of polymer nanocomposites.

Regardless of the approach used - analytical or computational, hierarchical or concurrent - when modelling nanocomposite materials, researchers have to tackle the issue of the interphase property determination. The most common approach, to this end, consists in MD simulations.

Yang et al. [9] resolved to employ MD simulations to obtain the elastic properties of the interface between the reinforcement and the matrix and used them in a micromechanical model. Song et al. [10] modelled the tensile properties of a nanoclay-reinforced epoxy in a FE code using cohesive elements to model the interphase, and employing MD simulations to obtain the required traction-separation law. Scocchi et al. [5] resolved to a more intensive approach, developing a multi-scale model which ranges from the quantum/atomistic simulation up to the FE analysis, for polymer-clay nanocomposites.

While the multiscale approach has imposed itself as the main path in studying nanocomposite materials, the research activity at the nanoscale is still in progress. In terms of computational tools, no software for nanocomposite simulations is able to offer an efficacy analogue to that of a commercial FE code in simulating microcomposites. The sheer amount of new Force Fields (FF) and FF parameters that are produced every year, along with new algorithms to better model chemical behaviours, requires a continuous update of the software and foster the development of in-house scripts aimed to solve very specific issues that relentlessly emerge. For instance, LAMMPS [11], which is an open-source MD code, had about 30 different releases due to major feature additions from 2004 to 2014 and 12 patches to fix bugs just during May 2014. The direct consequence of this proliferation of alternatives is that it is difficult to compare researches carried out with

just few years of difference, and the rate of obsolescence of their scientific value is dismantling.

Another common issue lies in the validation of simulation results: MD simulations are the most common approach to determine interphase properties because there are not other viable alternatives. Experimental testing at this length-scale is still pioneering, hence the validation is performed comparing the material bulk properties, obtained from experimental tests, with the output of the whole multiscale model or the predicted properties from Representative Volume Elements (RVEs) simulated directly in MD [12].

Considering several papers from the literature, it seems a common practice to assume the morphology of the interphase and look just for its mechanical properties. In [10], for instance, the authors consider perfectly round and flat clays and perfectly aligned reinforcements within stacks, as well as an interphase of uniform thickness over the external flat surfaces of each stack: the actual morphology of the interphase is disregarded and this unavoidably affects the validity of the analysis at the microscale. Even if MD simulations are performed to infer the traction-separation law between the polymer and the clay, edge-effects are not considered, while it is common engineering knowledge that points of stress concentration are likely to be critical in material behaviour. In [13] the authors carried out a parametric investigation on the effect of the interphase on thermal and elastic properties of polymer nanocomposites with FE analyses: they considered the interphase as a "homogeneous and isotropic covering layer of the outer surface of fillers with a distinct thickness" and created RVEs with random distributions of reinforcements. They assumed the morphology of the interphase and no comments are reported about that. This is true even in [14], where both numerical and analytical models are presented to study the stiffness of polymer-clay nanocomposites with oriented particles: in this case the authors used clays of rectangular shape with a constant thickness interphase lying on the top and bottom faces.

The considerations reported above highlight some weak spots of the mainstream research approach:

1. MD tools are still being developed, hence it is not possible to retrieve, in the literature, consolidated methods to infer material properties at the nanoscale.
2. Validation of results from MD simulations is an issue, both if MD is used to analyse interphase properties - due to the lack of experimental testing means - or if

MD is used to simulate whole nanocomposite RVEs - due to the computational cost.

3. In multiscale modelling the actual morphology of nanoreinforcements and interphase is commonly disregarded at the microscale both in computational and in analytical approaches.

According to the points reported above, a promising research approach would be to use MD in the simulation of whole RVEs of nanocomposite materials, using the results not just to predict the mechanical properties of the material, but also to refine micromechanical tools. Experimental validation of the model developed seems mandatory, not only to validate the tool itself, but the correct prediction of mechanical properties for a specific material system would also, reasonably, protect research results from the above mentioned obsolescence.

2. OBJECTIVES

The goal of the research activity is to study the shape and mechanical properties of the interphase around nanoclays. In particular:

1. Odegard approach [7] based on the density profile will be used to define the extension of an effective interphase around exfoliated clays. Particular care will be used to define the characteristic of the material along the edge of the clay, where the reduction in the surface density of cations unavoidably reduce the local density of the surfactant itself, and therefore affects the material properties.
2. Obtain a traction-separation curve for the mode I failure in the nancomposite and obtain the elastic properties of the effective interpahse.

3. POLYMER SIMULATION

In this section, the detailed procedure developed to simulate the elastic properties of an epoxy resin is listed. The software used and the actions performed to prepare the files are carefully reported. The goal is to give to the reader all the details which are usually skipped in published papers, but which are fundamental to perform the simulations.

3.1 Preparation of the Force Field.

OPLS-All Atom Force Field [15] has been implemented to simulate the evolution of the polymer until the end of the polymerization step. First of all, the basic file of the Force Field (FF), named oplsaa.prm, has been edited removing all the entries relative to un-used

chemical species: obviously the choice of the atom types affect the simulation, and care must be taken. This is performed to reduce the computational resources required in the following operation.

By means of the script oplsaa_moltemplate.py (included in LAMMPS tools) the edited .prm file is transformed into a .lt file for further processing (command: ./ oplsaa_moltemplate.py filename.prm).

3.2 Generation of the monomer molecules.

Avogadro modeller [16] has been used to generate the epoxy monomer, DGEBA, and the hardener monomer, DEDTA. The molecules are in a pre-reacted configuration: the epoxy molecule shows the epoxy rings already opened, by means of a H-atom addition to the O-atom, as well as in the hardener H-atoms have been removed from the N-atoms (see Figure 1-2). This modelling approach has been used by [17] to ease the reticulation process: in fact, the molecules are already in a reactive configuration, and the opening of the epoxy rings itself does not need to be simulated. The monomer files have been saved with .xyz extension.

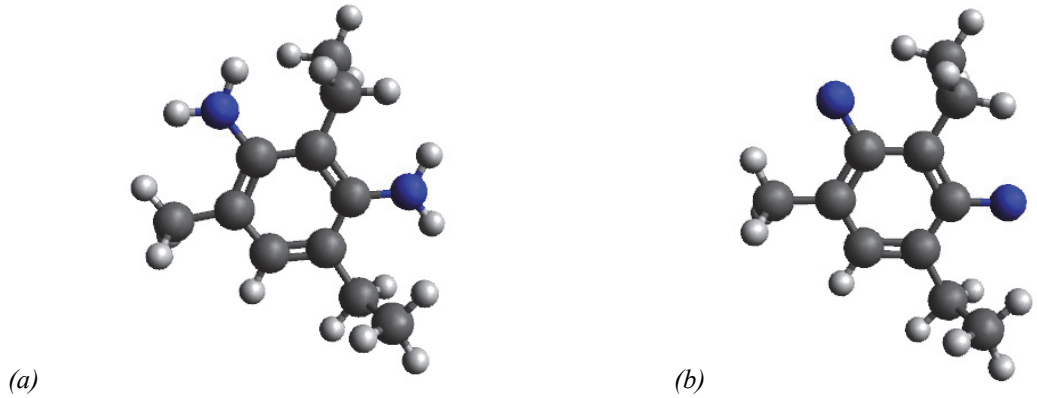

(a) *(b)*

Figure 1. (a) Stable DEDTA molecule. (b) DEDTA molecule with active polymerization sites. Colour map: dark gray : C-atom; light gray : H-atom; blue : N-atom.

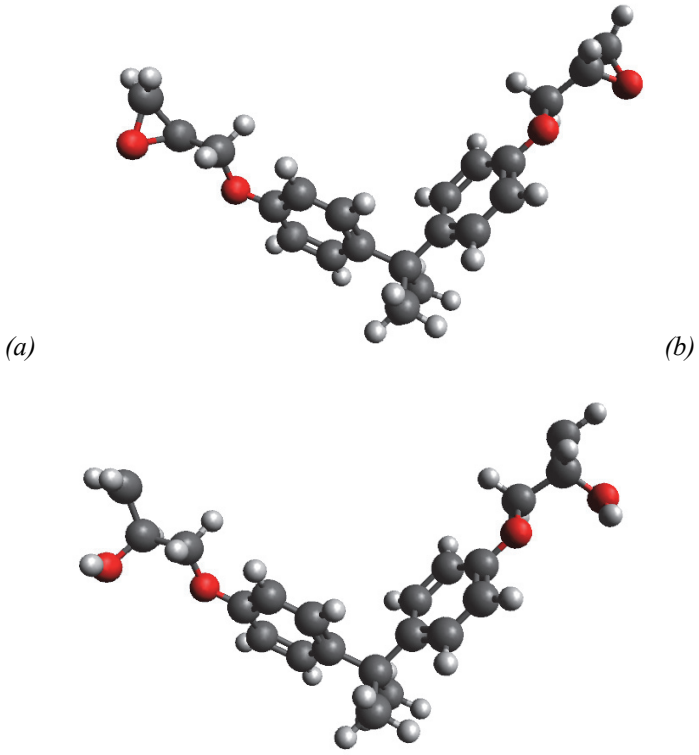

Figure 2. (a) Stable DGEBA molecule. (b) DGEBA molecule with opened epoxy rings. Colour map: dark gray : C-atom; light gray : H-atom; red : O-atom.

3.3 Generation of LAMMPS input files.

The next step consists in the generation of the topology file for the MD software. In this phase a stoichiometric amount of monomers is distributed within a cubic space and a file ready-to-be-read by the MD software is generated. To this end the files obtained at step 3.1 and 3.2 are further processed according to the following steps:

1. Use Packmol [18] to distribute a stoichiometric amount of monomers within the RVE box. In the Packmol input file set packmol.xyz as the output file. In order to successfully generate the RVE with small computational resources set the size of the box very big (which means to obtain a density in the order of 0.01 g/cm^3): the density will be corrected in the following steps.
2. Using Visual Molecular Dynamics [19] software with the plug-in topotools, the .xyz files are processed in an intermediary file. Commands:

   terminal : vmd

   in VMD : File → New Molecule... → Browse... → file.xyz → Load

   Menù : Extension → Tk Console

   Tk Console : topo writelammpsdata outputFile full

3. The script ltemplify.py, available in ../LAMMPS/tools/moltemplate/src directory, is used next. Command:

   ./ltemplify.py -name moleculeName file.in outputFile > output.lt (note: in this case file.in is an empty file)

4. It is now necessary to modify output.lt in the following way:
   - Add import "oplsaa.lt" as a first row of the file.
   - Remove or comment the mass section.
   - Find the expression moleculeName{ and substitute it with moleculeName inherits OPLSAA {.
   - In Data Atoms section modify the expressions @atom:type with the atom type from OPLSAA. This task requires some efforts and a conjoint use of the modeller Avogadro is suggested.
   - Find Data Bonds and rewrite it as Data Bond List.
   - In the same section, remove the expression @bond:type from each row.
5. Finally Moltemplate has been used to generate LAMMPS input files. After the preparation of the input file system.lt as per Moltemplate manual, issue the command: ./moltemplate.sh -xyz packmol.xyz system.lt.

3.4 Pre-relaxation of the polymeric system

Before executing the routine to reticulate the polymer, the density of the system is increased to about 1g/cm^3 in a NPT ensemble, performing a run of 300ps with a timestep of 1fs at 300K and 100atm. The system is made of 512 DGEBA and 256 DEDTA molecules: the relative high number of monomers (which results in about 33,000 atoms) is used in accordance with the observations of [20] which highlights how the simulation of polymer mechanical properties requires a number of atoms of this order. The evolution of the system is plotted in Figure 3.

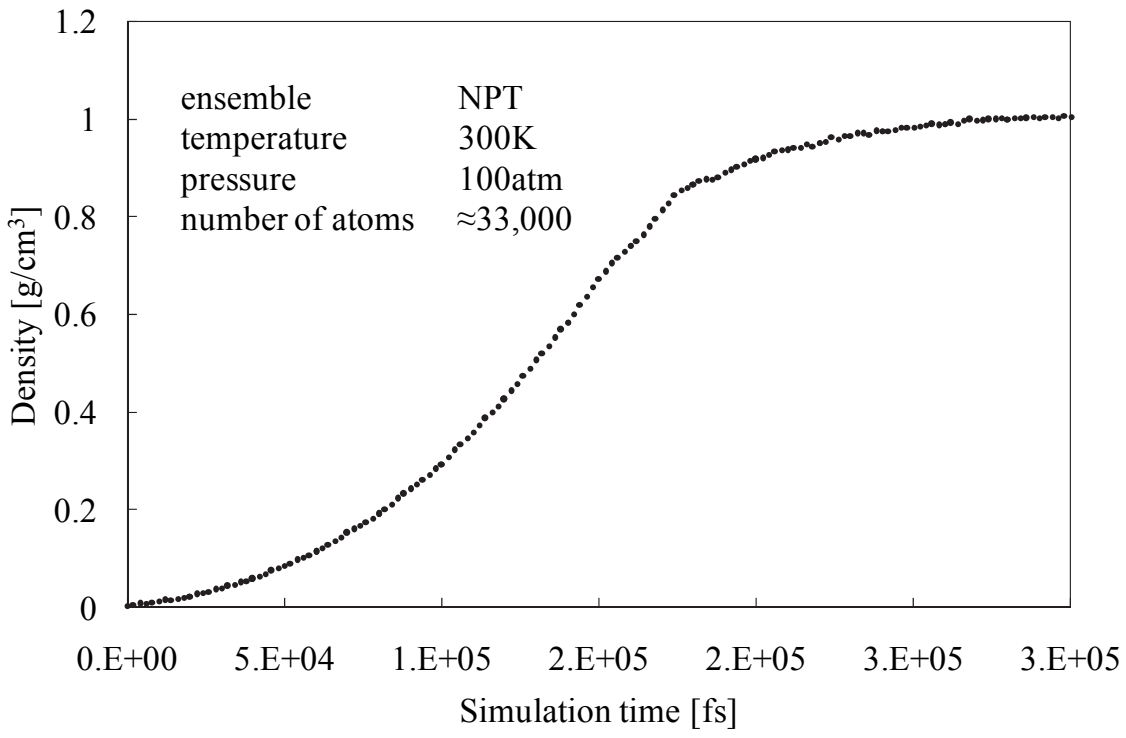

Figure 3. Density evolution as a function of the simulation time during the pre-relaxation of the polymeric systems. Simulation parameters are reported in the figure.

3.5 Polymerization

The polymerization of the system is performed following the approach reported in [17]: bonds are created between N-atoms of DEDTA molecules and terminal C-atoms of DGEBA molecules by means of fix bond/create of LAMMPS. In more details, within a NPT ensemble at 300K and 1atm, fix bond/create looks for reactive couples of atoms less than 4 Å afar and creates up to 2 bonds for each Nitrogen. After 100ps with timesteps of 0.1fs a curing of 78.5% is reached (see Figure 4). The timestep is reduced with respect of step 3.4 in order to smooth the atom displacements induced by the sudden generation of bonds. The overall density remains consistently at 1g/cm^3 regardless the different pressure in the ensemble: this behaviour is a consequence of the reticulation taking place.

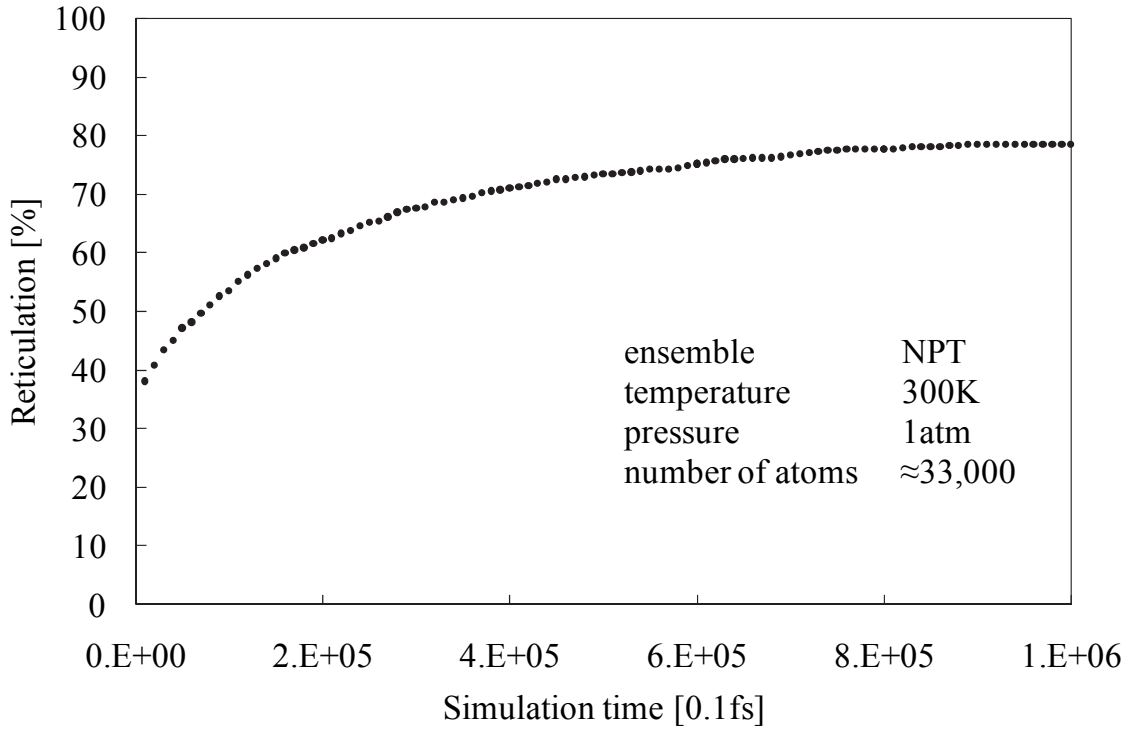

Figure 4. Reticulation within the polymeric system as a function of the simulation time

A useful remark is that in order to perform the reticulation just between the C and N atoms that are supposed to bind, a fictitious atom type for the C atoms has been used.

3.6 Change of Force Field

In order to simulate the damaging evolution within the polymer, the approach developed by Odegard *et al.* has been implemented [17]: OPLSAA is exchanged with a reactive Force Field, REAX [21], using the parameters of Liu *et al.* [22]. The system is allowed to relax in a NPT ensemble at 300K and 1atm, for an overall time of 50ps with timesteps of 0.5fs. During the simulation a charge equilibration is performed with fix qeq/reax of LAMMPS [23]. At the end of the simulation the density of the polymer is of about 1.18 g/cm^3, in agreement with experimental evaluations of the density of this kind of material [24].

Figure 5 reports the evolution of the system with and without qEq. The trends highlight the importance of studying the correct parametrization for the FF, in order to obtain meaningful results.

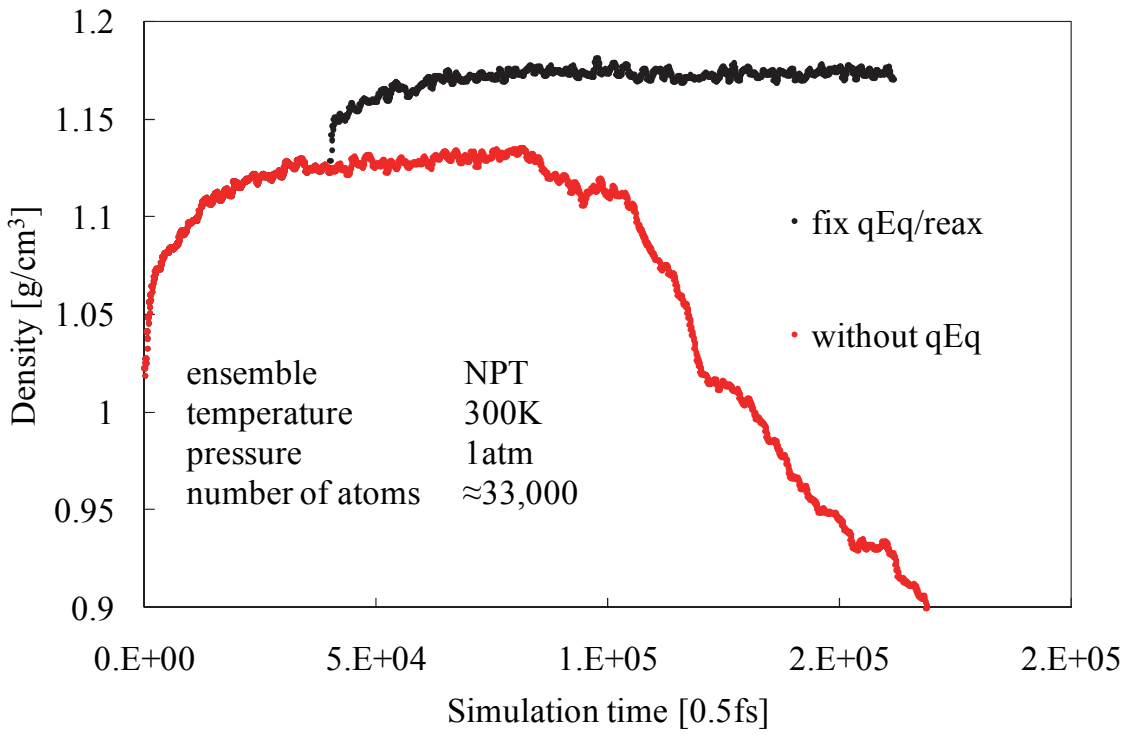

Figure 5. Evolution of the system at FF change (from OPLSAA to REAX): in red, with suppressed charge equilibration, in black, with activated charge equilibration at step 40,000.

3.7 Traction tests

A first attempt to perform the traction test was structured in this way: the command replicate 3 1 1 was used to replicate the RVE in X-direction 2 times. Then atoms in the first and the last block were put into two groups and fix move linear x.x NULL NULL was used to simulate a uniaxial traction. The ensemble was fix NPH.

Two issues have been identified:

1. It was not possible to remove the atoms in excess (e.g. keeping just a fraction of RVE in each "grip site", as in Figure 6) without changing the box size, because the evaluation of the stress did not work properly. Not removing these atoms results in a heavy computational cost.
2. It is not possible to use replicate with a not-reactive FF: in fact the software is currently unable to manage the un-wrapping of a continuous molecule which loops through RVE faces. As a consequence the command must be used before reticulating the polymer, therefore increasing the computational cost and altering the periodicity of the RVE.

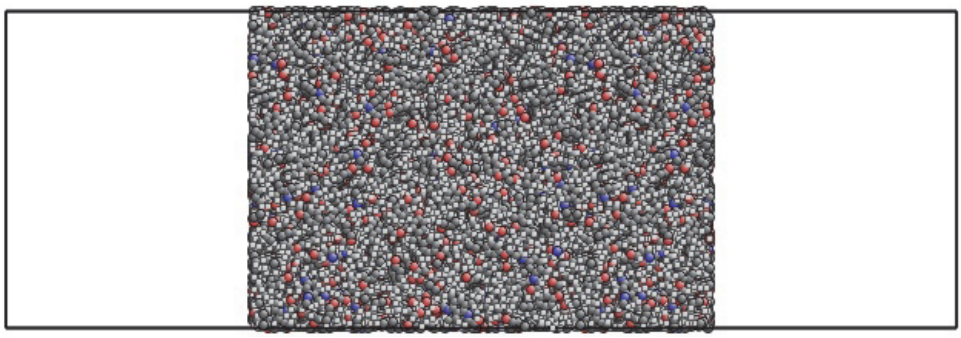

Figure 6. Representation of the system before traction in the first attempt tryed. Part of the atoms that are "frozen" by fix move have been removed to enhance the computational efficiency.

The alternative current approach consists in using the commands:

fix 1 all nvt temp 300.0 300.0 100.0

fix 2 all deform 1 x vel 0.0001 remap v

which result in an uni-axial strain in X-direction. "remap v" does not-remap atom positions and therefore impedes the re-distribution of the stress to "not-structural" atoms (e.g. H atoms), avoiding fictitious load transfers. To move from the stress evaluated in uni-axial strain to the elastic properties, basic theory of elasticity concepts can be used.

In Figures 7-8, results from traction tests performed with OPLSAA FF and REAX FF are reported.

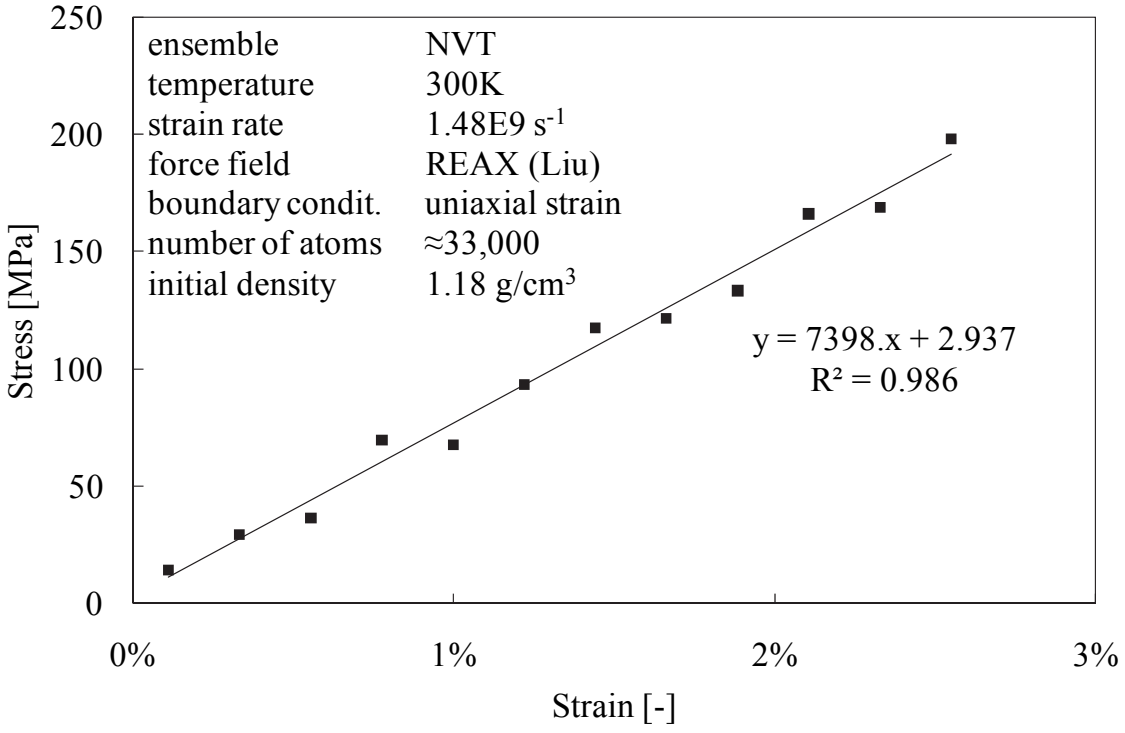

Figure. 7. Results of the traction test performed on the polymer with REAX FF. Stress values have been averaged every 1,500 timesteps.

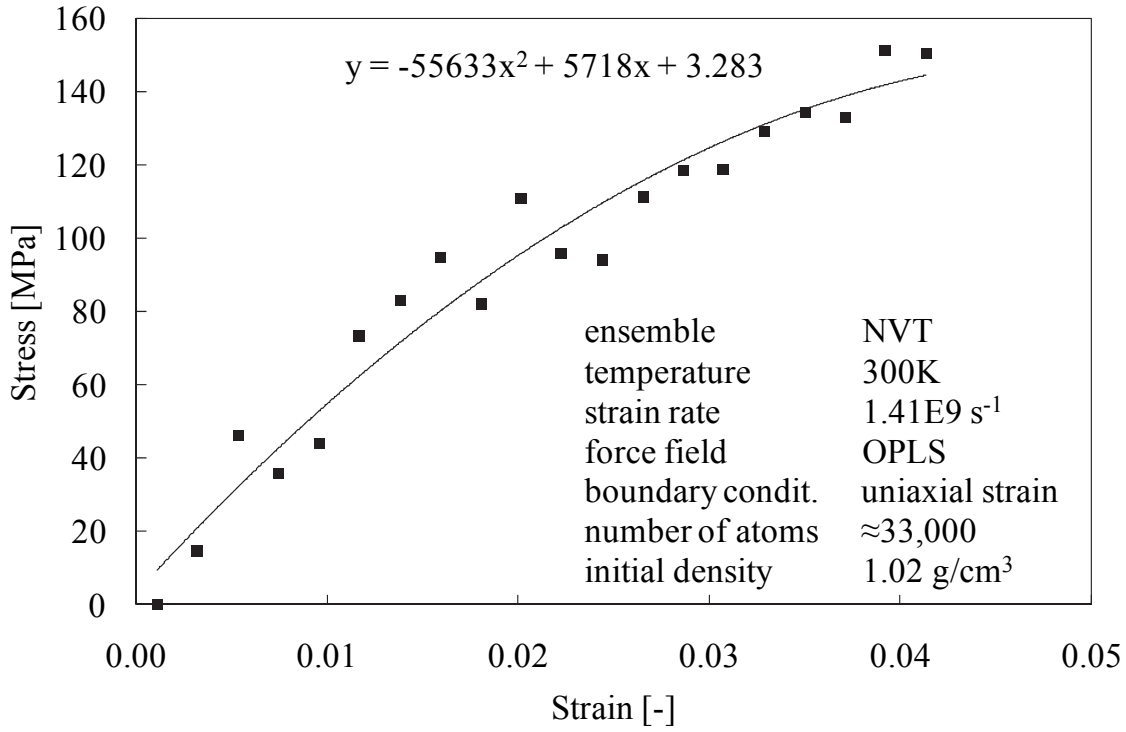

Figure 8. Results of the traction test performed on the polymer with OPLS FF. Stress values have been averaged every 1,500 timesteps.

Considering the longitudinal modulus averaged at 2%±0.5% strain, REAX results in about 7.6±0.2GPa, while OPLSAA in 5.1±0.2GPa: these results are consistent with each other, if the difference in the density of the polymer is taken into account.

Considering the generalized Hooke's law, $\varepsilon_{ii} = \frac{1}{E}\left(\sigma_{ii} - \nu\left(\sigma_{jj} + \sigma_{kk}\right)\right)$,under the hypothesis of isotropy it is possible to evaluate the average elastic modulus, E, and the Poisson's coefficient, ν. Doing so, REAX predicts and elastic modulus of 3.6±0.1GPa and a Poisson's coefficient of 0.36, while OPLSAA predicts 1.6±0.1GPa and 0.42 respectively.

It seems useful to point out how the evaluation of the elastic modulus is sensitive to the data range used in the computation: if all data points of Figure 7 are used to evaluate average stresses in x, y and z directions, the predicted elastic modulus is about 5.1GPa and ν is about 0.34.[1]

[1] values used in the computation of the elastic properties

	Sx [MPa]	Sy [MPa]	Sz [MPa]
Averaged at 2%	147	97.4	65.8
Averaged in 0%-2.55%	101	61.2	37.8

While results from REAX FF are reasonable if compared with experimental testing of epoxy resins (E≈3GPa)[24], [17], using a similar model but with a NPT ensemble and a strain rate on the order of 1.E8s^{-1}, evaluated an elastic modulus of about 5GPa and justified it considering the expected increase in elastic modulus due to the high strain rate. An initial attempt to run the simulations of OPLSAA and REAX with a strain rate reduced by one order of magnitude suggests that OPLSAA predicts a constant longitudinal modulus, while REAX predicts one about 15% higher. Further analyses are required.

Further possible researches:

- study the effect of the strain rate;
- study the strength of the material with REAX FF;
- study the effect of the polymerization ratio;
- study the effect of the temperature;
- modify the polymer adding additives actually presents in commercial products;
- add nanoreinforcements.

4. NANOCOMPOSITE SIMULATION

Preliminary remarks

The following part of the chapter is relative to a procedure to create a volume element of a nanoclay reinforced epoxy resin to be used within LAMMPS. This procedure is not completed yet, but to report the difficulties found and the solutions identified so far seems nonetheless worthy of few pages of this PhD thesis.

Nanoclay and surfactant material models

The Montmorillonite (MMT) model has been retrieved in the literature along with a dedicated FF developed by the research group of prof. H. Heinz [25]. PCFF Interface Force Field has been used with the model of a MMT with formula $K_{0.533}[Si_4O_8][Al_{1.467}Mg_{0.533}O_2(OH)_2]$, CEC=143 mmol/100g. Interface FF is meant to be an extension of common harmonic class-2 FFs (e.g PCFF), retaining their functional form but extending their capability of modelling organic/inorganic interfaces. Simulations carried out with this FF have been compared with experimental data showing a more than satisfactory agreement [25].

The surface of the MMT has been functionalise with an organic surfactant, in order to improve the compatibility with the polymer. To this end molecules of Stearylamine

($C_{18}H_{39}N$, see Figure 9) have been used: this kind of surfactant is commercially available from the same supplier of the MMT (Nanocor) and results with this compound are available in the literature both in terms of MD simulations (e.g. [26]) and experimental data (see Chapter 1).

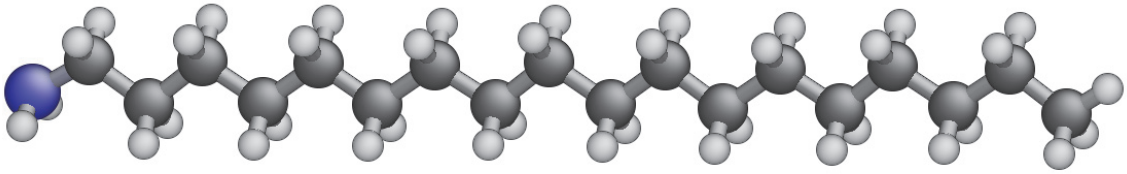

Figure 9. Representation of the Stearylamine model used in the simulation. Colour map: blue : N-atom; dark-gray : C-atom; light-gray : H-atom.

A FIRST ATTEMPT

Here follows the description of a failed attempt. It is reported to save others the time to try and implement it. The explanation of the issues found is reported after the description of the procedure

Creation of the input for LAMMPS.

The website of prof H. Heinz offers not only the FF and material models, but also a detailed description on how to generate LAMMPS input file. However, a different approach has been used here to allow the use of REAX FF for the surfactant. The tool msi2lmp_gcc32.exe, which is available in the referenced website, has been used to convert the model in a LAMMPS file. Separately, the model of the surfactant is created with Avogadro modeller and converted to a LAMMPS input file. Then, a dedicated C++ software has been prepared to deploy the desired amount of surfactant molecules within the simulation box of the MMT, retaining the LAMMPS input file format. Finally, a working simulation with hybrid potentials is set, using REAX FF with Liu parameters [22] for the surfactant and Interface FF for the clay. Pay attention that bonds, angles, dihedrals and impropers due to the former FF must be removed and non overlapped to the interactions of REAX.

It must be pointed out that the amount of surfactant that is able to stick to the clay unavoidably affect the mechanical properties of the system, affecting the compatibility between polymer and reinforcement.

The N-atoms of the surfactants are moved by means of the LAMMPS fix drag command over a cation in order to bind them to the MMT.

Issues

Some problems emerged employing the former approach:

- It appears reasonable to me that the former approach with a hybrid FF PCFF/REAX in which the surfactant is hold in place with a fix, results in an irrelevant presence of the MMT: in other words, the MMT model would be used only to define the position of the surfactant, missing the long range interactions.[2]
- The MMT model requires an interaction with the polymer, otherwise they don't see each other (e.g. it is the same as to try and model a contact interaction in FEA without contact elements: there is interpenetration). The hybrid parametrization needs to be carefully designed.
- Another problem is that the organic molecules have to be imported with OPLS in order to carry out the polymerization, and then the change in FF takes place. Moreover, fix bond/create does not work yet with class2 FF (date: 08-08-2014)[3].

SECOND ATTEMPT

To overcome the troubles reported in the section above, a different approach has been carried out: MMT, surfactant and monomers are all modelled in PCFF.

4.1. Creation of a running simulation of the MMT

The website of prof. H. Heinz offers not only the FF and material models, but also a detailed description on how to generate LAMMPS input file. However, just the first step has been carried out here, the modeller to create the organic molecules was not available .pdf and .pdb files. Instead, the tool msi2lmp_gcc32.exe, which is available in the referenced website, has been used to convert the MMT model (mont0_533_K_15_single_layer) in a LAMMPS file (mont0_533_K_15_single_layer.lammps05). Beware that the number of impropers is wrong (i.e. 525684) because, somehow, the tool generate many "virtual" impropers around atom type 1; they should be corrected (in this case, the removal of the wrong

[2] It is not straightforward to maintain electrostatic interactions with REAX (to keep the charge in the protonated N, for instance) and to obtain reasonable material behaviour(keep the charge→no qEq→see Figure 5).

[3] A work-around has been reported below, at point 6.Reticulation.

impropers results in 1860 impropers for the model). The input file needs the definition of interaction styles for the simulation:

```
units real
atom_style full
bond_style  class2
angle_style  class2
dihedral_style  class2
improper_style  class2
pair_style lj/class2/coul/long 20.0
kspace_style pppm 0.0001
```
[4]

Pay attention to the definition of pair_style: without coul/long, the model does not consider electrostatic interactions, but these interaction are the core of the MMT interaction with the surfactant and with the K cations.

4.2. Creation of the organic compound

Three organic species are considered in the simulation: the surfactant, the epoxy monomer and the hardener (i.e. Stearylamine, DGEBA and DEDTA). For these materials OPLS models can be obtained as described in the simulation of the polymer section, while the conversion to PCFF is described below. It is strongly suggested to check if it is possible to retrieve online a tool for the change of FF, which was not available when this procedure took place.

1. *Creation of the polymer compound*. With Packmol, it is possible to create a RVE of the organic compound, setting its boundaries to fill the space available in the MMT pre-constructed cell. In the available MMT RVE-cell, the space occupied by MMT atoms is just a fraction of the overall space, with atoms places at lower z coordinates: constraining Packmol to use the empty space simplifies the following operation of merging the composite phases.
2. *Identification of atom types*. It is necessary to link the atom type of the data file to a corresponding atom in PCFF. After identifying a molecule with its ID, it is possible to plot its atoms, for instance in a 2D Excel plot, and then identify the kind of molecule (e.g. DGEBA) and for each atom type its atomic specie and

[4] This configuration requires periodic boundary conditions. If non periodic BCs are needed, pair_style must be changed to lj/class2/coul/cut without kspace_style (therefore loosing the computation of long range interactions).

specific function (e.g. C in aromatic ring)[5]. A check could be performed comparing the parameters reported for pair coefficients in the data file and in OPLS.

3. *Reformulation of the FF coefficient file according to the new FF.* The following part requires the development of a script to be performed in a reasonable amount of time: using the data file, in which atoms, bonds, dihedrals and impropers are reported, the coefficient file is constructed ex-novo from PCFF. If the molecules involved in the simulation remain the same, reasonably the file does not need updates; this is not true if new molecule types are used.

At the end of this procedure a new file with the coefficients for the data file is created. Parameter styles are the same as the one reported in step 1.

4.3. Creation of the simulation cell

The organic and the inorganic materials are joined by simply adding their definition files, using the MMT files as a base and adding the organic informaton. Using Packmol to generate polymer coordinates which do not overlap to the MMT ones, this task is trivial. In system.data the overall indexes in the header section must be updated as well as atom, bond, dihedral and improper organic IDs.[6]

4.4. Surface modification of the clay

From here on the procedure is still a work-in-progress

Before proceeding with the simulation, the surfactant has to be bound to the MMT. The following description assumes a RVE composed of 1 clay platelet, 4 surfactant molecules, 30 DGEBAs and 15 DEDTAs.

The first operation consists in the deletion of 4 K-cations:

```
#remove 4 cations from the MMT (atom type 15), two per face
group           K2remove id 601 602 603 605
delete_atoms    group K2remove
```

[5] Note: it is possible that 1 OPLS atom type finds its equivalence in different PCFF atom types (e.g. the N in DEDTA and the N in Stearylamine are well different in PCFF, but they may not differ in the OPLS model). If such is the case, care must be taken in the following operations, and a manual fix of the final file will be required.

[6] I suggest to use Excel to perform the task of updating atom IDs. Pay attention to update also the atom IDs within bond, angle, dihedral and improper definitions.

This will allow to the protonated amine of the surfactant to substitute the missing cations and equilibrate the MMT. In this way the correct (electrostatic) interaction between surfactant and MMT is modelled.

Then the surfactant molecules are moved toward the MMT:

```
#attract surfactant toward the MMT
group           Np type 29
fix             moveNp Np drag NULL NULL 4.5 1000.0  6.0
```

This allows to move the surfactant charged head in the interaction radius defined by pair style lj/class2/coul/long. The position of the MMT has to be fixed in space, to allow fix drag to move the surfactant in the correct area:

```
#I have to fix the position of the MMT
group           SiAtoms type 2 3
fix             blockMMT SiAtoms move linear NULL NULL 0.0
```

Finally, the simulation is run according to:

```
#a limit has been used to help with surfactant dragging
fix             1 all nve/limit 0.1
```

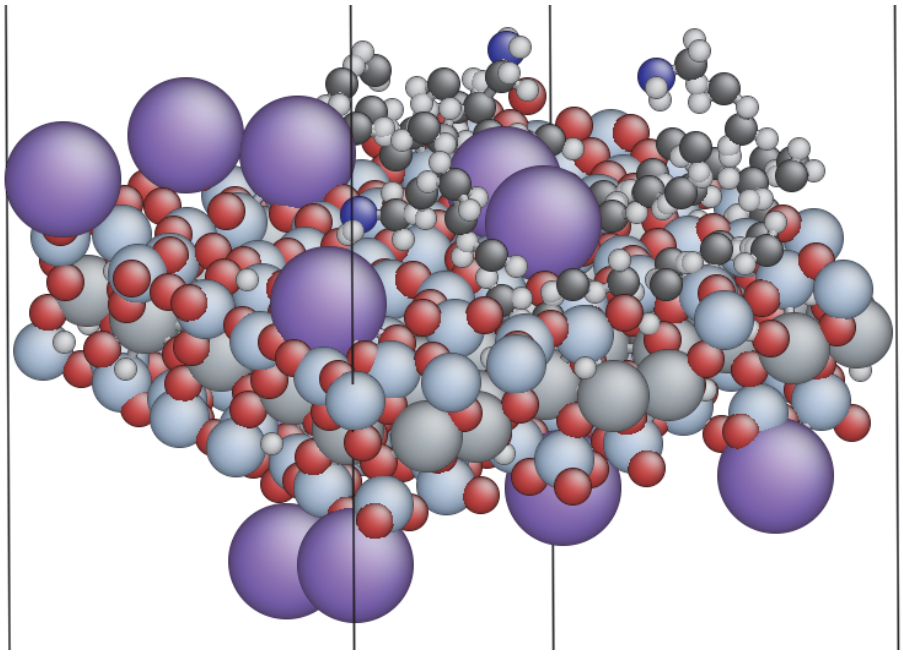

Figure 10. Representation of the clay with surfactant molecules attached to the surface. Colour map: light-gray : H-atom; dark-gray : C-atom; red : O-atom; middle-gray : Al/Mg-atom; violet : K-atom; blue : N-atom.

4.5. Compression

The NPT ensemble does not seem capable of performing the compression of the system up to the required density. A work-around could be to calculate the dimension of the RVE (without the space occupied by the MMT) with the correct density and then proceed with compression according to an approach similar to:

#deform the whole simulation box, in a uni-axial strain approach

```
fix             0 all nve/limit 0.1
fix             1 all langevin 300.0 300.0 100.0 1587
fix             2 all deform 1 z vel -0.001 remap v
```

performing the required amount of timesteps.

4.6. Reticulation

Reticulation requires some efforts, because the current version of LAMMPS (08-08-2014) invoke an error when a class 2 FF is used with fix bond/create, even if the bond created is harmonic instead of class 2. To solve the issue hybrid bond style is implemented as:

```
bond_style      hybrid harmonic class2
```

which requires a redefinition of the input file according to the hybrid approach:

```
bond_coeff      1  class2      2.0433      430   0      0
```

Then, the file fix_bond_create.cpp needs to be edited, commenting the rows from 241 to 245, and LAMMPS needs to be recompiled. In this way the check on the employment of class 2 FF is not performed, and it is up to the user the selection of a correct FF. A new bond type is then defined in the input file, retrieving the needed parameters from PCFF in the quadratic bond section:

```
bond_coeff      88      harmonic      356.5988      1.4700
```

As a next step, fix bond/create is employed as in the case of the simple polymer:

```
fix             1 all bond/create 2  26 28 4.0 88 iparam 2 26 jparam 1  28
```

Finally, the simulation can be run according to:

```
timestep        0.1
fix             2 all nve/limit 0.1
```

and reticulation process can be followed with:

```
thermo_style    custom step f_1[1] f_1[2] bonds
```

AKNOWLEDGMENTS
Even if this activity has not given results (yet) I would like to thanks Professor Chandra Veer Singh of the University of Toronto and his research group who hosted me. Their support and knowledge essential.

BIBLIOGRAPHY

[1] Chen, C., Justice, R. S., Schaefer, D. W., & Baur, J. W. (2008). Highly dispersed nanosilica–epoxy resins with enhanced mechanical properties.Polymer, 49(17), 3805-3815.

[2] Ma, J., Mo, M. S., Du, X. S., Rosso, P., Friedrich, K., & Kuan, H. C. (2008). Effect of inorganic nanoparticles on mechanical property, fracture toughness and toughening mechanism of two epoxy systems. Polymer, 49(16), 3510-3523.

[3] Liang, Y. L., & Pearson, R. A. (2009). Toughening mechanisms in epoxy–silica nanocomposites (ESNs). Polymer, 50(20), 4895-4905.

[4] Quaresimin, M., Salviato, M., & Zappalorto, M. (2014). A multi-scale and multi-mechanism approach for the fracture toughness assessment of polymer nanocomposites. Composites Science and Technology, 91, 16-21.

[5] Scocchi, G., Posocco, P., Danani, A., Pricl, S., & Fermeglia, M. (2007). To the nanoscale, and beyond!: Multiscale molecular modeling of polymer-clay nanocomposites. Fluid Phase Equilibria, 261(1), 366-374.

[6] Rahman, A. (1964). Correlations in the motion of atoms in liquid argon.Physical Review, 136(2A), A405.

[7] Odegard, G. M., Clancy, T. C., & Gates, T. S. (2005). Modeling of the mechanical properties of nanoparticle/polymer composites. Polymer, 46(2), 553-562.

[8] Wang, H. W., Zhou, H. W., Peng, R. D., & Mishnaevsky Jr, L. (2011). Nanoreinforced polymer composites: 3D FEM modeling with effective interface concept. Composites Science and Technology, 71(7), 980-988.

[9] Yang, B. J., Shin, H., Lee, H. K., & Kim, H. (2013). A combined molecular dynamics/micromechanics/finite element approach for multiscale constitutive modeling of nanocomposites with interface effects. Applied Physics Letters,103(24), 241903.

[10] Song, S., Chen, Y., Su, Z., Quan, C., & Tan, V. B. (2013). Effects of clay structural parameters and gallery strength on the damage behavior of epoxy/clay nanocomposites. Composites Science and Technology, 85, 50-57.

[11] Plimpton, S. (1995). Fast parallel algorithms for short-range molecular dynamics. Journal of computational physics, 117(1), 1-19.

[12] Smith, G. D., Bedrov, D., Li, L., & Byutner, O. (2002). A molecular dynamics simulation study of the viscoelastic properties of polymer nanocomposites. The Journal of chemical physics, 117(20), 9478-9489.

[13] Mortazavi, B., Bardon, J., & Ahzi, S. (2013). Interphase effect on the elastic and thermal conductivity response of polymer nanocomposite materials: 3D finite element study. Computational Materials Science, 69, 100-106.

[14] Pahlavanpour, M., Hubert, P., & Lévesque, M. (2014). Numerical and analytical modeling of the stiffness of Polymer–Clay Nanocomposites with aligned particles: One-and two-step methods. Computational Materials Science, 82, 122-130.

[15] Jorgensen, W. L., Maxwell, D. S., & Tirado-Rives, J. (1996). Development and testing of the OPLS all-atom force field on conformational energetics and properties of organic liquids. Journal of the American Chemical Society,118(45), 11225-11236.

[16] Hanwell, M. D., Curtis, D. E., Lonie, D. C., Vandermeersch, T., Zurek, E., & Hutchison, G. R. (2012). Avogadro: An advanced semantic chemical editor, visualization, and analysis platform. J. Cheminformatics, 4, 17.

[17] Odegard, G. M., Jensen, B. D., Gowtham, S., Wu, J., He, J., & Zhang, Z. (2014). Predicting mechanical response of crosslinked epoxy using ReaxFF.Chemical Physics Letters, 591, 175-178.

[18] Martínez, L., Andrade, R., Birgin, E. G., & Martínez, J. M. (2009). Packmol: A package for building initial configurations for molecular dynamics simulations.Journal of computational chemistry, 30(13), 2157-2164.

[19] Humphrey, W., Dalke, A., & Schulten, K. (1996). VMD: visual molecular dynamics. Journal of molecular graphics, 14(1), 33-38.

[20] Yang, S., & Qu, J. (2012). Computing thermomechanical properties of crosslinked epoxy by molecular dynamic simulations. Polymer, 53(21), 4806-4817.

[21] Van Duin, A. C., Dasgupta, S., Lorant, F., & Goddard, W. A. (2001). ReaxFF: a reactive force field for hydrocarbons. The Journal of Physical Chemistry A,105(41), 9396-9409.

[22] Liu, L., Liu, Y., Zybin, S. V., Sun, H., & Goddard III, W. A. (2011). ReaxFF-lg: Correction of the ReaxFF reactive force field for London dispersion, with applications to the equations of state for energetic materials. The Journal of Physical Chemistry A, 115(40), 11016-11022.

[23] Aktulga, H. M., Fogarty, J. C., Pandit, S. A., & Grama, A. Y. (2012). Parallel reactive molecular dynamics: Numerical methods and algorithmic techniques.Parallel Computing, 38(4), 245-259.

[24] Elantas Italia srl. EC157 epoxy resin product datasheet.

[25] Heinz, H., Lin, T. J., Kishore Mishra, R., & Emami, F. S. (2013). Thermodynamically consistent force fields for the assembly of inorganic, organic, and biological nanostructures: the INTERFACE force field. Langmuir,29(6), 1754-1765.

[26] Chen, Y., Chia, J. Y. H., Su, Z. C., Tay, T. E., & Tan, V. B. C. (2013). Mechanical characterization of interfaces in epoxy-clay nanocomposites by molecular simulations. Polymer, 54(2), 766-773.

ACKNOWLEDGEMENTS

I wish to express my gratitude to all the people who worked with me in these three years. To my supervisor, Dr. Michele Zappalorto, who advised me from the beginning of my doctorate, when I knew virtually nothing about polymer nanocomposites, and addressed my research activities in this young and exciting research field. To the chief of the research group, Prof. Marino Quaresimin, who gave me the opportunities and the means to prosecute the research activities contained in this thesis. To my colleagues, the older ones (Marco, Paolo, Christian) and the newer ones (Alberto, Pasquale, Lucio), who gave me precious advices and support. To the technicians, who take care of the laboratories and without whom it would not have been possible to carry out the experimental activities reported in these pages. To the Masters' students I co-advised in my doctorate (Matteo and Michele), and with whom I shared the weight of the experimental activities.

My gratitude is also to Prof. Gianmaria Concheri, the supervisor of my Masters' thesis, who believed in my skills and encouraged me to pursue a PhD.

My thankfulness to Fondazione CA.RI.PA.RO. for the scholarship they granted me.

Finally, I would like to express my gratitude to my family. Their support and sacrifices the foundation of my resolve.